2018

AN OPTIMIZED SOLID-PHASE REDUCTION AND CAPTURE STRATEGY FOR THE STUDY OF REVERSIBLY-OXIDIZED CYSTEINES AND ITS APPLICATION TO METAL TOXICITY

John Andrew Hitron
University of Kentucky, a.hitron@uky.edu
Digital Object Identifier: https://doi.org/10.13023/etd.2018.356

AN OPTIMIZED SOLID-PHASE REDUCTION AND CAPTURE STRATEGY FOR THE STUDY OF REVERSIBLY-OXIDIZED CYSTEINES AND ITS APPLICATION TO METAL TOXICITY

_____

DISSERTATION
_____

A dissertation submitted in partial fulfillment of the
requirements for the degree of Doctor of Philosophy in the
College of Medicine at the University of Kentucky

By
John Andrew Hitron

Lexington, Kentucky

Director: Dr. Xianglin Shi, Professor of Toxicology and Cancer Biology

Lexington, Kentucky

2018

ABSTRACT OF DISSERTATION

AN OPTIMIZED SOLID-PHASE REDUCTION AND CAPTURE STRATEGY FOR
THE STUDY OF REVERSIBLY-OXIDIZED CYSTEINES AND ITS APPLICATION
TO METAL TOXICITY

The reversible oxidation of cysteine by reactive oxygen species (ROS) is both a
mechanism for cellular protein signaling as well as a cause of cellular injury and death
through the generation of oxidative stress. The study of cysteine oxidation is complicated
by the methodology currently available to isolate and enrich oxidized-cysteine containing
proteins. We sought to simplify this process by reducing the time needed to process
samples and reducing sample loss and contamination risk.

We accomplished this by eliminating precipitation steps needed for the protocol
by (a) introducing an in-solution NEM-quenching step prior to reduction and (b)
replacing soluble dithiothreitol reductant with a series of newly-developed high-capacity
polyacrylamide-based solid-phase reductants that could be easily separated from the
lysate through centrifugation. These modifications, collectively called *resin-assisted
reduction and capture* (RARC), reduced the time needed to perform the RAC method
from 2-3 days to 4-5 hours, while the overall quality and quantity of previously-oxidized
cysteines captured was increased.

In order to demonstrate the RARC method's utility in studying complex cellular
oxidants, the optimized methodology was used to study cysteine oxidation caused by the
redox-active metals arsenic, cadmium, and chromium. As(III), Cr(VI), and Cd(II) were
all found to increase cysteine oxidation significantly, with As(III) and Cd(II) inducing
more oxidation than Cr(VI) following a 24-hour exposure to cytotoxic concentrations.
Label-free proteomic analysis and western blotting of RARC-isolated oxidized proteins
found a high degree of commonality between the proteins oxidized by these metals, with
cytoskeletal, translational, stress response, and metabolic proteins all being oxidized.
Several previously-unreported redox-active cysteines were also identified.

These results indicate that cysteine oxidation by As(III), Cr(VI), and Cd(II) may
play a significant role in these metals' cytotoxicity and demonstrates the utility of the

RARC method as a strategy for studying reversible cysteine oxidation by oxidants in oxidative signaling and disease. The RARC method is a simplification and improvement upon the current state of the art which decreases the barrier of entry to studying cysteine oxidation, allowing more researchers to study this modification. We predict that the RARC methodology will be critical in expanding our understanding of reactive cysteines in cellular function and disease.

KEYWORDS: Resin-Assisted Capture, Reversible Cysteine Oxidation, Immobilized Reductants, Cysteine Redox Proteomics, Heavy Metals

John Andrew Hitron

8-24-2018
Date

AN OPTIMIZED SOLID-PHASE REDUCTION AND CAPTURE STRATEGY FOR
THE STUDY OF REVERSIBLY-OXIDIZED CYSTEINES AND ITS APPLICATION
TO METAL TOXICITY

By

John Andrew Hitron

Xianglin Shi
Director of Dissertation

Isabel Mellon
Director of Graduate Studies

8-24-2018
Date

To my Mom, Dad, and Emily. Thank you for believing in me.

ACKNOWLEDGEMENTS

TABLE OF CONTENTS

LIST OF TABLES

LIST OF FIGURES

Chapter 1 : INTRODUCTION

Reactive oxygen and nitrogen species are both a natural byproduct of cellular aerobic processes and toxic compounds that are implicit in cellular disease, carcinogenesis, and aging. While the role of ROS and RNS in cellular signaling and disease has been well-documented, there is still significant debate as to what the initial targets for these species are upstream of any cellular signaling cascades. There has been mounting evidence that protein thiols may be the link between ROS and RNS and cellular signaling cascades.

However, the role of cysteines in ROS- and RNS-mediated signaling and disease is still poorly understood. This is no accident, as cysteine oxidative status is difficult to interrogate experimentally both *in vitro* and *in vivo*. Unlike phosphorylation, which is relatively stable post-lysis barring phosphatase activity, the simple act of lysis can introduce significant artefactual cysteine oxidation due to our oxidizing atmosphere.

Despite these hurdles, several techniques have been developed to study cysteine oxidation. These techniques are for the most part cumbersome and tedious, typically taking multiple days and requiring several precipitation and/or purification techniques. By requiring so many steps and sample handling, the risk of sample loss, modification loss, and contamination is greatly enhanced. Additionally the long workup time and many steps involved relegates cysteine oxidation experiments towards the esoteric since they require both a significant devotion of time as well as significant researcher experience.

With that in mind, it was our goal to streamline the experimental workflow to address these issues, and then utilize these streamlined methods to study cysteine oxidative modifications induced by environmental and occupational metal toxins. By decreasing the amount of handling and precipitation steps, the overall ease in studying cysteine oxidative modifications would be increased, pushing this post-translational modification into the experimental mainstream.

Cysteine is one of the least common amino acids in the human proteome, comprising only an estimated 1.7% of the amino acid composition. However the rate of cysteine incorporated into the proteome has increased over evolutionary history, coinciding both with a transition from a reducing to oxidizing environment as well as an increase in organismal complexity [1, 2]. This increase in cysteine incorporation over the course of evolution indicates the importance of cysteine for complex cellular functions. Cellular cysteines play significant roles in protein structure and function. They provide covalent inter- and intrachain linkages, act as catalytic centers for cellular enzymes, and act as cellular antioxidants to prevent cellular oxidative damage.

There has been an increased interest recently in examining the role of cysteine in cellular signaling networks. Since the sulfhydryl in cysteine can undergo reversible redox *in vivo*, protein cysteines may act as cellular switches. Under oxidative stress a switch cysteine would oxidize, altering protein structure or activity to induce a signaling cascade; cellular antioxidants could then reduce the cysteine to "turn off" the signaling cascade.

Protein Thiol Oxidation

Characteristics of Cysteine

Cysteine, chemical formula $C_3H_7NO_2S$, is a non-essential amino acid. Cysteine and methionine are the two sulfur-containing amino acids in the human proteome, with cysteine having a non-substituted thiol (-SH) in its side chain.

Sulfur has several characteristics that make it particularly useful. Due to its lower electronegativity, it is a better nucleophile than oxygen. Sulfur's electron configuration of $1s^2,2s^2,2p^6,3s^2,3p^4$ allows for 8 oxidation states (+2,+1,-1,-2,-3,-4,-5,-6) compared to oxygen's four (2,1,-1,-2). This increase in oxidation states allows for a wider range of reduction-oxidation reactions as well as an increase in binding partners for a sulfur center.

The sulfur in cysteine is a thiol (RSH, S(II)) [3]. While is similar in most respects to a hydroxyl group, thiols generally act as better nucleophiles under cellular conditions. Therefore this allows for the cysteines to bind more, and more readily to, cellular targets. Additionally, due to its decreased electronegativity it is easier to reduce the cysteine thiol than a hydroxyl, such that cellular cysteines can readily undergo both oxidation *and* reduction under cellular conditions.

While other amino acids can be oxidized *in vivo*, only the two sulfur-containing amino acids cysteine and methionine are readily reduced. In the case of cysteine, this reversibility allows for cysteine to be act as a redox center for enzymatic catalysis, a target for cellular oxidants, and a malleable component of protein structure.

The propensity for the cysteine thiol to be oxidized is dependent upon pH. Cysteine is oxidized only in its thiolate state. As discussed below, the thiol pKa is ~8.5; therefore at physiological conditions cysteine would exist primarily as a protonated thiol and be incapable of undergoing redox. How, then, can cysteine exist as a thiolate under physiological conditions?

The influence of nearby groups on thiol pKa has been clearly demonstrated through multiple studies, as summarized in Table 1.1. The presence of positively-charged groups in close proximity to the thiol will reduce the pKa, while the presence of negatively-charged groups will generally increase the pKa. As seen in Table 1.1, the substitution of an alcohol group in β-mercaptoethanol to an amine group in β-mercaptoethylamine decreases the thiol pKa from 9.72 to 8.35. Thiol pKa increases as the distance between the thiol and an amine increases, as seen in the series from 2-diethylaminoethanethiol to 2-diethylaminohexanethiol [4].

Cysteine contains three dissociable protons (those of the carboxylic acid, thiol, and ammonium), which would give three separate pKas. While the pKa of the carboxyl group can be clearly identified, the pKas of the thiol and ammonium groups overlap and, as mentioned above, affect each other greatly. Therefore determining the pKa of the cysteine side chain thiol has been the subject of many studies. Through using spectrophotometric measurements Benesch and Benesch measured the cysteine thiol pKa as 8.53 [5]. Thurlkill et al. used potentiometric titration on peptide hexamers consisting of Ala-Ala-Cys-Ala-Ala-Ala to arrive at a thiol pKa of 8.55 [6].

Table 1.1. The experimentally-determined pK_{SH} of simple and physiological thiol-containing compounds.

Chemical Name	Chemical Formula	pK_{SH}	Reference
Ethanethiol	C_2H_5-SH	10.61	
β-mercaptoethanol	HO-C_2H_4-SH	9.72	
β-mercaptoethylamine	H_2N-C_2H_4-SH	8.35	
2-diethylaminoethanethiol	$(C_2H_5)_2$-N-C_2H_4SH	7.8	[4]
2-diethylaminopropanethiol	$(C_2H_5)_2$-N-C_3H_6SH	8.0	[4]
2-diethylaminobutanethiol	$(C_2H_5)_2$-N-C_4H_8SH	10.10	[4]
2-diethylaminohexanethiol	$(C_2H_5)_2$-N-C_6H_{12}SH	10.10	[4]
l-cysteine	$HO_2CCH(NH_2)$-CH_2SH	8.53	[5]
Glutathione	Glu-Cys-Gly	9.20	

The influence of neighboring charged groups on cysteine thiol pKa means that protein cysteines may have measurable pKas that are far different than that of free cysteine. Positively charged groups from adjacent or proximate amino acids such as arginine, histidine, and lysine could significantly shift the thiol pKa; furthermore the burying of cysteines within a protein may lead to a dehydration of the area surrounding the thiol, leading to a far different dielectric constant. These different variables allow for large variability in reported protein cysteine values, ranging from 2.5 – 11.1, with a mean protein cysteine pKa of 6.8 ± 2.7 [7].

At a physiological pH of 7.4, free cysteine will be primarily in the protonated thiol (-SH) state; however a significant portion of cysteines will be in an unprotonated thiolate (-S⁻) state due both to the pK_{SH} as well as conformationally-induced pK shifts. This is in sharp contrast to the cellular antioxidant tripeptide glutathione, which has a pKa of 9.2. As thiolates are nucleophilic and readily undergo redox reactions, cysteines will be oxidized more readily and at a faster rate than glutathione under physiological

conditions [8]. Glutathione is present intracellular at millimolar concentrations, making

it the predominant cellular thiol and a significant cellular antioxidant [9]. However the

greater reactivity of cysteines towards oxidants, coupled with the critical roles that

cysteines play in protein structure and activity means that cysteine oxidation could act as

an early sensor of oxidative stress, affecting protein structure and function and mediating

downstream signaling.

Therefore it is important to understand the different forms of oxidized cysteine

that may be encountered in the cell, as well as their characteristics. Cysteine oxidation

products can generally be categorized as *reversible* or *irreversible*, based upon the ease

with which the oxidation product can be reduced back to a thiol under physiological

conditions.

Cysteine Modifications by Radical Species

Oxidative Modifications

Cysteine oxidative products are those that are generated by the radical attack of

reactive oxygen species (ROS) on cysteine thiols. These oxidative products have been

classically organized into two groups: *reversible* and *irreversible*. The reversible

oxidative products are those that were perceived to be easily reversed under physiological

conditions through a reduction-oxidation reaction by cellular antioxidants, such as

glutathione, and antioxidant proteins, such as thioredoxin and peroxiredoxin. The

irreversible oxidative products were perceived to be biologically irreversible, although it

is now understood that some modifications that were considered to be irreversible are in

fact reversible *in vivo* under certain conditions [10, 11].

Irreversible cysteine oxidation. Irreversible cysteine oxidation to a sulfinic acid ($-SO_2H$) or sulfonic acid ($-SO_3H$) may result in inactivation of protein function. For instance, hyperoxidation of the active-site cysteine of GAPDH to a sulfinic acid leads to an irreversible inactivation of enzymatic function [12, 13]. Likewise oxidant-mediated active-site selenocysteine hyperoxidation of glutathione peroxidase 1 (GPX) [14, 15] and active-site cysteine hyperoxidation of superoxide dismutase 1 (SOD1) and catalase [16] cause irreversible inactivation of key cellular antioxidant enzymes. While sulfiredoxin is capable of reducing cysteine sulfinic acids to thiols, its substrate specificity of 2-Cys peroxiredoxins [10] means that cysteine and selenocysteine hyperoxidation of these enzymes is physiologically irreversible.

However not all hyperoxidized proteins are necessarily inactivated by cysteine sulfinic and sulfonic acids. An excellent example of hyperoxidation-mediated protein function is the cellular redox sensor DJ-1/PARK7. DJ-1/PARK7 is a multifunctional protein which contains three cysteines: Cys46, Cys53, and Cys106. Under oxidative stress Cys106 is irreversibly hyperoxidized to a sulfinic acid, leading to conformational changes and causing subcellular redistribution to the mitochondria [17] and nucleus. Hyperoxidized DJ-1/PARK7 acts as a pro-survival agent within cells undergoing oxidative stress, inhibiting apoptosis signaling kinase 1 activation by preventing ASK1-Daxx interaction [18] and Trx1-ASK1 complex dissolution [19]. Hyperoxidized DJ-1/PARK7 also inhibits apoptotic MEKK1-SEK1-JNK1 signaling [20], inhibits PTEN dephosphorylation of Akt/PKB [21], sequesters p53 from transcriptional activation [22], and increases antiapoptotic ERK1/2 signaling [22]. These activities, all triggered by DJ-

1/PARK7 C106 sulfinylation, delay cellular apoptosis under oxidative stress to allow time for antioxidant recovery.

Reversible cysteine oxidation and sulfenic acids. Reversible oxidative modifications include sulfenic acids (-SOH), disulfides (-SS-), and nitrosothiols (-SNO). Sulfenic acids are considered to be unstable intermediate oxidative products and generally will rapidly oxidize further to disulfides [23], sulfenamides [24], or sulfinic and sulfonic acids; this is due to the abstraction of oxygen by the electronegative oxygen to give a highly electrophilic sulfur which can undergo further nucleophilic attack.

However some proteins have been demonstrated to form stable sulfenic acids through conformational restriction of further oxidation [25]. Oxidoreductase enzymes, such as NADH peroxidase and NADH oxidase, utilize a stabilized sulfenic acid in their catalytic centers. Additionally stabilized sulfenic acids have been shown to form a rapid redox switch for cell signaling in transcription factors, antioxidant proteins, and cell survival and apoptotic proteins (reviewed in [26]).

Sulfenic acids play a significant role in cellular response to oxidative stress. The active-site cysteine Cys152 in glyceraldehyde-3-phosphate dehydrogenase is reversibly-oxidized to a sulfenic acid when exposed to nitric oxide generators such as sodium nitroprusside [27], leading to an inhibition of glycolysis and redirection of glyceraldehyde-3-phosphate towards the pentose phosphate pathway to generate NADPH for antioxidant response [28]. Cysteine sulfenic acid oxidation on the antiapoptotic protein Bcl-2 by hydrogen peroxide prevents its interaction with and suppression of apoptotic ERK1/2 signaling [29].

Disulfides. A disulfide is a thioether formed either between two cysteines (Cys-S-S-Cys) in the case of a cysteine disulfides, or between a cysteine and a non-cysteine thiol species (ex. Cys-S-S-Glutathione) in the case of mixed disulfides. Cysteine disulfides are a crucial structural element of proteins, contributing to secondary, tertiary, and quaternary structure [30]. Disulfides are a key non-primary structural motif due to the energetic favorability of disulfide formation. Under oxidizing physiological conditions cysteines will readily undergo oxidation to form disulfides [31], although disulfide formation is *in vivo* is catalyzed and error-corrected in the endoplasmic reticulum by the oxidorectase protein disulfide isomerases [32, 33].

While protein cysteines will form disulfides spontaneously, incorrect and disulfide formation can cause severe perturbations to protein structure and cell function. Protein disulfide misfolding caused by protein disulfide isomerase disruption results in ER stress and has been linked to apoptosis [34], neurodegeneration [35], and diabetes [36].

In addition to structural elements and protein folding, disulfides have been shown to act as redox sensors. Cysteine-cysteine disulfides and mixed glutathione-cysteine disulfides regulate Nrf2 stabilization ([37]), phosphatase and kinase activity, proteosomal function, and apoptosis (reviewed in [38]). Beyond their role in unfolded protein response, PDIs have been proposed to be key oxidative stress regulatory hubs through disulfide formation, driving a variety of signaling cascades [39].

Nitrosothiols. Reactive nitrogen species such as nitric oxide can induce the formation of cysteine-S-nitrosothiols (Cys-SNO). Nitric oxide is generated endogenously by the

constitutively-expressed family of nitric oxide synthases (NOSs), including eNOS, iNOS, and nNOS.

As with the other reversible oxidative products discussed previously, S-nitrosylation of cysteines has been shown to regulate protein cell signaling cascades. Cardiovascular regulation of vasodilation by nitric oxide is driven by S-nitrosylation [40]. Nitric oxide has also been linked to inflammation [41], UPR signaling, diabetes [42], neurodegeneration [43], antiapoptotic signaling [44], autophagic resistance [45], and inhibition of cellular kinases [42].

Methods for Detecting Cysteine Oxidation

Given the widespread impact of cysteine oxidative adducts on both homeostasis and cellular pathology, the presence of cysteine oxidative modifications and their contribution to protein structure and function has been a topic of research for the past century. While early studies focused on the relationship between cysteine and cysteine, as well as cysteine's role in urinary calculi, by the 1960s researchers had identified that cysteine played a significant role in protein stability and structure.

Early studies into cysteine oxidation states relied upon several methods. These methods included X-ray crystallography [46], amino acid analysis, nonreducing/reducing diagonal gel electrophoresis [47], and protein mass-shifts induced by cysteine alkylation by high-molecular weight alkylating reagents [48]. While these methods used different approaches and arrived at different endpoints for their analyses, they were collectively slow, laborious, and were inefficient as methods to discover previously unidentified reversibly-oxidized cysteines.

In 2001 Jaffrey et al. first described the basic framework of the biotin-switch assay (BSA) [49]. The BSA used ascorbate to reduce nitrosothiols, leaving all other oxidative cellular modifications unperturbed. In the BSA cellular thiols are blocked using the methyl methanethiosulfonate (MMTS), after which excess MMTS is removed, nitrosothiols are reduced with ascorbate, and the newly-reduced thiols are biotinylated using biotin-HPDP.

The development of the biotin-switch assay was a significant advancement in the field of cysteine redox signaling. Since the endpoint for the BSA was biotinylation of nitrosothiols, it allowed the enrichment and study of the nitrosothiol-containing fraction of the proteome. The BSA was not without its drawbacks, however. Ascorbate has been shown to be capable of reducing some cellular disulfides, reducing the overall specificity of the BSA [50, 51]; furthermore the biotinylation endpoint adds undue complexity to the assay since it requires the removal of excess biotinylation prior to streptavidin pulldown.

In the decades following the first description of the BSA, researchers have developed modifications and improvements of the BSA to alleviate these issues and broaden its applicability. Leichert and Jakob introduced a disulfide quench step consisting of direct lysis of samples in 10% trichloroacetic acid (TCA) prior to alkylation. The rapid decrease in pH and protein denaturation caused by the TCA was presumed to eliminate disulfide exchange, freezing the cellular thiol status [52]. The alkylation reagent used has changed from the haloalkanes iodoacetate (IAA) and iodoacetamide (IAM) to N-ethylmaleimide (NEM), which has the advantage of faster cysteine alkylation at neutral and slightly acidic pH (pH 6.5-7.5). Reduction methods were expanded to probe for all manner of cysteine oxidation products, including protein disulfides. Finally,

the most fundamental change in the BSA technique has been the transition away from biotin itself towards resin-assisted capture (RAC).

In RAC the biotin-streptavidin capture is replaced by substituting an activated-disulfide thiopyridine resin [53]. Following alkylation and reduction, the newly-reduced cysteines are bound covalently to the solid-phase resin through mixed disulfide bonds. The benefits of RAC are threefold. Using RAC instead of biotin-streptavidin pulldown eliminates the need to remove any excess biotin from the sample. Furthermore, since the capture is through a covalent bond the reaction can occur under highly denaturing conditions, and more stringent wash conditions can be used to eliminate any non-specific interactions. Finally, since the cysteine is bound to the resin through a disulfide bond the protein can be gently eluted by the addition of a reducing agent.
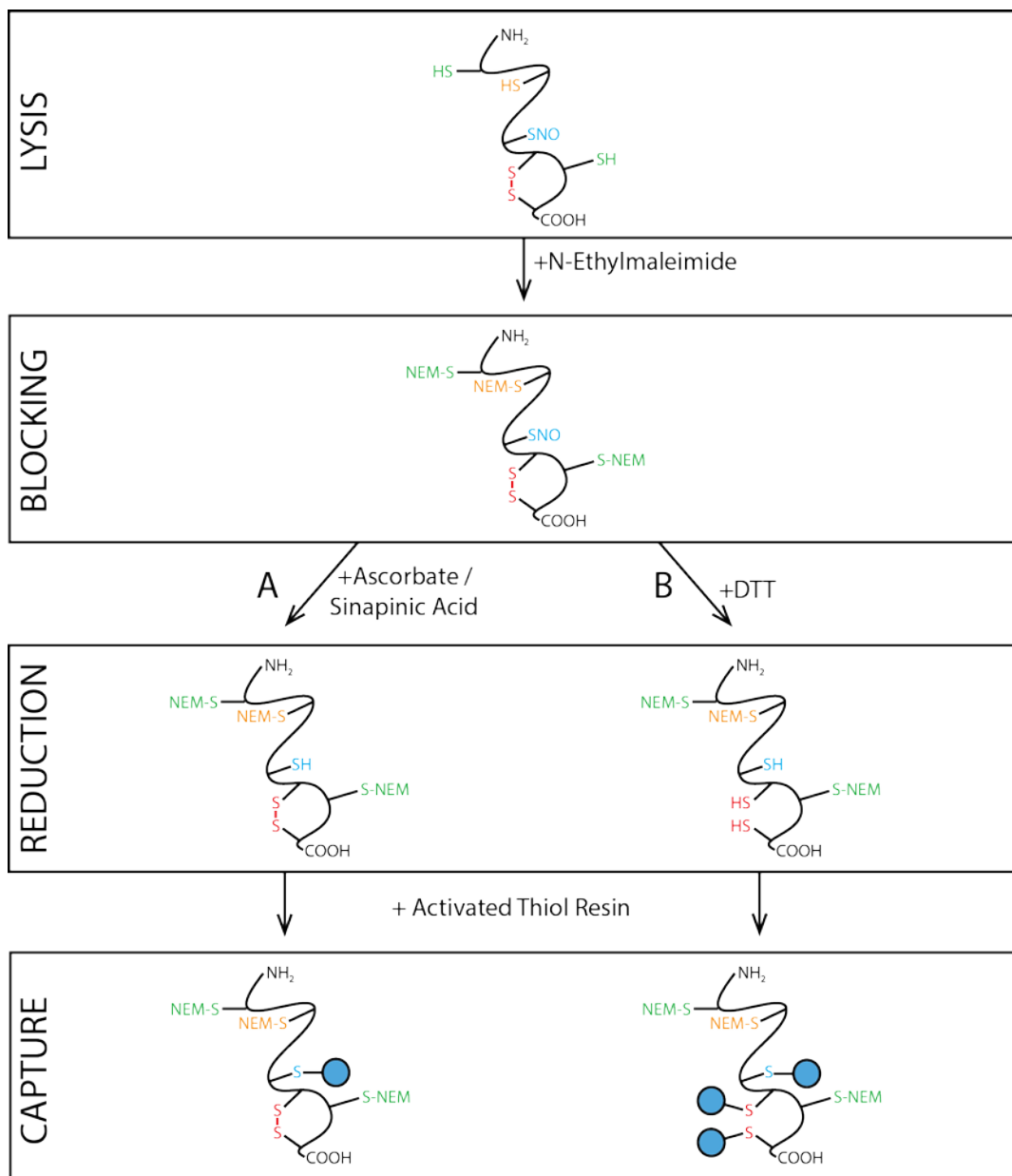
Figure 1.1. The resin-assisted capture (RAC) methodology. Cells are lysed in the presence of cysteine alkylating reagents such as N-ethylmaleimide (NEM), which alkylate reduced cysteine thiols, blocking them from being captured by activated thiol resins. Reversibly-oxidized cysteines, including cysteine s-nitrosothiols and disulfides, are then reduced by reducing agents. The newly-reduced cysteines then form mixed disulfides with an activated thiol resin, which allows the proteins containing previously-oxidized cysteines to be captured and separated from non-oxidized proteins. Captured proteins can be eluted from the resin with the simple addition of a cysteine reductant such as dithiothreitol (DTT) or tris(carboxylethy)phosphine (TCEP).

13

As a technique, RAC is dependent upon the reductant used to determine what kind of cysteine oxidative adducts it captures (Fig. 1). The use of ascorbic or sinapinic [54, 55] acids will result in the reduction and capture of S-nitrosothiols, while using sodium arsenite will lead to the reduction and capture of sulfenic acids. The use of a nonspecific thiol reductant like dithiothreitol (DTT) will reduce and capture all reversible cysteine oxidative adducts present.

Unfortunately using RAC for studying total protein oxidation comes with significant drawbacks. Since the reduction of nitrosothiols and sulfenic acids is specific for those species, reduction and capture can occur at the same time. However since the dithiopyridyl capture resin is based on an activated disulfide, any attempt to reduce cellular disulfides at the same time as capture would result in at best the immediate cleavage of any newly-formed mixed disulfides, and at worst would neutralize the capturing resin entirely. Therefore total protein oxidation studies require a two-step reduction and capture, wherein the proteins are reduced with DTT, after which the excess reductant must be removed by precipitation, ultrafiltration, or dialysis prior to capture.

The necessary removal of the reductant prior to capture limits the throughput of the RAC when it comes to studying total protein oxidation. As it stands this method requires, from start to finish, at least two days to finish using chloroform-methanol precipitation; using the more quantitative acetone precipitation would require at least three days to prepare a sample for capture and analysis. Additionally each step requires significant user manipulation, risking sample contamination and/or loss.

Tangible improvements have been made in streamlining methodology for nitrosothiol RAC through thiosulfonate switching [56, 57]. However very little advancement has been done on its sister technique in this regard. An alternative approach to total protein oxidation RAC was developed by the Cross group [58] which eliminated the precipitation step between alkylation and reduction in order to reduce the time needed to perform the RAC technique. However this method has not been adopted by the wider community, nor has it been compared to the classical RAC method in order to determine whether its modifications have conferred tangible improvements to the technique beyond processing time reduction.

We therefore saw an opportunity to reevaluate total protein oxidation RAC and improve upon it. Using the iterative improvements to date as a starting point, our goal was to reduce the time needed to process samples with the RAC technique to one that could be performed in a single workday, with a reduced need for precipitation and handling. It was intended that optimization of the RAC technique would allow for lower sample variability and error, higher throughput, increased ease of use, and the potential of automation. These benefits would decrease the barrier to entry for researchers interested in using RAC to study cysteine oxidation, increasing the body of knowledge surrounding cysteine oxidative signaling and redox modifications.

Chapter 2 : OPTIMIZATION OF INCUBATION CONDITIONS FOR RESIN-ASSISTED CAPTURE OF TOTAL OXIDIZED CYSTEINES.

Background

There are two distinct workflows used for resin-assisted capture of reversibly-oxidized cysteines: the Purification of Reversibly-Oxidized Proteins (PROP) method [58] and the Oxidized Resin-Assisted Capture (Ox-RAC) method [59, 60]. Both of these techniques follow the same basic structure, alkylation-reduction-capture, but they differ in a few key respects. The Ox-RAC technique adheres closely to the BSA workflow; it uses an SDS-based lysis buffer, either NEM or IAM as an alkylating reagent, and most importantly uses a two-step alkylation/reduction where the alkylating reagent is first removed from the lysate by organic precipitation and washing, then the lysate is resuspended in reducing buffer.

The PROP technique differs from the Ox-RAC technique in that it uses a guanidine-based lysis buffer, specifically identifies NEM as the preferred alkylating reagent, and uses a one-step alkylation/reduction buffer where following alkylation an overwhelming amount of DTT is added to the lysate to both quench the NEM and reduce cysteines. The benefit of the PROP workflow is that by removing one precipitation/wash step, sample loss is reduced and the procedure is shortened by one day.

Given the variations between the two methods, it was important that these differences were compared to determine the optimal conditions for analysis. Additionally it highlighted several areas in which the Ox-RAC method could be improved upon to decrease handling steps, sample loss, and method time. While these improvements

would naturally make the method shorter, it would also reduce or eliminate the use of hazardous organic solvents, decrease sample variability, and make the method more user-friendly.

Therefore we identified the key differences between the two methods and compared them. These variables included the inclusion of an acid-quenching step, the denaturant and alkylating reagent used, and using either a one- or two-step alkylation/reduction. We then altered the method further by using solid-phase reducing resins to eliminate the need for precipitation and buffer exchange.

Materials and Methods

Materials. The immortalized human bronchial epithelial cell line BEAS-2B was purchased from American Type Culture Collection (ATCC CRL-9609). Cell culture medium (Gibco DMEM+GlutaMAX, Gibco 10569), HBSS pH 7.4 (Gibco 14025), PBS pH 7.4 (Gibco 10010), trichloroacetic acid (Fisher BP555, Lot# 165234), 5,5'-dithiobis-(2-nitrobenzoic acid) (Thermo Scientific 22582, Lot# OG189149A), and screw cap microcentrifuge spin columns (Pierce 69705) were purchased from Thermo Fisher Scientific (Waltham, MA). Sepharose 6B (Aldrich 6B100, Lot# MKCG3369), sodium borohydride (Aldrich 452882 Lot# SHBF1327V), ethyl 3-benzoylacrylate (Aldrich 260614, Lot# STDB7349V), ethyl vinyl sulfone (Aldrich 282839, Lot# MKCB3364V), phenyl vinyl sulfone (Aldrich 241717, Lot# 0001451652), methyl propiolate (Aldrich 171859, Lot# BCBT5514), ethyl propiolate (Aldrich E46607, Lot# STBG4123V), 3-phenyl 2-propynenitrile (Aldrich 672645), methyl sulfonylbenzothiazole (Enamine

ENA069848532), and 1-(2-aminoethyl)maleimide (Aldrich 809322) were purchased

from Millipore Sigma (St. Louis, MO). Epichlorohydrin (Alfa Aesar A15823, Lot#

Y13B038), sodium thiosulfate (Alfa Aesar A17629 Lot# 10205369), N-ethylmaleimide

(Alfa Aesar 40526, Lot#P290042), acrylamide (Alfa Aesar J62100 Lot# P17C510),

methyl acrylate (TCI FII01-RPGO), iodoacetamide (Amresco M216 Lot# 1835C142), 2-

mercaptoethylamine hydrochloride (Alfa Aesar A14377, Lot# 10173644), dithiothreitol

(VWR 97061), and all other ancillary materials and consumables were purchased from

VWR (Radnor, PA).

Cell Culture. The human bronchial epithelial cell line BEAS-2B was grown at 37° C in a

humidified incubator with a 5% CO2 atmosphere in DMEM+GlutaMAX, 10% FBS, 1%

penicillin-streptomycin. BEAS-2B was subcultured prior to confluence and plated at a

density of 3,000-5,000 cells/cm^2. Following plating, the cells were grown to ~65-80%

confluence for treatment, and only passages 60-90 were used for experiments.

Synthesis of Epoxide Resins

Epoxide Resin. Epoxide resin was synthesized as described by Axen et al. [61] using the

modifications provided by Matsumoto et al. [62] Sepharose or sephadex resin was

washed free from its storage buffer using deionized water under vacuum on a fritted glass

filter, then allowed to dry under vacuum until no more water passed through the filter. 2g

of the washed resin was added to 3 ml of 56% DMSO in deionized water, to which 1.3 ml

of 2M sodium hydroxide and 0.3 ml of epichlorohydrin were added in order. The

suspension was incubated at 40°C for 2 hours with mixing, after which the resin was

washed with 50 ml of deionized water. The epoxide resin was not stable enough to store long-term, so subsequent reactions were conducted immediately.

S-Alkyl-Thiosulfate Resin. 2g of epoxide resin was washed with 0.5M sodium phosphate buffer, pH 6.3. It was then resuspended in 4 ml of the same buffer, to which 2 ml of 2M sodium thiosulfate was added. The suspension was incubated for 6 hours at RT with end-over-end mixing. The resin was then washed with deionized water and resuspended in phosphate buffered saline. The resin was stored at 4° C in 20% ethanol/PBS.

Thiol Resin. 2g of S-alkyl-thiosulfate resin was washed with deionized water followed by methanol and allowed to dry on a fritted glass filter. The resin was then resuspended in 10 ml of methanol in a peptide synthesis vessel. 700 mg of sodium borohydride (20 mmol) was added to the suspension, and nitrogen was bubbled through the vessel. The suspension was incubated for 1 hour at RT. The resin was then dried under vacuum and washed with 50 ml of 0.1M acetic acid to neutralize any remaining borohydride. The resin was stored short-term in 0.1M acetic acid at 4° C.

Thiopropyl Resin. 2g of thiol resin was washed with 60% acetone/40% 0.05M sodium bicarbonate/1 mM EDTA. It was then resuspended in 5 ml of the same solvent, to which 0.3M of 2,2'-dipyridyl disulfide in the same solvent was added. The suspension was incubated for 1 hour at RT in the dark with end-over-end mixing. The resin was washed with 60% acetone, followed by 1 mM EDTA in water. The resin was stored in 20% ethanol/PBS in the dark at 4° C or lyophilized [63] for long-term storage.

Cell Lysis. BEAS-2B cells were plated onto 10-cm^2 dishes and grown to 65-80% confluence. Upon reaching the desired % confluency the cell culture medium was

replaced with culture medium containing treatment compounds or vehicle alone. Following treatment exposure the plates were washed 3x with HBSS, the cells were detached from the plate with a cell lifter, collected into 1.5ml tubes, pelleted, and lysed in 400 μl of degassed lysis buffer (20 mM NaHPO$_4$, 1 mM EDTA, 0.1% IGEPAL CA-630, 2% SDS unless otherwise noted). Lysate DNA was sheared by sonicating the samples using 10 30-second cycles in a BioRuptor Pico (Diagenode, Denville, NJ). The supernatant was transferred to a clean tube and either used immediately in downstream assays or flash frozen and stored at -80°C.

Thiol Measurement. Sample thiol content was measured using the 5,5'-dithiobis-(2-nitrobenzoi acid) (DTNB) assay [64, 65]. Thiol-containing samples were solubilized in DTNB assay buffer (100 mM Tris, pH 7.8, 1 mM EDTA), then mixed with DTNB assay buffer containing 10 mM DTNB; for 96-well plates the volume ratio of sample:DTNB was 1:2. The samples were mixed thoroughly and allowed to incubate at RT in the dark for 10 minutes, after which sample absorbance was measured at λ=405 nm on a BioTek EL800 spectrophotometer (BioTek Instruments, Winooski, VT). An internal set of thiol standards consisting of known concentrations of mercaptoethylamine was included in each run to verify accuracy of the measurements.

Trichloroacetic Acid Disulfide Quenching. Pelleted BEAS-2B cells were thoroughly resuspended in 1 ml of 4% trichloroacetic acid (TCA) by pipetting and incubated for 10 minutes at room temperature. Following incubation the proteins were pelleted by centrifugation at 16,000g for 5 minutes. The pellet was washed 1x in 4% TCA, then 3x in cold methanol; the pellet was thoroughly resuspended for each wash by pipetting.

Following the final wash the pellet was allowed to dry briefly to remove residual

methanol, then the pellet was resuspended in degassed lysis buffer.

Prelysis Quenching. Following treatment the cell culture medium was exchanged with

HBSS containing NEM (50 mM unless otherwise noted) and incubated briefly. After

incubation the HBSS + NEM was removed, the plates were washed 3x with HBSS, the

cells were detached from the plate with a cell lifter, collected into 1.5ml tubes, pelleted,

and resuspended in degassed lysis buffer.

Lysate Alkylation and Reduction. BEAS-2B cells were lysed in 400 μl of degassed lysis

buffer containing 20 mM NEM in opaque 2-ml microcentrifuge tubes. The samples were

incubated for 2 hours at RT with gentle end-over-end mixing. The samples were then

precipitated by the addition of 4 volumes (1.6 ml) of prechilled acetone, vortexed, and

precipitated overnight at -20°C. The precipitated protein was collected by centrifugation

at 4,000g for 5 minutes in a 4° C microcentrifuge. The supernatant was removed and the

protein pellet was washed 3x with cold 80% acetone. The samples were then allowed to

dry briefly to remove excess acetone, then resuspended by pipetting in 400 μl of lysis

buffer containing 50 mM DTT. After a one-hour incubation the samples were again

precipitated with cold acetone, allowed to incubate overnight at -20°C, and washed 3x

with cold 80% acetone before resuspension for RAC.

Resin-Assisted Capture. Alkylated and reduced sample pellets were resuspended by

pipetting in 400 μl of capture buffer (20 mM CH_3COONa pH 4.5, 2% SDS, 1 mM

EDTA). Sample concentration was measured by BCA assay [66], and equal

concentrations of lysates were added to microcentrifuge spin columns containing 35 mg

of buffer-equilibrated thipropyl resin. The columns were sealed and the slurry was incubated for one hour at RT with rotation. Following incubation the columns were unsealed, placed into waste collection tubes, and centrifuged at 1,000g for 1 minute to remove all nonbound proteins. The columns were washed with 5 column volumes of capture buffer, 5 column volumes of diH$_2$O, and 1 column volume of Laemmli sample buffer. After the final wash 100 μl of Lammli buffer containing 50 mM DTT was added to the columns, which were sealed and rotated at RT for 30 minutes. The columns were then unsealed, placed in clean 1.5 ml microcentrifuge tubes, and centrifuged at 1,000g to collect the bound fraction.

Gel Electrophoresis and Staining. Equal volumes of sample bound fractions were loaded in adjacent wells of NuPAGE Bis-Tris gels. Equal concentrations of input fractions were loaded to verify equivalent loading of the spin columns between samples. Gels were run in MOPS SDS-PAGE running buffer at 200V. Following electrophoresis the gels were removed from the gel cassettes, cut, and placed directly into fixation solution (10% acetic acid, 50% methanol) and incubated with RT for 15 minutes at RT. The fixation solution was decanted and replaced with staining solution (0.025% Coomassie G-250, 10% acetic acid), and the samples were incubated with rocking for 30 minutes at RT. The staining solution was decanted and the gels were destained with two 30-minute incubations in 10% acetic acid. Following destain the gels were imaged using a ChemiDoc XRS (Bio-Rad, Hercules, CA).

Results and Discussion

Use of Trichloroacetic Acid for Disulfide Quenching

The use of trichloroacetic acid (TCA) as an acid-quench step was first proposed by Leichert and Jakob [52]. By adding a denaturing amount of TCA to intact cells the cells would be lysed, proteins would be denatured, and the free cysteine thiols would be protonated; this would prevent disulfide exchange and giving a cellular "snapshot" of cysteine oxidation status. Therefore TCA quenching has become an integral step in the BSA technique [60].

However the use of TCA quenching has been called into question. Curbo et al. found that diamide, a potent thiol oxidant, was still able to oxidize protein thiols during TCA quenching [67]. Since cysteine oxidation post-lysis during the quench step would be stochastic, this would increase non-specific oxidative "noise" in subsequent steps of the assay.

An additional concern regarding the use of TCA quenching which was of great concern to our research field was the possibility of generating more-reactive metal species during the acid quench. It is well-known that some transition metals, such as chromate, are highly oxidative at low pH. There was a concern that these metals could induce post-lysis oxidation of the samples during TCA quench. We therefore wanted to determine whether acid-quenching in the presence of redox-active metals could cause post-lysis oxidation in a manner similar to that of diamide.

BEAS-2B pellets were lysed in 4% TCA [68] either alone or in the presence of metals (As(III), Cd(II), or Cr(VI)) at concentrations commonly used for *in vitro* experiments for 10 minutes to demonstrate whether these metals were capable of inducing protein cysteine oxidation over a short exposure period at low pH. Fig. 2.1

shows the results of this experiment. While arsenic caused no discernable increase in

cysteine oxidation relative to the control, both cadmium and chromium caused post-lysis

oxidation with Cr(VI)-induced oxidation being much higher than Cd(II)-induced

oxidation (Fig. 2.1A). Cr(VI) is known to be a highly oxidizing agent at low pH, so post-

lysis metal-induced oxidation was not unexpected.
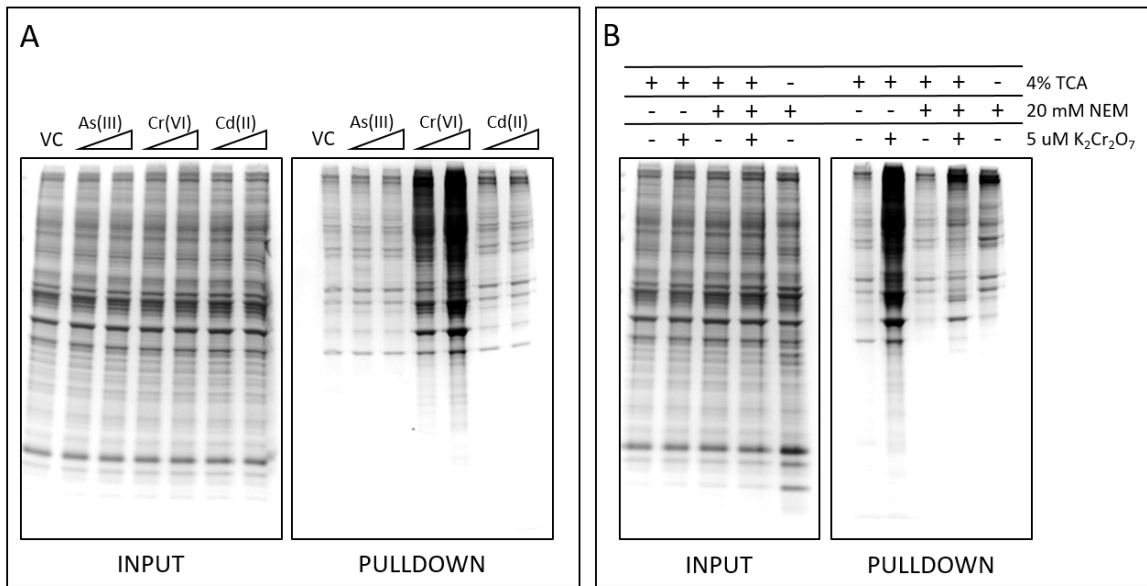
Figure 2.1. TCA disulfide quenching causes postlysis oxidation by reactive metals. BEAS-2B cells were quenched by the addition of trichloroacetic acid (TCA) to starvation medium (DMEM) to a final concentration of 4% TCA. During quenching the cells remained untreated or were treated with $NaAsO_2$, $K_2Cr_2O_7$, or $CdCl_2$ in the acidified medium for 10 minutes. Following quench in the presence acidified metals, cells were collected, washed, and processed for resin-assisted capture (RAC) analysis as described in the Methods. Input fractions are 5 µg of total lysate for each sample. Pulldown fractions are equivalent volumes of resin-assisted capture eluate representing reversibly-oxidized proteins for each sample. (**A**) BEAS-2B cells were treated with 5-10 µM of As^{3+}, Cr^{6+} or Cd^{2+} for 10 minute in the presence of 4% TCA. Equivalent amounts of RAC-processed whole cell lysates as determined by bicinchoninic acid assay were loaded onto thiopropyl-sepharose columns to capture oxidized proteins, washed, and eluted (RAC pulldown). The lanes on the left side of the figure were loaded with 5 µg of RAC-processed whole cell lysate (INPUT), and the lanes on the right side of the figure were loaded with 20 µl of eluate (PULLDOWN) containing only oxidized proteins from each treatment. (**B**) BEAS-2B cells were pretreated with 20 mM N-ethylmaleimide (NEM) (lanes 3-5, 8-10) prior to TCA quenching and treatment with diH_2O vehicle (Lanes 1, 3, 6, 8) or 10 µM Cr(VI) (Lanes 2, 4, 7, 9) for 10 minutes as in part A. Lanes 5 and 10 are

from BEAS-2B cells which were pretreated with NEM but not acid-quenched. Equivalent amounts of RAC-processed whole cell lysates were loaded into thiopropyl-sepharose columns to capture oxidized proteins, washed, and eluted. The lanes on the left side of the figure were loaded with 5 μg of RAC-processed whole cell lysate (INPUT), and the lanes on the right side of the figure were loaded with 20 μl of eluate (PULLDOWN) containing only oxidized proteins from each treatment. The gels were visualized after electrophoresis using Coomassie G-250.

Cysteine oxidation by chromic acid during the TCA quench would only occur in the presence of free, reduced cysteines. We wanted therefore to see whether alkylating free thiols prior to lysis and quench, thereby eliminating the pool of free thiols available for oxidation, would be an effective way to avoid chromic acid post-lysis oxidation. We pretreated BEAS-2B cells with 20 mM N-ethylmaleimide prior to TCA quenching alone or in the presence of Cr(VI) (Fig. 2.1B). Pre-lysis treatment with NEM significantly decreased post-lysis cysteine oxidation by chromic acid, reducing it to nearly that of control.

Pre-Lysis Disulfide Quenching with N-Ethylmaleimide

TCA quenching was originally conceived of as a way to prevent cysteine oxidation and disulfide exchange by the rapid denaturation of proteins in a low-pH solution. Unfortunately as we have shown above, the presence of certain metals in the TCA solution, whether due to metal treatment or as trace contaminants, can induce post-lysis oxidation upon acidification; this effect was greatly reduced by the pretreatment of cells with NEM prior to TCA quenching, since the membrane-permeable NEM would alkylate accessible cysteines *in vitro* prior to lysis, thereby greatly reducing the population of free thiols at risk of post-lysis oxidation.

In addition to using NEM prior to TCA quenching, we also tested NEM treatment without TCA quenching (Fig. 2.1B, Lanes 5 and 10). We found that NEM prelysis treatment reduced post-lysis cysteine oxidation to levels comparable to that obtained by TCA quenching (Fig. 2.1B, Lanes 1 and 6). Due to this we reasoned that NEM prelysis quenching of accessible cysteines could potentially replace TCA disulfide quenching as a viable approach to reducing or eliminating postlysis cysteine oxidation and disulfide exchange. The benefits of eliminating TCA from the workflow would be elimination of a precipitation and resuspension step at the start of the procedure, as well as avoiding the use of a potentially hazardous acid.

This approach has been used in previous studies, although there is a lack of available data regarding both the efficiency of the pre-lysis blocking, as well as the optimization of conditions for the blocking step. Therefore we sought to fill in these blanks to determine whether pre-lysis blocking was a viable alternative to TCA quenching. We blocked BEAS-2B cells prior to lysis by exchanging their culture medium with HBSS containing NEM immediately prior to harvesting. Figure 2.2 shows the results of the blocking experiments.

As can be seen in Fig. 2.2A, significant cysteine blocking was achieved by all concentrations of NEM trialed. A 15-minute incubation with 1 mM NEM at room temperature resulted in a decrease in available free thiol of over half, while increasing NEM concentrations resulted in even further decreases in the free thiol pool. While this loss of free thiol increased with increasing NEM concentration, the alkylation demonstrably slowed as the concentration was increased from 25-100 mM; this is most likely due to the effective alkylation of surface-exposed cysteines, with the remaining

~25% of free thiols representing conformationally buried cysteines which are inaccessible to NEM in the proteins' native configuration.

Given the decreasing cost-benefit ratio of increasing NEM concentration for prelysis quench, we settled on 50 mM NEM as an optimal concentration of NEM to use in prelysis quench to both achieve maximal cysteine alkylation while preventing excessive waste of alkylant.   However we wanted to determine whether incubation time and/or temperature would have a significant effect on prelysis quenching. Therefore we tested altering the incubation time (Fig. 2.2B), as well as altering the incubation temperature (Fig. 2.2C), would lead to increased alkylation with a sub-maximal NEM concentration of 25 mM.

The prelysis quench was essentially finished at 5 minutes, with no substantive increase in alkylation being gained as the incubation was extended out to 30 minutes. A slight but non-significant gain in alkylation occurred when the cells were quenched at 37°C instead of RT. Based on these results the optimal prelysis quench conditions were determined to be incubation with 50 mM NEM for 5 minutes at RT or 37°C, with further time or concentration increases being unnecessary.
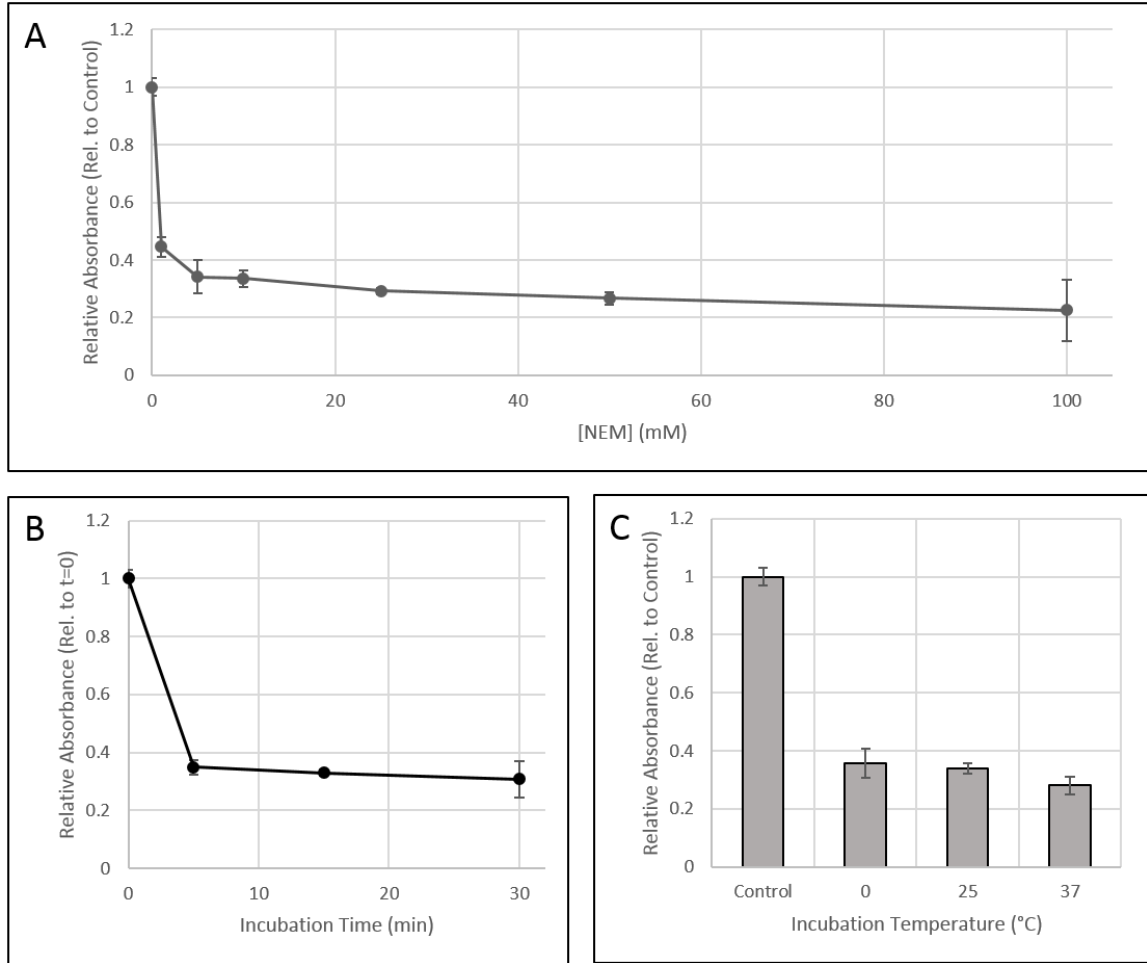
Figure 2.2. N-ethylmaleimide (NEM) incubation of cell pre-lysis causes significant cysteine alkylation. 100 μl of the supernatant was pipetted into 3 replicate wells of a 96-well plate. To these wells 200 μl of 5,5'-dithio-bis-(2-nitrobenzoic acid) (DTNB) assay solution (100 mM NaH_2PO_4 pH 7.8, 1 mM EDTA, 10 mM DTNB) was added. The plates were briefly shaken to mix and allowed to incubate for 10 minutes in the dark prior to reading at λ=405 nm. All DTNB measurements were normalized to cell lysate protein concentrations, determined by BCA assay. (**A**) BEAS-2B cells were incubated for 15 minutes at RT in the dark with increasing concentrations of NEM. (**B**) BEAS-2B cells were incubated with 25 mM NEM at RT in the dark for various incubation times. (**C**) BEAS-2B cells were incubated with 25 mM for 5 minutes in the dark at varying temperatures. HBSS media used was acclimated to the incubation temperature prior to addition to the BEAS-2B culture dish. Bars and data points represent mean ± SD, n=3.

Investigation of Alternative Alkylating Reagents

While maleimides are the most commonly-used class of cysteine alkylants in RAC, they are not without their drawbacks; as Michael acceptors maleimides can undergo a retro-Michael reaction in the presence of a base. This retro-reaction means that maleimide-cysteine adducts are reversible in basic media or in the presence of a competing Michael donor.

Due to this we wanted to investigate alternative cysteine alkylants from alternative classes of cysteine alkylants reported thus far (reviewed in [69]). This includes halo-acetamides, alternative Michael donors, electron-deficient alkynes, and Julia-Kocienski-like reagents. Since the intention of this comparison was to determine whether NEM was the best-available cysteine alkylant, we limited the compounds screened to only those compounds which were commercially-available at high purity (>99%) in reasonable quantity.

We therefore compared the efficacy of NEM to that of the commonly-used halo-acetamide iodoacetamide (IAM), the alkenes acrylamide (AAm) [70, 71], butyl acrylate (BA), methyl acetylacrylate (MAA), ethyl 3-benzoylacrylate [72], ethyl vinyl sulfone (EVS), and phenyl vinyl sulfone (PVS), the alkynes methyl propiolate (MP) [73, 74], ethyl propiolate (EP) [74], and 3-phenyl 2-propynenitrile (PPN) [75], the Julia-Kocienski-like reagent methyl sulfonylbenzothiazole (MSBT) [76], and finally the self-hydrolyzing maleimide 1-(2-aminoethyl)maleimide (NAEM) [77]. While this list of reagents is by no means comprehensive, each compound we tested has been shown to irreversibly alkylate cysteine and has either been proposed or used as an alternative to

NEM alkylation in prior studies, although the quality of alkylation was variable between the reagents used.

We expected some alkylating reagents, such as acrylamide, to be poor alkylating agents in comparison to NEM, since previous studies using acrylamide for cysteine alkylation prior to proteomic analysis used molar concentrations of acrylamide. However we were hopeful that some of the more modern reagents, such as MSBT, PPN, and ethyl 3-benzoylacrylate would prove to be effective replacements for NEM. MSBT [76], PPN [75], and ethyl 3-benzoylacrylate [72] had been shown to be similarly effective as an equivalent concentration of NEM; Both MSBT and PPN had also been demonstrated to generate irreversible alkylation products with cysteine, while ethyl 3-benzoylacrylate alkylated cysteines at a faster rate than NEM but the alkylation product was known to be unstable and slowly decompose. NEM-cysteine alkylation products likewise have been demonstrated to decompose due to NEM's tendency, as with other Michael donors, to undergo anti-Michael additions at basic pH in the presence of competing thiols to regenerate free cysteine thiols [78].

This base-catalyzed reversibility of NEM-cysteine alkylation products was addressed in a prior study by the addition of a basic amino group to maleimide to generate 1-(2-aminoethyl)maleimide (NAEM) [77]. Maleimides can undergo hydrolysis at the imine, resulting in succinimide ring opening and resulting in a non-reactive succinimic acid [79-81]. When this hydrolysis occurs to a maleimide-cysteine alkylation product, it results in a non-reactive thiosuccinimic acid derivative which cannot undergo anti-Michael addition. NAEM showed equivalent conjugation rates as NEM, but

underwent hydrolysis at a much faster rate, resulting in irreversible NAEM-cysteine alkylation products.

Based off the success of these prior studies in developing alternatives to NEM as a cysteine alkylating reagent, we wanted to compare the alkylating reagents directly to determine their relative efficiencies at alkylating a simple monothiol, mercaptoethylamine, at both neutral and mildly acidic pHs; since N-ethylmaleimide has been shown to be an effective and specific cysteine alkylating reagent within the pH range of 6.5-7.5, we examined alkylating reagent efficacies at both pH 6.5 and pH 7.4.

The results of this comparison are shown in Fig. 2.3. With the exception of the maleimides and methyl acetylacrylate, reaction rates were higher for alkylants at pH 7.4 than at pH 6.5; this is to expected as more thiols would be deprotonated at pH 7.4, facilitating nucleophilic attack of the electrophilic alkylants. NEM was by far the fastest thiol alkylant at both pH 7.4 and pH 6.5, with only NAEM and MAA showing similar reactivity. However MAA-thiol adducts showed significant reversibility as the incubation timeframe was extended from 10 minutes to overnight (Fig. 2.3B). Only NEM and the similar maleimide NAEM showed both the rapid reactivity and adduct stability required for RAC. NAEM is more irreversible than NEM due to its self-hydrolysis to maleimic acid. However NAEM is also far more expensive than NEM and not available in bulk quantitites. Therefore for routine RAC analysis NEM would seemingly be the preferable alkylant; however for any experiment which requires long-term processing or storage NAEM could be easily substituted for NEM to avoid any adduct loss.

Given the potential risk for NEM-adduct reversibility at basic pH, conducting the RAC procedure at pH 6.5 instead of pH 7.4 would hopefully eliminate any retro-Michael reactions. Using this pH for the RAC would have benefits beyond just eliminating NEM-adduct reversibility, as previous studies have shown that restricting the reaction pH to below neutral also reduces non-specific NEM alkylation significantly [82]. By changing the pH of the alkylation reaction we can therefore both decrease NEM-adduct loss as well as improve any proteomic results downstream of the RAC technique.
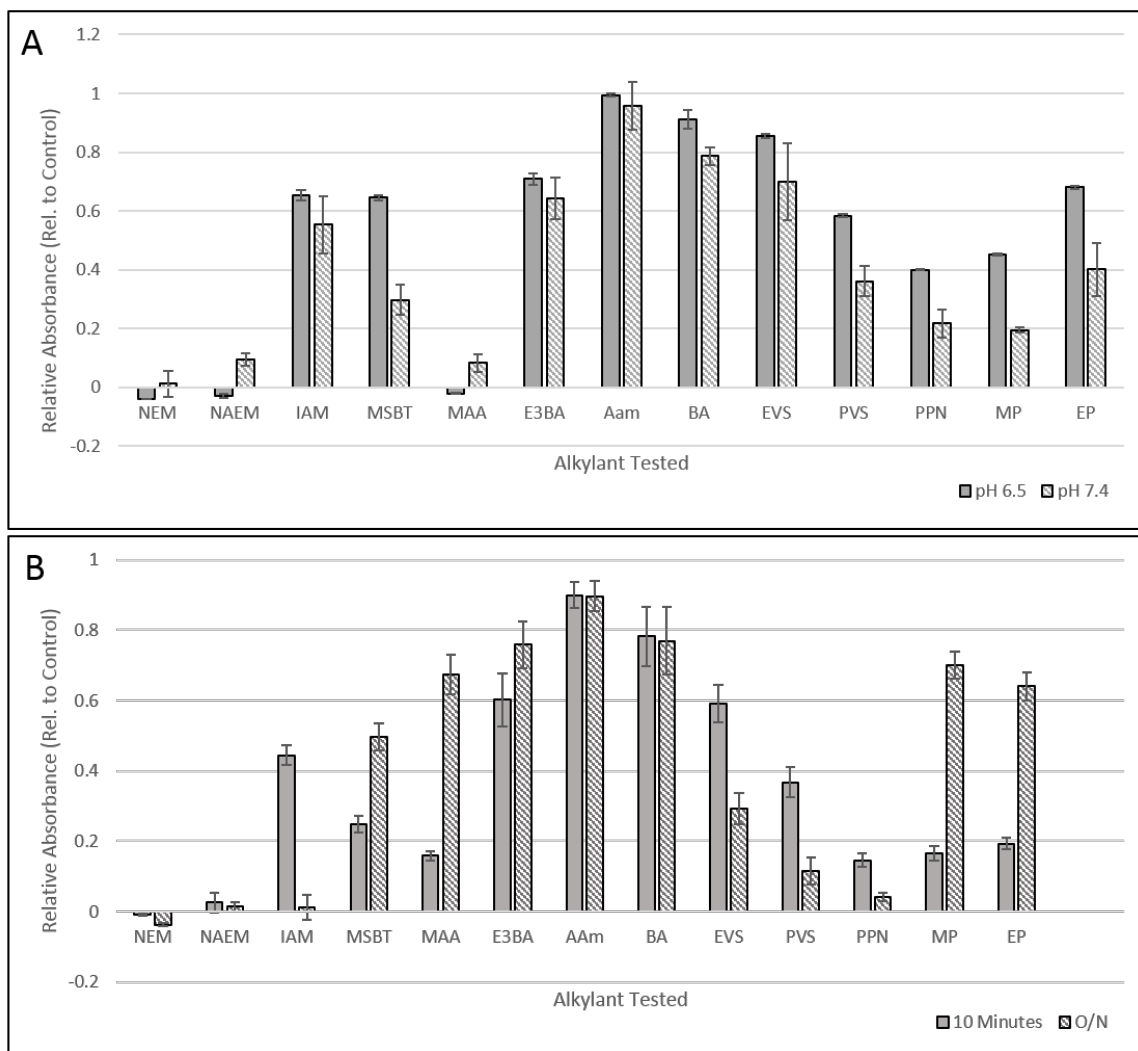
Figure 2.3. Comparison of commercially-available thiol alkylants. (**A**) 100 μl of 1 mM alkylant solution in 20 mM NaHPO$_4$ at either pH 6.5 or 7.4 was added to an equal

volume of 1 mM mercaptoethylamine in triplicate wells of a 96-well plate. The plates were gently shaken for 10 minutes at RT in the dark. Following incubation 200 μl of 5,5'-dithio-nitro-bis-(2-nitrobenzoic acid) (DTNB) assay solution containing 10 mM DTNB was added to each well. The plates were mixed, incubated in the dark at RT for 10 minutes, and absorbance was read at λ = 405 nm. (**B**) Alkylants were incubated with mercaptoethylamine at pH 7.4 as in Fig. 1.7A, but allowed to incubate either for 10 minutes or overnight prior to DTNB addition. Alkylant abbreviations in the figure are NEM: N-ethylmaleimide, NAEM: 1-(2-aminoethyl)maleimide, IAM: iodoacetamide, MSBT: methylsulfonylbenzothiazole, MAA: methyl acetylacrylate, E3BA: ethyl 3-benzoylacrylate, AAm: acrylamide, BA: butyl acrylate, EVS: ethyl vinyl sulfone, PVS: phenyl vinyl sulfone, PPN: 3-phenyl 2-propynenitrile, MP: methyl propiolate, EP: ethylpropiolate. Bars represent mean ± SD, n=3.

Choice of Denaturant for Alkylation

For PROP, its authors argued that using guanidine hydrochloride as the denaturant instead of SDS or urea during lysis facilitated more rapid alkylation by NEM. However guanidine is incompatible with SDS-PAGE and more difficult to remove by organic precipitation. The use of guanidine would not impact the oxidized cysteine fractions captured by RAC since the buffer could be easily exchanged on the columns, but it would impact any loading control used. Since guanidine forms a precipitate with SDS, precipitation or buffer exchange of the loading fractions would be required prior to electrophoresis; this would necessarily alter the sample concentration between the loading control and the actual amount loaded onto the columns, introducing an avoidable source of sample error. For these reasons it was therefore important to see whether the increase in alkylation caused by the denaturant choice was significant enough to necessitate the use of guanidine despite its incompatibility with downstream processes.

The three denaturants guanidine, urea, and sodium dodecyl sulfate (SDS) were compared to determine whether there was a difference in NEM-cysteine alkylation rates

caused by the denaturant used. BEAS-2B cells were lysed in lysis buffers that were identical except for the included denaturant. Denaturant concentrations were chosen based on literature values, settling on 6 M guanidine hydrochloride, 8 M urea, and 2% SDS. At these denaturant concentrations protein denaturation should be rapid, exposing all cysteines and eliminating conformational-dependent alterations in cysteine pKa.

The results of this experiment are summarized in Fig. 2.4A**.** It is clear that denaturant choice has a significant effect upon the cysteine alkylation rate, with guanidine hydrochloride facilitating NEM alkylation far more than either SDS or urea; the alkylation rates were guanidine> urea > SDS. The effect persisted at slightly acidic pH (Fig. 2.4B). These results agree with the findings of Templeton et al. that denaturant choice has an effect on NEM alkylation rate.

However, the above experiment was done in the absence of a prelysis quench step. Since prelysis quenching would alkylate the majority of protein cysteines, the NEM added in the lysis buffer would be more effective due to the increased molar ratio between NEM and the remaining free thiols. Therefore we wanted to see whether prelysis quenching could raise the effectiveness of SDS-denatured samples to that of guanidine-denatured samples, thereby permitting the use of the more-compatible denaturant in lieu of the more-effective one.

As seen in Fig. 2.4C, prelysis quenching of the samples prior to lysis and alkylation increased the alkylation efficiency of all tested denaturants. This is again most likely due to the increased molar ratio of NEM:cysteine in the samples since the only thiols left to alkylate by NEM were those which were conformationally obstructed from

prelysis alkylation. This eliminated the difference in effectiveness between guanidine and SDS, permitting the use of SDS as a lysis buffer for RAC and avoiding any denaturant interference in either cysteine alkylation rate or downstream analysis by SDS-PAGE.
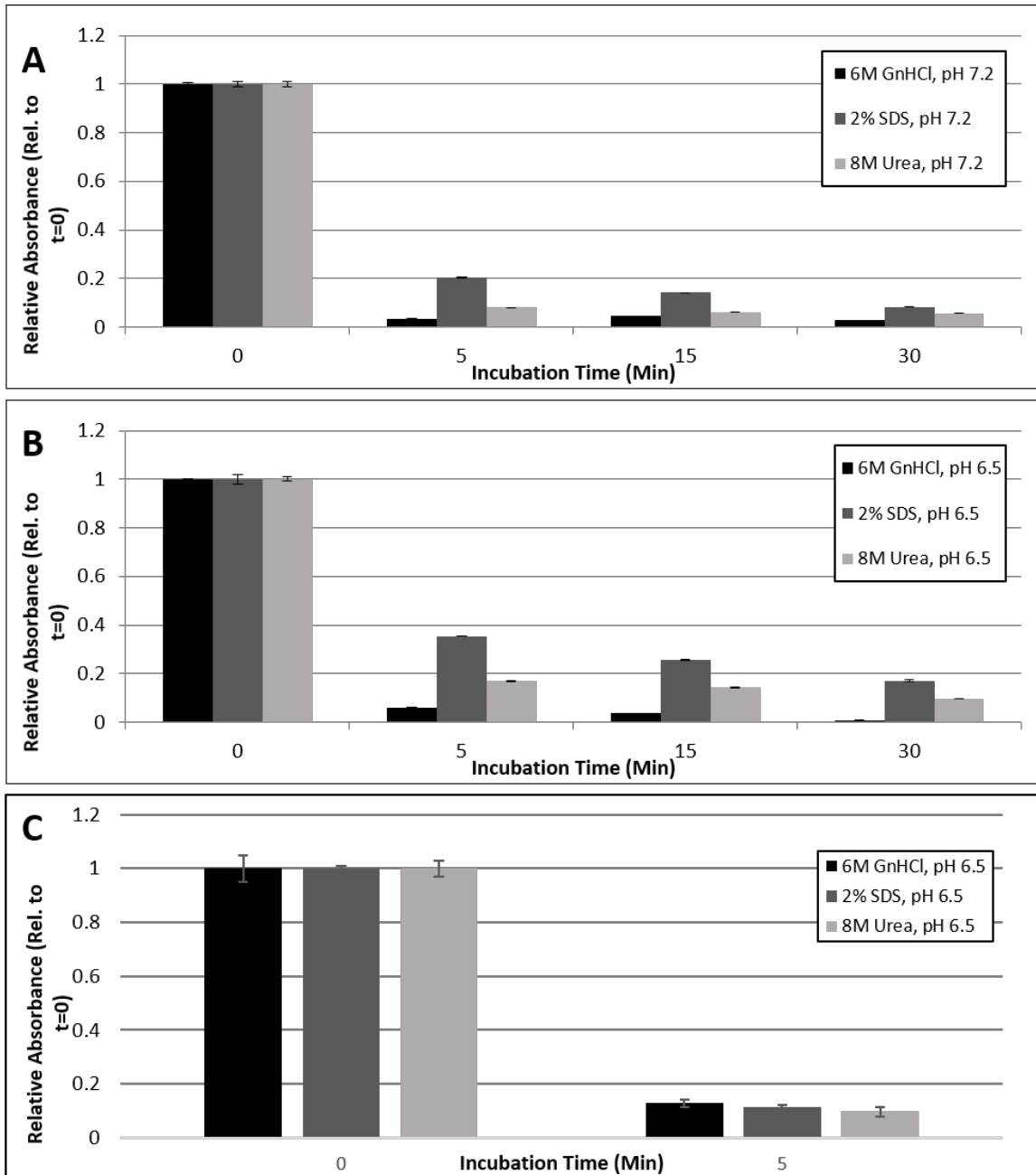
Figure 2.4. Cysteine alkylation by N-ethylmaleimide (NEM) was measured under different denaturing lysis conditions. BEAS-2B cells were washed with PBS, detached from plates, and lysed in degassed lysis buffers (20 mM MOPS, 0.1% NP-40, 150 mM NaCl, 1 mM EDTA) containing 25 mM NEM and one of three different denaturants (6M guanidine HCl (GnHCl), 8M urea, or 2% SDS) at (**A**) pH 7.2 or (**B**) pH 6.5. The lysates were incubated for the indicated time points, then 100 μl of each lysate was pipetted into three replicate wells of a 96-well plate. To these wells 200 μl of 5,5'-dithio-bis-(2-nitrobenzoic acid) (DTNB) assay solution (100 mM NaH_2PO_4 pH 7.8, 1 mM EDTA, 10 mM DTNB) was added. The plates were briefly shaken to mix and allowed to incubate for 10 minutes in the dark prior to reading at λ=405 nm. (**C**) BEAS-2B cells were treated with 50 mM NEM or HBSS vehicle (for zero time point controls) for 15 minutes, washed with PBS, detached from plates, pelleted, and lysed in g 25 mM NEM and one of three different denaturants (6M guanidine HCl (GnHCl), 8M urea, or 2% SDS) at pH 6.5 for 5 minutes. All DTNB measurements were normalized to cell lysate protein concentrations, determined by bicinchoninic acid assay. Bars represent mean relative absorbance ± SD, n=3.

One- vs. Two-Step Alkylation/Reduction

Having determined that NEM alkylation at pH 6.5 using both prelysis quenching

and SDS denaturation as optimal conditions for a streamlined RAC, we wanted to

compare the one-step PROP method, which features a single precipitation step between

reduction and capture, vs. two-step Ox-RAC method, which features two precipitation

steps between the alkylation-reduction and reduction-capture steps. By eliminating one

of two precipitation steps one-step would significantly shorten processing time for RAC

analysis; however combining NEM quenching and sample reduction into one step risks

potential NEM alkylation of previously-oxidized cysteines if the NEM quenching is not

rapid enough or insufficient.

We therefore compared control and peroxide-treated samples processed using

either one-step alkylation/reduction, where DTT is added directly to the NEM-containing

sample to both quench and reduce, or the two-step which removes the NEM by

precipitation prior to reduction. As seen in Fig. 2.5 the one-step procedure showed lower

signal fidelity than the two-step procedure with the difference between control and

treated samples being far lower for one-step. This would indicate that one-step

alkylation/reduction results in poor sample quality, likely due to insufficient quenching of

NEM during reduction allowing NEM alkylation of newly-reduced cysteines. However

the decreased workflow required by one-step was a tantalizing goal, and as such we

wanted to determine whether one-step could be modified in such a way as to both

eliminate the need for NEM removal prior to reduction *as well as* preserve sample

fidelity.
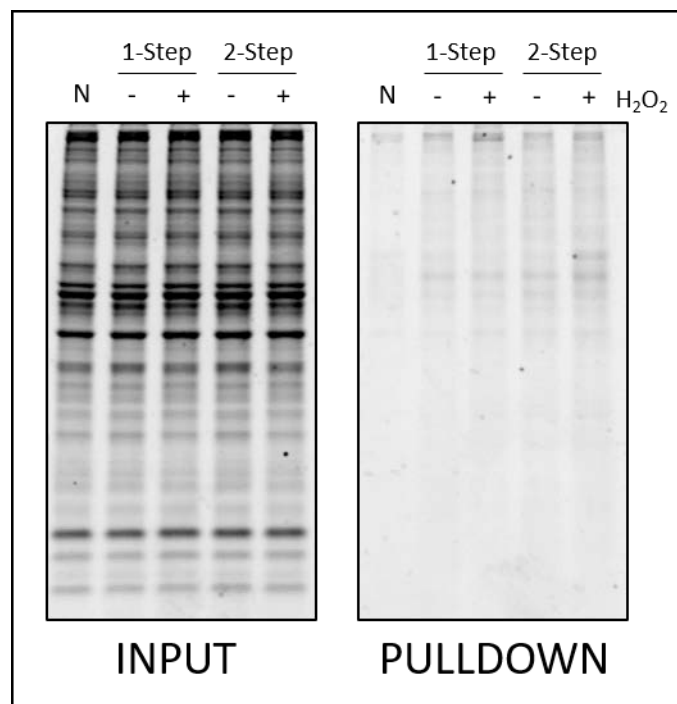
Figure 2.5. Two-precipitation-step resin-assisted capture as exemplified by Ox-RAC
yields higher capture of proteins following peroxide treatment than one-precipitation-step
resin-assisted capture as exemplified by PROP. BEAS-2B cells were treated with PBS or
0.5 mM H_2O_2 for 1 hr in serum-free DMEM. Following treatment cells were prelysis
quenched with 50 mM N-ethylmaleimide (NEM), pelleted, lysed in PNIES 1.5% lysis
buffer (20 mM NaH_2PO_4 pH 7.0, 150 mM NaCl, 0.1% Igepal CA-630, 1 mM EDTA,
1.5% SDS), and alkylated with 20 mM NEM as described. Following alkylation 50 mM

dithiothreitol (DTT) was added directly to the NEM-containing buffer for the samples in lanes 1-2 (1-step) while the samples in lanes 3-4 (2-step) were precipitated with acetone, washed 3x with 80% acetone, and resuspended in PNIES lysis buffer containing 50 mM DTT. Following reduction samples were precipitated with acetone, washed and processed for resin-assisted capture as described in the Methods. Equivalent amounts of RAC-processed whole cell lysates as determined by bicinchoninic acid assay were loaded onto thiopropyl-sepharose columns to capture oxidized proteins, washed, and eluted (RAC pulldown). The lanes on the left side of the figure were loaded with 5 µg of RAC-processed whole cell lysate (INPUT), and the lanes on the right side of the figure were loaded with 20 µl of eluate (PULLDOWN) containing only oxidized proteins from each treatment. NC indicates samples which were alkylated with N-ethylmalemide but not reduced as a negative control for thiopropyl capture. The gels were visualized after electrophoresis using Coomassie G-250.

In order for a one-step alkylation/reduction to be feasible, the alkylating reagent must be completely quenched either before addition of the reductant, or by the reductant itself. Without total quenching of NEM's alkylating ability, any newly-reduced thiols exposed by the reductant will be immediately alkylated, decreasing detection. Therefore we wanted to determine whether dithiothreitol (DTT), the reductant used in PROP, was suitable for a one-step procedure. We incubated equimolar concentrations of four reductants with NEM. The reductants chosen were two monothiols, l-cysteine and 2-mercaptoethanol, as well as DTT and dithiobutylamine (DTBA) [83], a dithiol with a lower pK_{SH} than DTT.
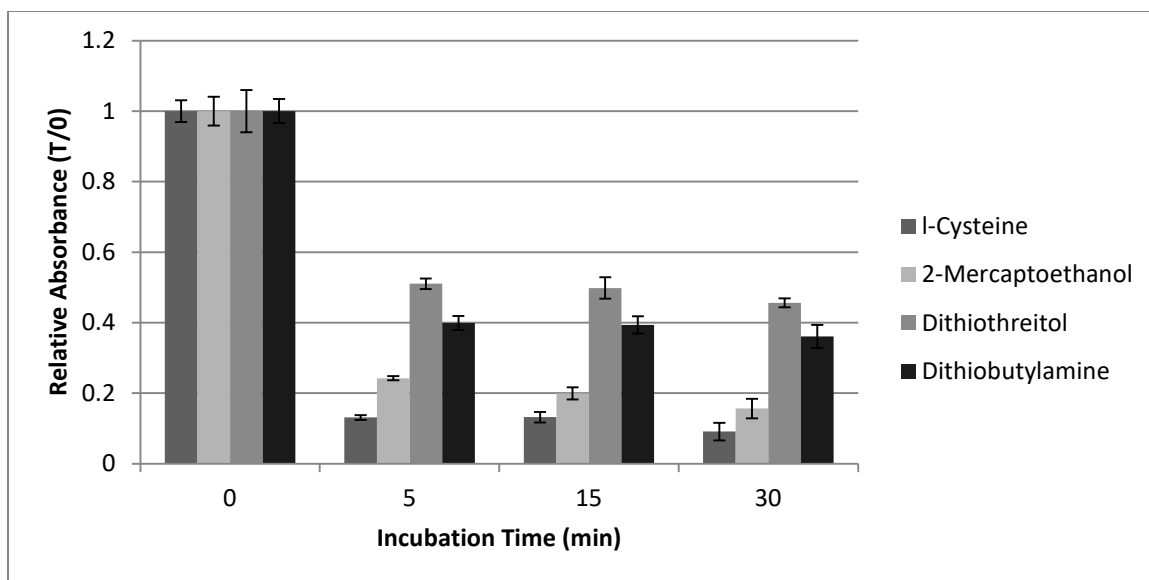
Figure 2.6. Four thiol-containing compounds were compared for their ability to quench an equimolar concentration of N-ethylmaleimide (NEM) over time. 50 μl of either l-cysteine (2 mM), β-mercaptoethanol (2 mM), dithiothreitol (1 mM), or dithiobutylamine (1 mM) in 25 mM MOPS, pH 6.5 were added to 50 μl of 2 mM NEM in the same buffer in triplicate wells of a 96-well plate; for the zero-minute control each thiol compound was added to 50 μl of buffer alone. After incubation for the indicated amounts of time, 150 μl of a 5 mM 5,5'-dithio-bis-(2-nitrobenzoic acid) solution (100 mM Tris, pH 8.0) was added to each well and allowed to incubate with mixing for 5 minutes. Following incubation the wells were read at 405 nm on a BioTek EL800 spectrophotometer. Bars represent mean relative absorbance ± SD, n=3.

The results (Fig. 2.6) indicate that both DTT and DTBA were poor NEM quenchers, leaving 51% and 39%, respectively, of free NEM after a 5-minute incubation. Based on these results, if the PROP one-step approach is used a significant portion of NEM would still be available to alkylate the newly-reduced cysteines, reducing signal. However the two monothiol reductants were far better at quenching NEM, with l-cysteine leaving only 13% free NEM in solution after 5 minutes. This shows that the idea of quenching NEM prior to reduction in a one-step approach may be viable using a low-

pK$_{SH}$ monothiol such as cysteine as a quenching reagent prior to the addition of DTT as a reductant.

We therefore tested this revised one-step method. In lieu of l-cysteine, which is relatively difficult to solubilize at neutral pH, we used the simple monothiol mercaptoethylamine. As seen in Table 1.1 mercaptoethylamine has a pK$_{SH}$ of 8.35, which is slightly lower than that of l-cysteine; therefore it should have similar quenching properties as l-cysteine. Additionally mercaptoethylamine is readily soluble in neutral aqueous solutions and so can easily be prepared immediately prior to use.

Using mercaptoethylamine as an NEM-quenching agent followed immediately by the addition of DTT as the reducing agent in a one-step approach resulted in a significant signal improvement over the traditional two-step methodology (Fig. 2.7). Both the one-step and two-step approaches showed an increase in cysteine oxidation with increasing peroxide concentration, although the increase was more pronounced for the one-step samples than the two-step. Aside from the increased signal the samples were identical between one- and two-step; every band that was visible in the two-step sample lanes corresponded to a band visible in the one-step lanes. The increase in signal fidelity for the revised one-step is likely due to decreased sample loss and processing time by eliminating the second precipitation step.
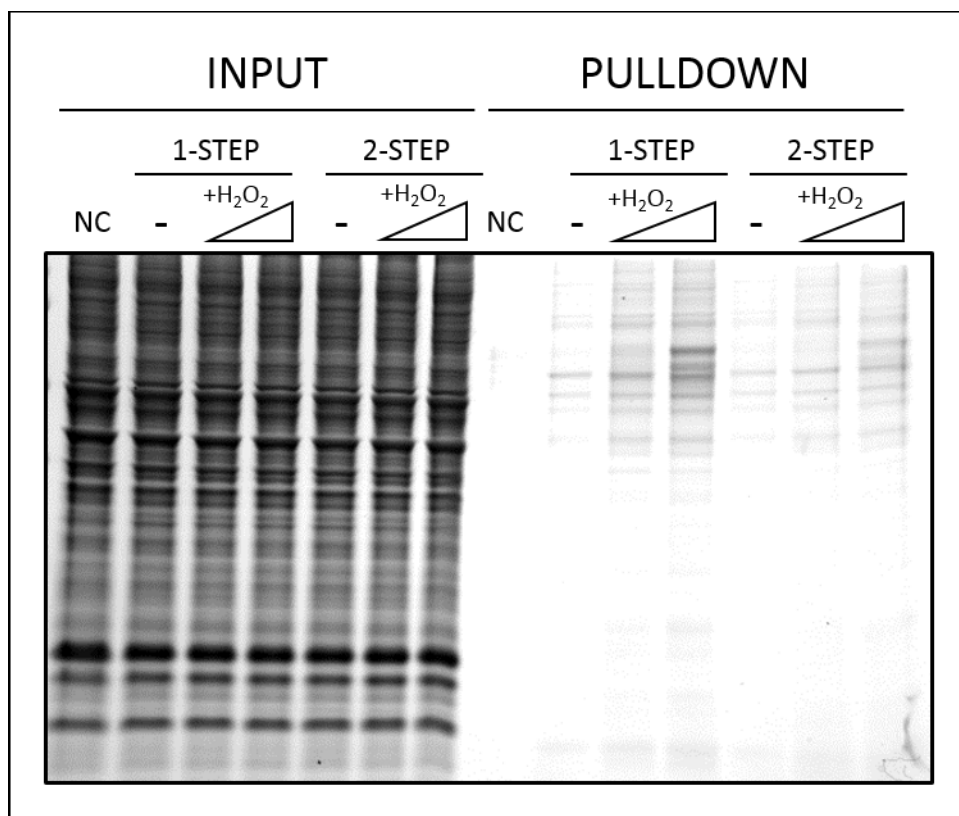
Figure 2.7. Oxidized cysteine yield by the optimized one-step resin-assisted capture is higher than with the two-step resin-assisted capture method. Control and 0.1 mM or 0.5 mM hydrogen peroxide-treated BEAS-2B samples were prelysis quenched, pelleted, lysed, and alkylated with 20 mM N-ethylmaleimide (NEM) as described in the Methods. Following alkylation 20 mM mercaptoethylamine was added directly to the NEM-containing buffer and, after a 5 minute incubation, 50 mM dithiothreitol (DTT) was added for the samples in lanes 9-11 (1-step). The samples in lanes 12-14 (2-step) were precipitated with acetone, washed 3x, and resuspended in reduction buffer containing 50 mM DTT. Following a one-hour reduction all samples were precipitated with acetone and processed for resin-assisted capture as described in the Methods. Equivalent amounts of RAC-processed whole cell lysates as determined by bicinchoninic acid assay were loaded onto thiopropyl-sepharose columns to capture oxidized proteins, washed, and eluted (RAC pulldown). The lanes on the left side of the figure were loaded with 5 μg of RAC-processed whole cell lysate (INPUT), and the lanes on the right side of the figure were loaded with 20 μl of eluate (PULLDOWN) containing only oxidized proteins from each treatment. NC indicates samples which were alkylated with N-ethylmalemide but not reduced as a negative control for thiopropyl capture. The gels were visualized after electrophoresis using Coomassie G-250.

Conclusions

In comparing the characteristics which differentiated the two resin-assisted capture techniques, Ox-RAC and PROP, we arrived at an optimized workflow for RAC which improves upon its predecessors. We determined that TCA quenching, which could introduce post-lysis oxidative artifacts by trace metals and other oxidants, could be eliminated by quenching surface-exposed thiols with NEM prior to lysis. The incorporation of prelysis quenching into the workflow permitted the use of SDS as the lysis denaturant without a decrease in the alkylation efficiency as compared to GnHCl. The separation of the alkylant quenching and reduction steps in the one-step PROP workflow into two distinct steps, with mercaptoethylamine being added as a quenching agent prior to DTT addition, increased the quality and speed of the RAC procedure immensely as compared to the conventional two-step RAC method.

These changes to the RAC workflow are inexpensive and easy to incorporate into existing protocols. The optimized methodology we have developed will save time and decrease sample error caused by precipitation and handling. This study has indicated that there are still iterative improvements upon the RAC methodology to be made in order to develop it into a mature experimental staple. An obvious source for future improvement and streamlining based on our experience would be the elimination of the final precipitation step, thereby transforming RAC into a one-day, one-pot technique.

Chapter 3 : SYNTHESIS AND APPLICATION OF HIGH-CAPACITY THIOL REDUCTANT-POLYACRYLAMIDE BEADS FOR SOLID-PHASE REDUCTION OF OXIDIZED CYSTEINES.

Background

The introduction of the two-step quench/reduction into the RAC method was effective in eliminating the organic precipitation step previously used between alkylation and reduction. However if the downstream assay is for total cysteine oxidation it was still necessary to remove the reductant by organic precipitation followed by resuspension since any excess DTT in the solution would reduce the disulfide bonds formed between the cysteine thiols and solid-phase resin, thereby preventing capture. We theorized that if we could remove the reductant without requiring organic precipitation then this could drastically improve the workflow since as mentioned before each precipitation step incurs sample loss and increased risk of contamination and user error.

Therefore it was considered highly advantageous to determine some means of removing reductant without precipitation. Unlike in the case of the alkylant, there was no easy way to quench or oxidize the reductant without also risking oxidation of the newly-reduced cysteine thiols. DTT's reducing capacity could be drastically decreased by decreasing the pH of the sample solution, thereby protonating DTT's thiols, but those thiols would still be available for capture by the solid-phase resin – in essence crowding out the cysteine thiols, preventing sample capture. However if we instead conjugated the reductant to a neutral resin, thereby making a solid-phase reductant, we could remove the

reductant from the lysate by a simple centrifugation step in a spin column – in essence an inversion of the downstream resin-assisted capture.

Solid-phase reductants have been previously applied to the reduction of samples prior to western blotting and protease digestion. The utility of a solid-phase reductant was observed as far back as 1973, when Gorecki and Patchornik described the conjugation of dihydrolipoic acid to polymers [84]. Since that time commercially-available reducing resins have become available. Additionally Grazu et al. [85] demonstrated that an agarose resin that was highly-substituted with monothiols had act as a suitable reductant. Therefore the incorporation of a solid-phase reductant into the RAC workflow was both reasonable and viable in principle.

However the aforementioned solid-phase reductants were designed around reduction of samples prior to western blotting or protease digestion, and therefore do not contain the high reductant concentrations made necessary by the inherent limitations of the optimized RAC method. In order to properly study cysteine oxidation caused by treatments a quantitative reduction of oxidized cysteines is necessary. During RAC this is typically achieved by using 50 mM or higher concentrations of DTT; furthermore since RAC uses a microcentrifuge spin column the upper limit for the sample volume is fixed at ~600 μl which allows for ~200 μl of resin.

While this is not difficult to achieve using concentrated stock solutions of soluble DTT, to achieve the same results using an immobilized reductant would require a highly-substituted resin. As both the sample and reductant resin would compete for the limited volume of the spin column, having a higher reductant substitution on the resin would

allow the use of a smaller volume of resin, thereby allowing for a much larger fraction of the column volume to be occupied by the sample.

As an example, for a 600 μl sample being processed for RAC 30 μmol of DTT are added to arrive at a final concentration of ~50 mM DTT. Therefore in order to achieve the same reductant concentration using a solid-phase reductant the resin would need to have a conjugated reductant amount of 30 μmol/200 μl resin, or 150 μl/ml resin. Unfortunately commercially-available reducing resins are low-substitution, with a quantity of reductant available of only 8-25 μmol/ml. In order to utilize a solid-phase reductant for RAC it was necessary to synthesize a much higher-capacity reducing resin. Additionally it was hoped that the reducing resin could be synthesized in a manner which required no specialized equipment or techniques, as well as limiting the use of toxic or hazardous reagents.

Choice of Solid-Phase Substrate

With these requirements in mind a suitable insoluble substrate was needed to generate the immobilized reductant. Agarose has been extensively used as an insoluble support for chemical conjugation [61, 86, 87] due to its low cost and the uncharged hydrophilic structure of the polysaccharide. Agarose can be relatively easily substituted with thiols through an epoxidation of the polysaccharide backbone's hydroxyl groups using epichlorohydrin, requiring only moderate heating. While Grazu et al. [85] reported success in generating a high-capacity reducing resin of 1 mmol thiol/g resin (approx. 333 μmol thiol/ml resin with 3 ml/g swell ratio), substitution ranges of 200-250 μmol/ml resin are more commonly observed [61, 62] using agarose.

Although less common, polyacrylamide (PAAm) resin has also been used successfully for small-molecule immobilization to the amide group of the PAAm backbone. As a solid-phase support PAAm has several advantages over agarose. Both PAAm and agarose are hydrophilic, but since agarose is derived from polysaccharides it has much lower chemical stability and durability than the polyethylene-derived PAAm; PAAm can be easily dried under vacuum for storage without damage, whereas agarose requires lyophilization with stabilizing additives to prevent structural damage [88]. PAAm can achieve much higher theoretical substitution rates than agarose since the amide groups in PAAm repeat much more frequently than the hydroxyl groups on the agarose polysaccharide. Additionally the amide group on PAAm allows for greater flexibility in its conjugation reactions, since the amide can be derivatized to an amine, carboxylic acid, or hydrazide [89]. Furthermore the different porosities available for PAAm resins allow for very narrow fractionation ranges, allowing the complete exclusion of the sample proteins from the interior of the beads.

PAAm substitution rates of >2 mmol/g have been routinely reported [84, 89]. PAAm resin swell rates depend upon the porosity of the PAAm beads and range from 3-12 ml/g resin [90]; based on this, it was estimated that the substitution of PAAm resin would range from ~250-670 μmol/ml resin depending upon the chosen resin porosity. As this substitution range was comparable to that of agarose, PAAm was chosen as the immobilization substrate due to its numerous other advantages.

The selection of PAAm allowed for a wide latitude of strategies for thiolation, given the range of derivatives available. However most of the derivation reactions required refluxing conditions and toxic chemicals, such as ethylenediamine or hydrazine

[89]. We therefore sought derivations that could be achieved using relatively mild conditions and/or reagents more likely to be encountered in a molecular biology lab. Accordingly we developed a strategy based on conjugation of a dialdehyde to PAAm to give an activated aldehyde-PAAm, which would allow for further conjugation to a variety of reducing groups (Fig. 3.1).

Glutaraldehyde-Conjugation of PAAm

Glutaraldehyde will rapidly react with amines and amides over a wide pH range ($\geq$ pH 3) and will react with thiols in the presence of a primary amine [91]. While glutaraldehyde has been used to immobilize antigens to PAAm through crosslinking between the PAAm amide group and amines present on the antigen [92, 93], to date no one has utilized glutaraldehyde-PAAm reactivity and glutaraldehyde-amine or glutaraldehyde-thiol reactivity to generate an immobilized solid-phase reductant (Fig. 3.1B.2-3). If possible this synthetic reaction would be highly advantageous since it uses the aqueous, relatively non-toxic glutaraldehyde as its reactive group instead of the highly toxic and potentially carcinogenic compounds used in previous syntheses, such as epichlorohydrin [94-96] and ethylene diamine [97].

We further sought to utilize the versatile nature of PAAm-conjugated glutaraldehyde to conjugate cysteine reductants which contained neither an amine nor a thiol. Using acid-catalyzed acetal formation we predicted that we could synthesize high-capacity DTT-PAAm (Fig.3.1B.4) and non-thiol reductant tris(hydroxylpropyl)phosphine-PAAm (THP-PAAm) resins (Fig. 3.1B.5). The non-thiol reductant tris(carboxyethyl)phosphine (TCEP) could additionally be conjugated via an

47

EDC-mediated amide linkage to amino-PAAm (Fig. 3.1C). This range of synthetic

reactions would allow us to generate a panel of immobilized thiol reductants.
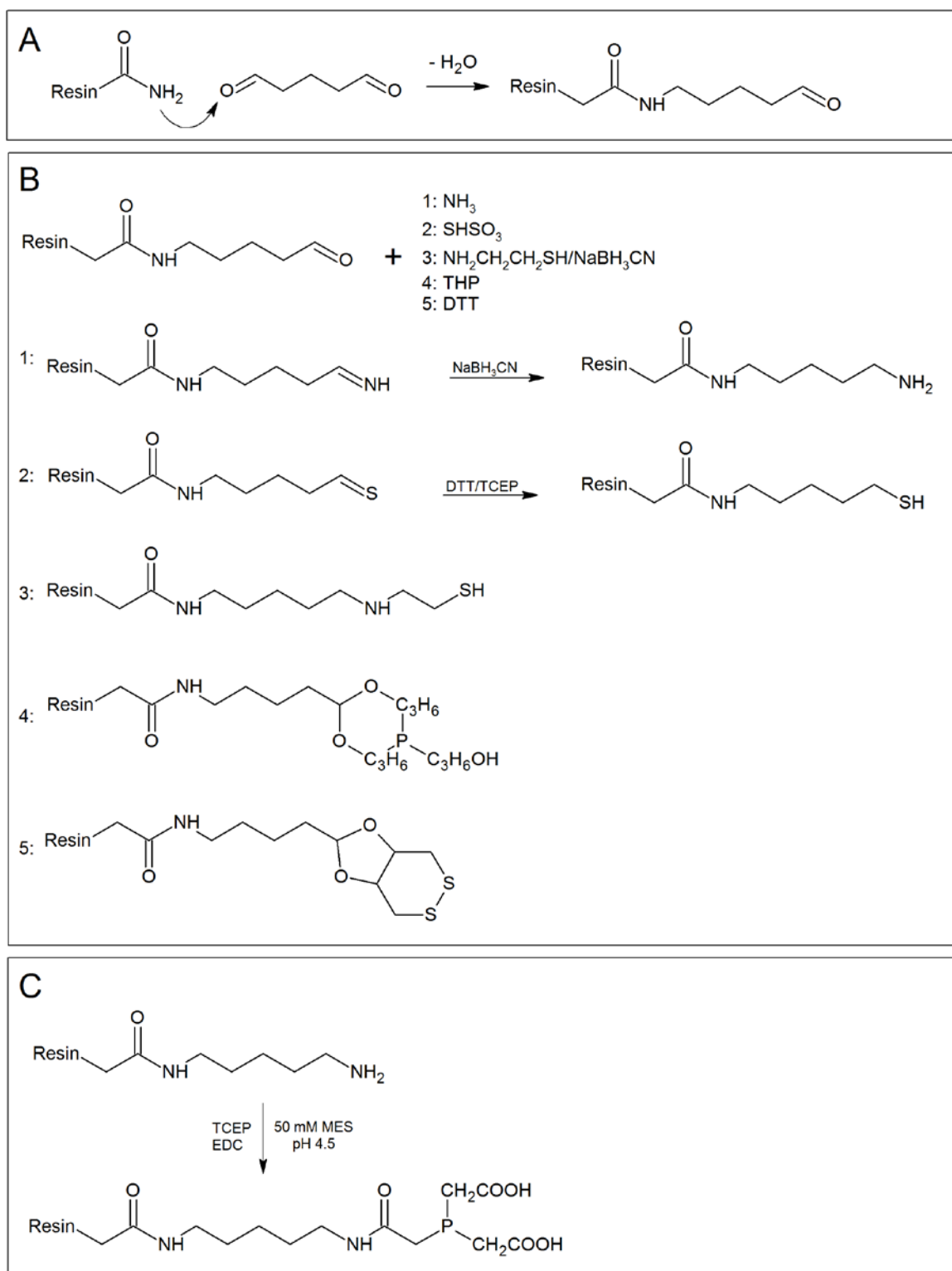
Figure 3.1. Synthetic routes and structures for polyacrylamide-based reducing resins. (**A**) Conjugation reaction between amide group of acrylamide and aldehyde group of glutaraldehyde. (**B**) Synthetic routes for aminopropyl-polyacrylamide (1), thiopropyl-

polyacrylamide (2), mercaptoethylamine-polyacrylamide (3), tris(hydroxylpropyl)phosphine-polyacrylamide (4), dithiothreitol-polyacrylamide (5). For all structures "Resin" represents a polyacrylamide backbone. For compounds 1-3 the reaction conditions were 0.1M NaPO$_4$, pH 7.7, 25°C, 3 hr incubation. For the acetal-conjugated compounds 4-5, the reaction conditions were 10 mM HCl, pH 2.2, 25°C, ON. All reductant compounds were added in molar excess of available aldehyde groups on the polyacrylamide. The imine formed by the addition of (1) to aldehyde was reduced with sodium borohydride. Thiol containing compounds (2, 3, 5) were reduced with excess dithiol or phosphine reductants following conjugation. (**C**) Synthesis of tris(carboxylethyl)phosphine-polyacrylamide (TCEP-PAAm) using carbodiimide amide formation. TCEP and EDC were added in excess to pentaneamine-polyacrylamide. The reaction conditions were 50 mM MES, pH 4.5, 25°C, 4hr.

Materials and Methods

Materials. The immortalized human bronchial epithelial cell line BEAS-2B was

purchased from American Type Culture Collection (ATCC CRL-9609). Cell culture

medium (Gibco DMEM+GlutaMAX, Gibco 10569), HBSS pH 7.4 (Gibco 14025), PBS

pH 7.4 (Gibco 10010), 5,5'-dithiobis-(2-nitrobenzoic acid) (Thermo Scientific 22582,

Lot# OG189149A), thiopropyl-sepharose 6B resin (GE Healthcare 17042001) and screw

cap microcentrifuge spin columns (Pierce 69705) were purchased from Thermo Fisher

Scientific (Waltham, MA). Bio-Gel P6DG (Bio-Rad 150-0738 Lot# 64053706) was

purchased from Bio-Rad (Hercules, CA). Tris(carboxylethyl)phosphine (TCEP25 Lot#

2801.042518A) was purchased from Gold Biotechnology (St. Louis, MO). Cystamine

dihydrochloride (Aldrich C121509 Lot# BCBQ0040V), tris(hydroxypropyl)phosphine

(Aldrich 777854), *trans*-4,5-dihydroxy-1,2-dithiane (Aldrich D3511), and

selenocystamine dihydrochloride (Sigma S0520 Lot# SLBS6606) were purchased from

Millipore Sigma (St. Louis, MO). 50% glutaraldehyde solution (VWR 0875 Lot#

0587C463), N-ethylmaleimide (Alfa Aesar 40526, Lot#P290042), dithiothreitol (VWR

97061), and sodium cyanoborohydride (TCI S0396 Lot# MMQED-MC) was purchased from VWR (Radnor, PA).

Cell Culture. The immortalized human bronchial epithelial cell line BEAS-2B (ATCC CRL-9609) was cultured in DMEM with 10% FBS, 1% Pen-Strep at 37°C, 5% CO_2 in a humidified incubator. Cells were subcultured prior to confluence and seeded at 3000 cells/cm^2. For experiments the cells were treated at 60-80% confluence, and treated with the concentrations of metals described in the figures or deionized water as a vehicle control.

Synthesis of Activated Carbonyl Resins

Activated Carbonyl PAAm Resin. Activated-carbonyl resin was synthesized as described by Weston and Avrameas [92] with modifications. 1g of polyacrylamide resin (Bio-Gel P6DG) was rehydrated with deionized water for 4 hours. Following rehydration the resin was washed with 0.5M sodium phosphate buffer, pH 8. It was then resuspended in 9 ml of the same buffer, and 6 ml of 50% glutaraldehyde (final 20% v/v) was added to the resin. The suspension was incubated at 40°C for 4 hours with end-over-end rotation. Following incubation the resin slurry was transferred to a fritted-glass filter and washed 4x with PBS under vacuum. The resin was allowed to dry until no more water passed through the filter, then it was resuspended in the specified downstream reaction buffer(s) and used immediately for downstream syntheses. Alternatively if the resin was to be stored at this point it was resuspended in PBS containing 10% EtOH and stored at 4°C.

Thiopropyl-PAAm Resin. 1g of activated-carbonyl resin was resuspended in 40 ml of 0.1M sodium phosphate buffer, pH 7.7. 1.58g of sodium thiosulfate was dissolved in 10

ml of 0.125M Tris-HCl buffer, pH 7.7, and this solution added to this suspension to make a final concentration of 0.2M sodium thiosulfate, 25 mM Tris-HCl. The suspension was incubated at 25°C overnight with end-over-end rotation. Following incubation the resin was washed 4x with diH2O and 4x with ethanol. Following the final wash the resin was dried overnight under vacuum in a desiccator.

Mercaptoethylamine-PAAm Resin. 1g of activated-carbonyl resin was resuspended in 40 ml of 0.1M sodium phosphate buffer, pH 7.7. 2.85g of cystamine dihydrochloride was dissolved in 10 ml of diH2O, and this solution added to this suspension to make a final concentration of 0.25M. An equimolar amount of $NaBH_3CN$ was added to the suspension. The slurry was incubated at 25°C for 3 hours with end-over-end rotation. Following incubation the resin was washed 4x with 0.1M acetic acid, 4x with deionized water, and 4x with ethanol. Following the final wash the resin was dried overnight under vacuum in a desiccator.

Aminopropyl-PAAm Resin. 1g of activated-carbonyl resin was resuspended in 7 ml of 0.1M sodium phosphate buffer, pH 7.7. 1.19g of ammonium bicarbonate was dissolved in 5 ml of diH2O, and this solution added to this suspension to make a final concentration of 1M. A molar equivalent of $NaBH_3CN$ was added to the solution. The suspension was incubated at RT for 3 hours with end-over-end rotation. Following incubation the resin was washed 4x with 0.1M acetic acid, 4x with deionized water, and 4x with ethanol before drying overnight in a vacuum dessicator.

Tris(carboxylethyl)phosphine-PAAm Resin. 1g of aminopropyl-PAAm was resuspended in 10 ml of 0.1M MES buffer, pH 4.5. 5 ml of a 0.5M tris(carboxyethyl)phosphine

(TCEP) stock solution, pH 4.5, was added to bring the final concentration of TCEP to 167 mM. 480 mg of 1-ethyl-3-(3-dimethylaminopropyl)carbodiimide hydrochloride (EDC) was added to the suspension. The suspension was sharply inverted end-over-end several times to dissolve and mix the EDC thoroughly, then incubated at 25°C for 4 hours with end-over-end rotation. Following incubation the resin was washed 4x with diH2O and 4x with ethanol. Following the final wash the resin was dried overnight under vacuum in a desiccator.

Tris(hydroxylpropyl)phosphine-PAAm Resin. 1g of activated-carbonyl resin was resuspended in 7 ml of 10 mM HCl, pH 2.2. 1.832 ml Tris(hydroxylpropyl)phosphine (THPP) was diluted in diH2O, pH-adjusted to pH 2.2 with HCl, and brought to 10 ml to give a 1M THPP stock solution. 3 ml of this THPP stock solution added to the suspension to make a THPP quantity of 3 mmol. The slurry was incubated at 25°C overnight wrapped in foil with end-over-end rotation. Following incubation the resin was washed 4x with 0.1M acetic acid, 4x with deionized water, and 4x with ethanol. Following the final wash the resin was dried overnight under vacuum in a desiccator.

Dithiothreitol-PAAm Resin. 1g of activated-carbonyl resin was resuspended in 7 ml of 10 mM HCl, pH 2.2. 456.72 mg of *trans*-4,5-dihydroxy-1,2-dithiane (3 mmol) was dissolved in 3 ml of 10 mM HCl, and this solution added to this suspension. The slurry was incubated at 25°C overnight with end-over-end rotation. Following incubation the resin was washed 4x with 0.1M acetic acid, 4x with deionized water, and 4x with ethanol. Following the final wash the resin was dried overnight under vacuum in a desiccator.

Reduction of thiol-containing resins. 1g of thiol-containing PAAm resin was rehydrated in 10 ml of PBS. Following rehydration the beads were centrifuged down and the supernatant removed. PBS was added to bring the total volume to 10 ml, then 5 ml of a 0.5M TCEP, pH 7.0 stock solution was added to bring the final TCEP concentration to 0.15M. The suspension was incubated at 25°C for 1 hour with end-over-end rotation. Following incubation the resin was washed with diH$_2$O until the flowthrough did not react with DTNB, indicating complete removal of TCEP (~25x). The resin was then washed 4x with ethanol and dried overnight under vacuum in a desiccator.

Measurement of PAAm Substitution. Substitution was measured using the DTNB assay [64] with modifications. 1 mg of resin was placed in a 2 ml microcentrifuge tube. 1 ml of a 10mM DTNB solution (100 mM sodium phosphate, pH 7.8, 1 mM EDTA) was added to the tube. The sample was vortexed and incubated with rotation at 25°C for 30 minutes in the dark. Following incubation the resin was pelleted by centrifuging at 16,000x g for 5 minutes. 100 µl of the supernatant was placed into a 96-well plate. The plate was read at λ=405 nm using a BioTek EL800 spectrophotometer. The absorbance values for the sample were compared against a mercaptoethylamine standard curve incubated under identical conditions.

Prelysis Quenching. Following treatment the cell culture medium was exchanged with HBSS containing NEM (50 mM unless otherwise noted) and incubated briefly. After incubation the HBSS + NEM was removed, the plates were washed 3x with HBSS, the cells were detached from the plate with a cell lifter, collected into 1.5ml tubes, pelleted, and resuspended in degassed lysis buffer.

Lysate Alkylation and Reduction. BEAS-2B cells were lysed in 400 µl of degassed lysis buffer containing 20 mM NEM in opaque 2-ml microcentrifuge tubes. The samples were incubated for 2 hours at RT with gentle end-over-end mixing. 20 mM mercaptoethylamine was then added to the samples to quench the NEM. After quenching for 5 minutes 50 mM DTT was added to reduce oxidized cysteines. After a one-hour incubation the samples were again precipitated with cold acetone, allowed to incubate overnight at -20°C, and washed 3x with cold 80% acetone before resuspension for RAC.

Resin-Assisted Reduction. Sample pellets were lysed, alkylated, and quenched as described above. Following quenching the samples were loaded into spin columns containing 50 mg of buffer-equilibrated solid-phase reductant resin. The columns were sealed and rotated end-over-end for one hour in the dark at RT. After incubation the columns were unsealed, placed into clean microcentrifuge tubes, and centrifuged at 16,000xG for 5 minutes to remove the sample from the reductant. Samples were then loaded into thiopropyl-resin spin columns for RAC.

Resin-Assisted Capture (RAC). Alkylated and reduced sample pellets were resuspended by pipetting in 400 µl of capture buffer (20 mM CH_3COONa pH 4.5, 2% SDS, 1 mM EDTA). Sample concentration was measured by BCA assay [66], and equal concentrations of lysates were added to microcentrifuge spin columns containing 35 mg of buffer-equilibrated thipropyl resin. The columns were sealed and the slurry was incubated for one hour at RT with rotation. Following incubation the columns were unsealed, placed into waste collection tubes, and centrifuged at 1,000xG for 1 minute to remove all nonbound proteins. The columns were washed with 5 column volumes of capture buffer, 5 column volumes of diH_2O, and 1 column volume of Laemmli sample

buffer. After the final wash 100 μl of Lammli buffer containing 50 mM DTT was added to the columns, which were sealed and rotated at RT for 30 minutes. The columns were then unsealed, placed in clean 1.5 ml microcentrifuge tubes, and centrifuged at 1,000xG to collect the bound fraction.

Gel Electrophoresis and Staining. Equal volumes of sample bound fractions were loaded in adjacent wells of NuPAGE bis-tris gels. Equal concentrations of input fractions were loaded to verify equivalent loading of the spin columns between samples. Gels were run in MOPS SDS-PAGE running buffer at 200V. Following electrophoresis the gels were removed from the gel cassettes, cut, and placed directly into fixation solution (10% acetic acid, 50% methanol) and incubated with RT for 15 minutes at RT. The fixation solution was decanted and replaced with staining solution (0.025% Coomassie G-250, 10% acetic acid), and the samples were incubated with rocking for 30 minutes at RT. The staining solution was decanted and the gels were destained with two 30-minute incubations in 10% acetic acid. Following destain the gels were imaged using a ChemiDoc XRS (Bio-Rad, Hercules, CA).

Results and Discussion

Determination of optimum activation pH. While Weston and Avrameas had previously described experimentally-determined condition optima for PAAm activation, their experimental conditions and endpoints are significantly far enough away from the current study that we felt it necessary to re-determine the optimal pH and time for the glutaraldehyde-PAAm incubation. The previous studies had been focused on protein

conjugation to polyacrylamide resins and therefore used highly-porous, low-crosslinked polyacrylamide resins (Bio-Gels P60-P300) to allow large proteins to entire into the bead macrostructure. For our purposes we wanted to restrict lysate proteins exclusively to the void volume to prevent protein retention by the resin, which necessitated using highly-crosslinked resins instead. How the difference in macroporosity between our chosen resin and the resins previously used would affect the ideal activation conditions needed to be determined.

To find the optimum activation pH, polyacrylamide beads were incubated at 40°C with glutaraldehyde for 2 hours at various pH values [92] using a pH-adjusted Britton-Robinson universal buffer system. Following this activation the glutaraldehyde-PAAm beads were incubated with sodium thiosulfate and then reduced to allow quantitation of thiol substitution of PAAm. Activation levels increased as the pH became slightly alkaline, with the thiol substitution of the resin being roughly equivalent from pH 8-9 (Fig. 3.2). Activation at pH 10 resulted in the beads forming large aggregates that required breaking up prior to downstream processing. The samples activated at pH 10 showed far lower thiol substitution than those activated at pH 9. It was also noted that the samples activated at pH 10 had a significantly smaller sample bead volume and were a dull yellow color as opposed to the off-white color of both the original resin and all other pH groups.
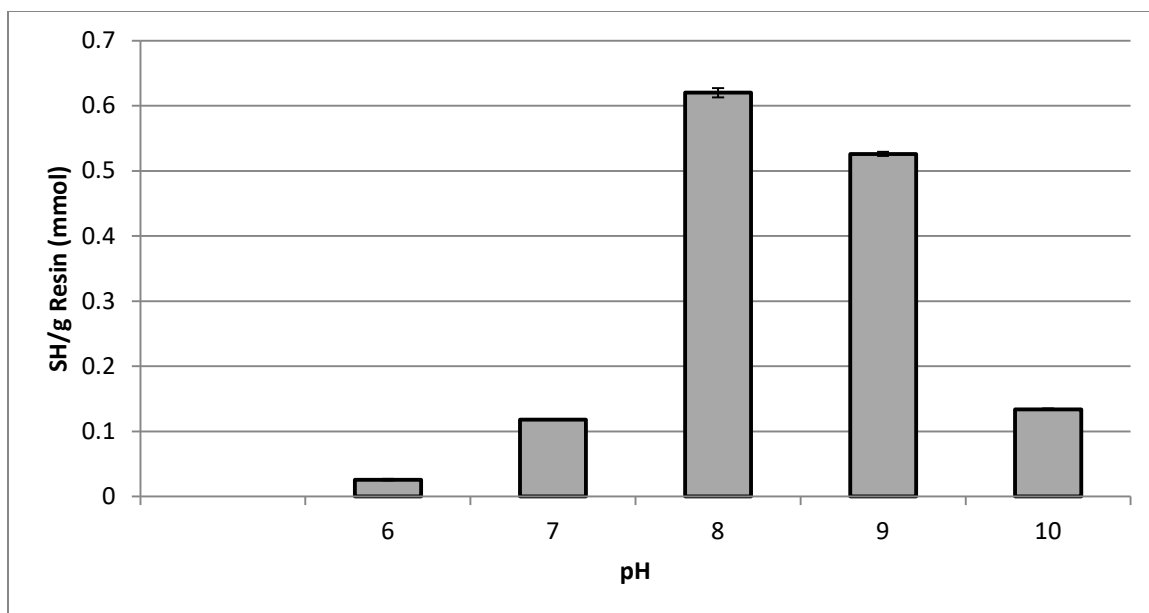
Figure 3.2. Thiol substitution of PAAm beads incubated at different pH. Bio-Gel P6 beads were incubated for two hours at 40 °C in the presence of 20% glutaraldehyde and 0.5M Britton-Robinson buffer at varying pH. After incubation the resin was washed extensively with PBS, then incubated with 2M $Na_2S_2O_3$ overnight. Thiolated resins were reduced with 0.5M tris(carboxylethyl)phosphine, then washed extensively. 1 mg of resin was added to 1 ml of 5,5'-dithio-bis-(2-nitrobenzoic acid) assay solution, allowed to equilibrate for 30 minutes, then measured at λ=405 nm to determine thiol content. Bars represent mean thiol content ± SD, n=3.

Since a large portion of the fractionation characteristics of PAAm resin can be attributed to their macrostructure, it was important to determine whether the activation had affected the bead diameter and overall structure. As can be seen in Figure 3.3 the macroscale structure of the PAAm beads does not change significantly from pH 6-8. At pH 9 there an increase in bead wall thickness, although the overall diameter of the beads did not change as compared to non-activated BioGel P6; this increase in thickness is most likely due to poly-glutaraldehyde formation. As expected the beads incubated at pH 10 had a much smaller diameter than the other groups. Additionally a significant portion of the beads showed a deformed and "rippled" exterior in sharp contrast to the smooth

exterior of both the control groups as well as those incubated at other pHs, due most

likely again to poly-glutaraldehyde crosslinking altering the bead structure.
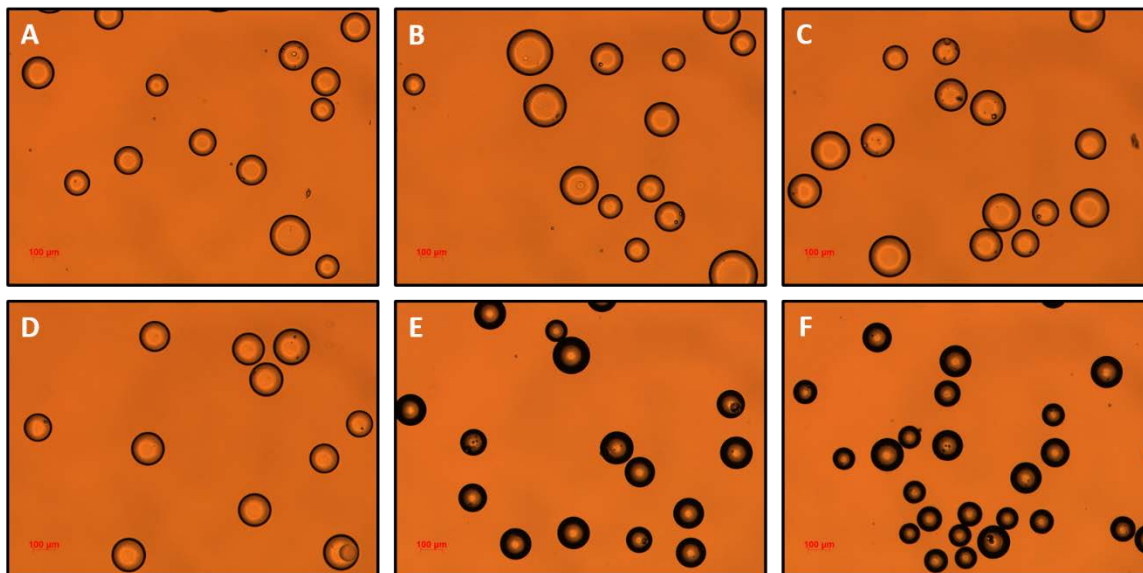
Figure 3.3. Polyacrylamide activation with glutaraldehyde at high pH causes significant alterations to bead structure. Optical microscopy images of thiolated-polyacrylamide beads activated at different pH. (**A**) control Bio-Gel P6. (**B**) pH 6, (**C**) pH 7, (**D**) pH 8, (**E**) pH 9, (**F**) pH 10. Images were captured using a Zeiss AxioObserver A.1 inverted microscope with an AxioCam MRc 5.

Determination of optimum activation incubation time. To find the optimal incubation

time, PAAm beads were activated at pH 7-9, 40°C for 1-12 hours. Following this

activation the beads were incubated with sodium thiosulfonate, reduced, and quantitated.

For both pH 7 and pH 8 activation levels increased with increasing incubation time in a

roughly linear fashion, with activation rates at each time point being higher for pH 8 than

pH 7. Activation at pH 9 peaked at 1 hour, after which the thiol substitution decreased

rapidly (Fig. 3.4).

Figure 3.4. Activated aldehyde conjugation to polyacrylamide resin increases with increasing incubation time. Bio-Gel P6 beads were incubated for the indicated times at 40°C in the presence of 20% glutaraldehyde and 0.5M Britton-Robinson buffer at pH 7, 8, and 9. After incubation the resin was washed extensively with PBS, then incubated with 2M $Na_2S_2O_3$ overnight. Thiolated resins were reduced with 0.5M tris(carboxylethyl)phosphine, then washed extensively. 1 mg of resin was added to 1 ml of 5,5'-dithio-bis-(2-nitrobenzoic acid) assay solution, allowed to equilibrate for 30 minutes, then measured at λ=405 nm to determine thiol content. Bars represent mean thiol content ± SD, n=3.

The macroscale structure of the beads was relatively unchanged from the non-activated control beads for both pH 7 and pH 8 over 1-2 hour activation (Fig. 3.5, B-C and E-F). As observed in the prior experiment the macroscale structure of the beads activated at pH 9 changed significantly, with a pronounced thickening of the bead wall in as little as 1 hour of activation (Fig. 3.5D). This thickening, again due to polyglutaraldehyde formation, would explain the rapid loss of activation with increased incubation times – as the activation continued, an increasing amount of free glutaraldehyde was polymerizing with the bound amide-bound glutaraldehyde and thickening the bead wall without contributing any further active aldehyde groups to the resin.
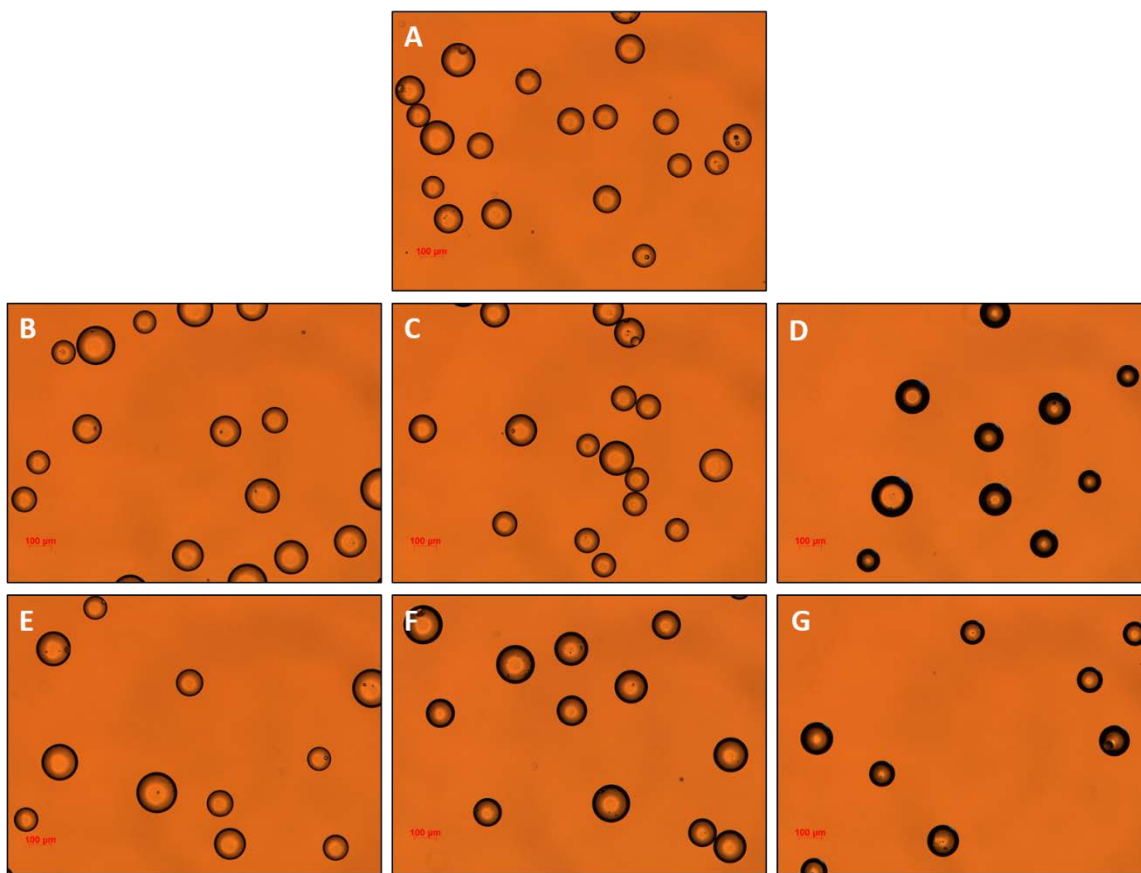
Figure 3.5. Polyacrylamide activation with glutaraldehyde at for increasing time at pH 8-9 causes bead diameter decrease and bead wall thickness increase. Optical microscopy images of thiolated-PAAm beads activated for different times at (**B,E**) pH 7, (**C,F**) pH 8, (**D,G**) pH 9. (**A**) control Bio-Gel P6. (**B-D**) 1-hour incubation. (**E-G**) 2-hour incubation. Images were captured using a Zeiss AxioObserver A.1 inverted microscope with an AxioCam MRc 5.

We observe this bead wall thickening in the pH 8-activated samples as well as the activation time is increased past 2 hours (Fig. 3.6C,E,G), however the thickening induced at pH 8 doesn't appear to coincide with decreased thiolation rates as seen in pH 9-activated samples. It is possible that the thickness increase observed in these beads is due to increased amide-glutaraldehyde loading instead of glutaraldehyde polymerization, or that the glutaraldehyde polymers formed at pH 8 are structurally distinct from those

formed at higher pHs and retain more activated aldehydes. The beads incubated at pH 7

showed minimal signs of bead wall thickening even as the activation time increased to 12

hours (Fig. 3.6F).
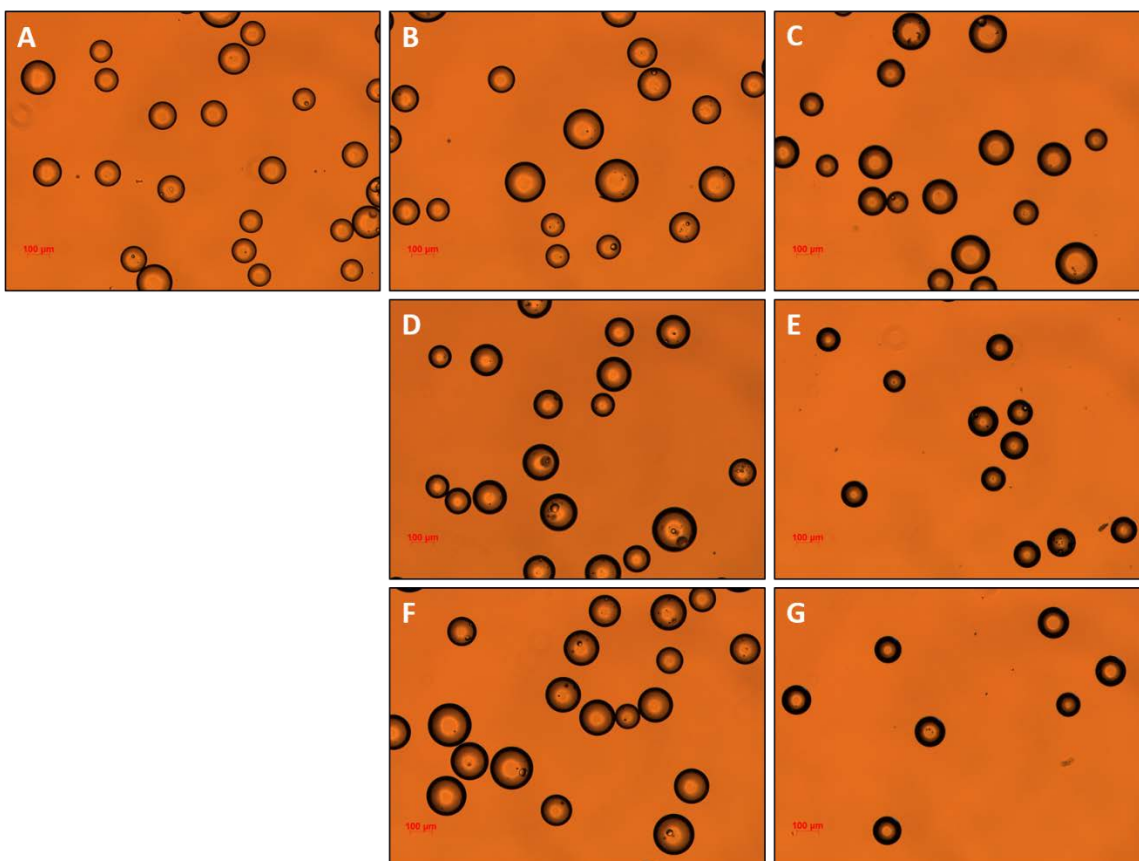
Figure 3.6. Polyacrylamide activation with glutaraldehyde for 4+ hours at pH 8 but not pH 7 causes bead diameter decrease and bead wall thickness increase. Optical microscopy images of thiolated-polyacrylamide beads activated for different times at (**B,D,F**) pH 7, (**C,E,G**) pH 8. (**A**) control Bio-Gel P6. (**B,C**) 4-hour incubation. (**D,E**) 8-hour incubation. (**F,G**) 12-hour incubation. Images were captured using a Zeiss AxioObserver A.1 inverted microscope with an AxioCam MRc 5.

Weston had described optimal reaction conditions for PAAm activation as

incubating for 17 hours at pH 6.8, 40°C. Based off our own pH and time-course

experiments it was clear that the previously-described conditions were far from maximizing glutaraldehyde loading. Due to this discrepancy between the previously-reported conditions and our own observations we wanted to investigate whether the activation rate or macroscale changes observed would be altered significantly if the activation reaction was conducted at room temperature instead of at 40°C (Fig. 3.7). As can be seen, the activation rate of beads incubated at pH 8 was significantly reduced at room temperature as compared to 40°C (Fig. 3.7A). However, when we activated beads at pH 9 at room temperature instead of 40°C the aforementioned decrease in activation due to polymerization was absent (Fig. 3.7B); with all other conditions equivalent, the beads activated at pH 9, RT showed an increasing activation level for the entire 6 hour-duration of incubation.
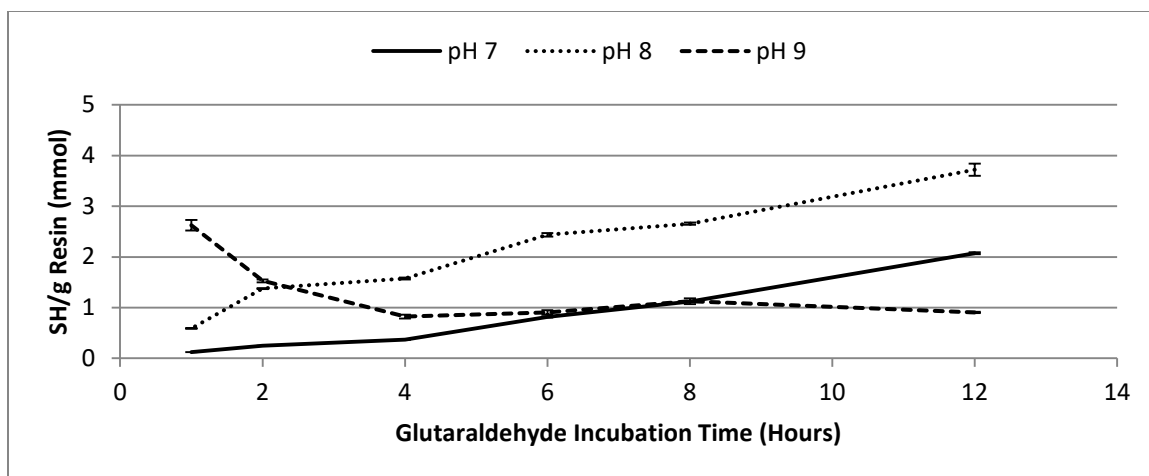

63
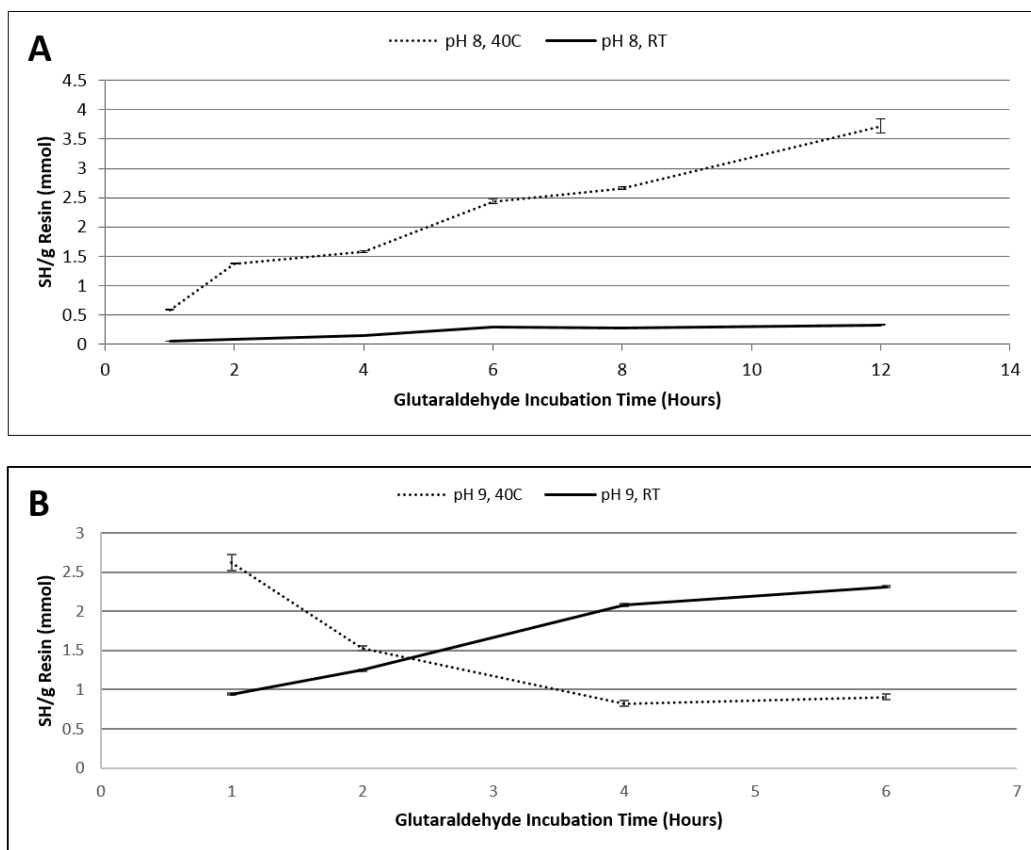
Figure 3.7. Activated aldehyde conjugation to polyacrylamide resin increases with increasing incubation temperature. Bio-Gel P6 beads were incubated for the indicated times in the presence of 20% glutaraldehyde and 0.5M Britton-Robinson buffer, at pH 8 (**A**) or pH 9 (**B**) at either room temperature or 40°C. After incubation the resin was washed extensively with PBS, then incubated with 2M $Na_2S_2O_3$ overnight. Thiolated resins were reduced with 0.5M tris(carboxylethyl)phosphine, then washed extensively. 1 mg of resin was added to 1 ml of 5,5'-dithio-bis-(2-nitrobenzoic acid) assay solution, allowed to equilibrate for 30 minutes, then measured at $\lambda=405$ nm to determine thiol content. Bars represent mean thiol content $\pm$ SD, n=3.

These results indicated that the activation conditions could be tailored depending upon the desired endpoint. Within the efficacious pH range (7-9) activation would, in a time-dependent manner, result in an increase in bead wall thickness. This increase was both pH-dependent, with thickening occurring faster at more alkaline pH, and time-dependent. Additionally carrying out the reaction at elevated temperature resulted in increased activation for pH 7-8, while it caused very rapid activation and, eventually, inactivation at pH 9.

These results indicated that the activation conditions which caused the least alterations to bead macrostructure was determined to be long-duration incubations (12 hours or more) at neutral pH. However for our reductant resins we chose instead to activate for 4-hours at pH 8/37° C. The reasoning behind this decision was that these incubation conditions were the best compromise between activation time, glutaraldehyde loading, and macroscale alterations; the use of these conditions meant that all synthesis steps for a reducing resin could be conducted in a single workday with the resin ready to use the following day.

The activated polyacrylamide was used to synthesize a panel of different reductant resins, the structures of which are reviewed in Fig. 3.1. These resins included

thiopropyl-polyacrylamide (SH-PAAm), dithiothreitol-polyacrylamide (DTT-PAAm), tris(hydroxypropyl)phosphine-polyacrylamide (THPP-PAAm), tris(carboxyethyl)phosphine-polyacrylamide (TCEP-PAAm), and mercaptoethylamine-polyacrylamide (MEA-PAAm). As shown in Table 2.1, the conjugation rate for the monothiol SH-PAAm was far higher than that of the dithiol DTT-PAAm or either of the two phosphine-based resins. Some of the discrepancy observed in conjugation rates between the monothiol and other resins could be due to reaction issues, as both DTT and THPP conjugation rates were likely lowered in part due to acid-catalyzed acetal hydrolysis. Additionally the reductant molecules could potentially bind to two aldehydes (forming hemiacetals for DTT and THPP, and large crosslink structures for TCEP). Despite this difference in conjugation the reducing ability of the resins would be similar, as twice the molar concentration of thiol groups would be needed as DTT or phosphine groups. We therefore expected similar reduction rates between the different resins.

Having developed a panel of different high-capacity reductant resins, we wanted to test whether the substitution of a solid-phase reductant for DTT in RAC was viable. The optimized RAC protocol developed previously was used to investigate total reversible cysteine oxidation in peroxide-exposed BEAS-2B; the protocol was either carried out as described previously with MEA quenching followed by DTT reduction and precipitation, or with the MEA-quenched sample loaded into spin columns containing solid-phase reductant resins. Following reduction the lysate was eluted from the spin columns with centrifugation and immediately loaded into spin columns containing thiopropyl capture resin without intermediate precipitation.

As can be seen in Fig. 3.8, some but not all of the solid-phase reductants were effective replacements for DTT use in RAC. SH-PAAm showed no significant reduction of cysteine thiols. DTT-PAAm showed a similar reduction amount as soluble DTT, while THPP-PAAm caused much higher cysteine reduction that DTT. Interestingly the other phosphine-based reductant used, TCEP-PAAm, was less effective than either DTT or THPP-PAAm in reducing cysteines.

Table 3.1. Synthesized Polyacrylamide-Conjugated Reductant Capacities as Determined by DTNB Assay.

Resin	Conjugated Reductant Amount (mmol/g resin)
PAAM-SH	1.944 ± 0.034
PAAM-DTT	0.702 ± 0.005
PAAM-THPP	0.634 ± 0.004
PAAM-TCEP	0.58 ± 0.004
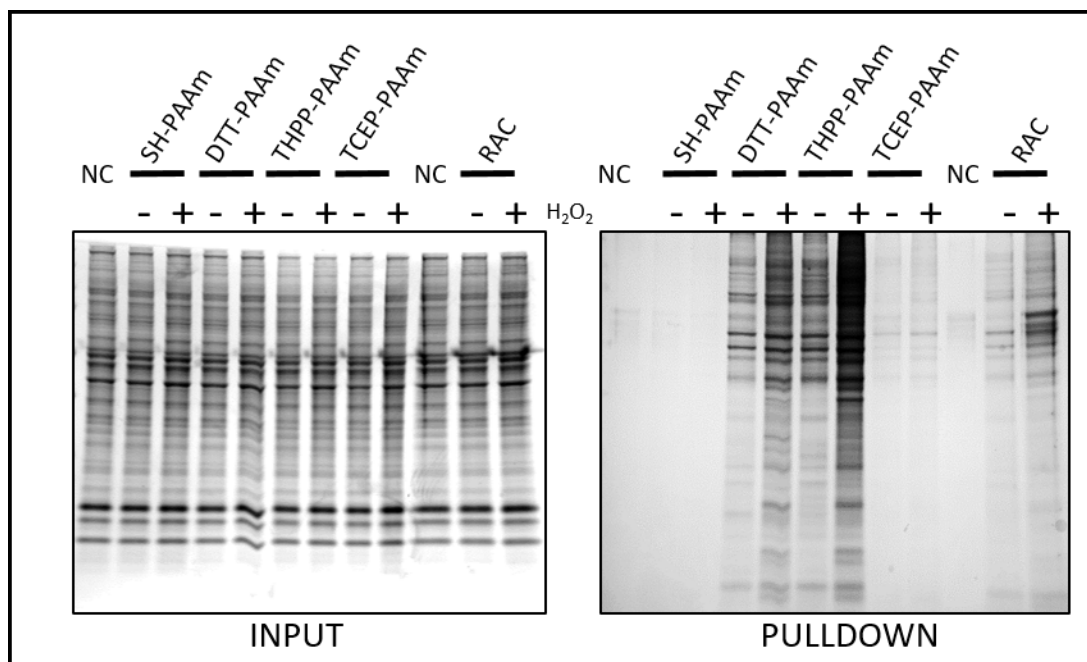
Figure 3.8. Solid-phase reductants are effective replacements for soluble dithiothreitol in resin-assisted capture of oxidized cysteines. BEAS-2B lysates treated with vehicle or 0.5

mM H_2O_2 were processed via the optimized resin-assisted capture (RAC) protocol as described in the Methods. Lanes 1-9 were reduced by the corresponding polyacrylamide reductant resins, while lanes 10-12 were reduced using dithiothreitol in a conventional optimized RAC using a precipitation step to remove the reductant post-reduction. Equivalent amounts of reduced whole cell lysates as determined by bicinchoninic acid assay were loaded onto thiopropyl-sepharose columns to capture oxidized proteins, washed, and eluted (RAC pulldown). The lanes on the left side of the figure were loaded with 5 μg of reduced whole cell lysate (INPUT), and the lanes on the right side of the figure were loaded with 20 μl of eluate (PULLDOWN) containing only oxidized proteins from each treatment. NC indicates samples which were alkylated with N-ethylmalemide but not reduced as a negative control for thiopropyl capture. The gels were visualized after electrophoresis using Coomassie G-250. SH-PAAm: thiopropyl-polyacrylamide. DTT-PAAm: dithiothreitol-polyacrylamide. THPP-PAAm: tris(hydroxypropyl)phosphine-polyacrylamide. TCEP-PAAm: tris(carboxyethyl)phosphine-polyacrylamide.

The difference between the resins were not entirely unexpected, although the intensity of the differences were interesting. Since the reducing group in SH-PAAm is mercaptopropylamide, the pK_{SH} of the thiol would be ~ 10.10 (Table 1.1), meaning that it was predicted to be a poor reductant at the reaction pH of 6.5. However the dramatic differences between the two phosphines was unexpected although easily explained. Since TCEP is conjugated to the polyacrylamide via an amide linkage it could be conjugated with up to three separate acrylamide molecules (Fig. 3.9A-C), thereby inducing structural impediments to easy cysteine access. Since THPP is instead conjugated via an acetal (Fig. 3.9D) it would not have the same conformational issues; if the THPP molecule bound to two or more acrylamides it would form unstable hemiacetals instead (Fig. 3.9E-F), which would be hydrolyzed in solution.

The increased reactivity of the THPP resin is likely due to its higher efficiency as a reductant at low pH than DTT [98]. This is most likely the case as the difference in cysteine oxidation between control and peroxide-treated resins was similar for both DTT-

PAAm and THPP-PAAm. However the increased cysteine reduction for THPP-PAAm may also been caused by phosphine-induced anti-Michael reactions with maleimide, as trialkylphosphines have been previously shown to act as Michael acceptors and undergo maleimide conjugation via Michael reaction [99]. Because of this potential side reaction we sought to develop a thiol-based reductant resin with an efficiency similar to THPP-PAAm which would reduce the risk of anti-Michael reactions at acidic pH.
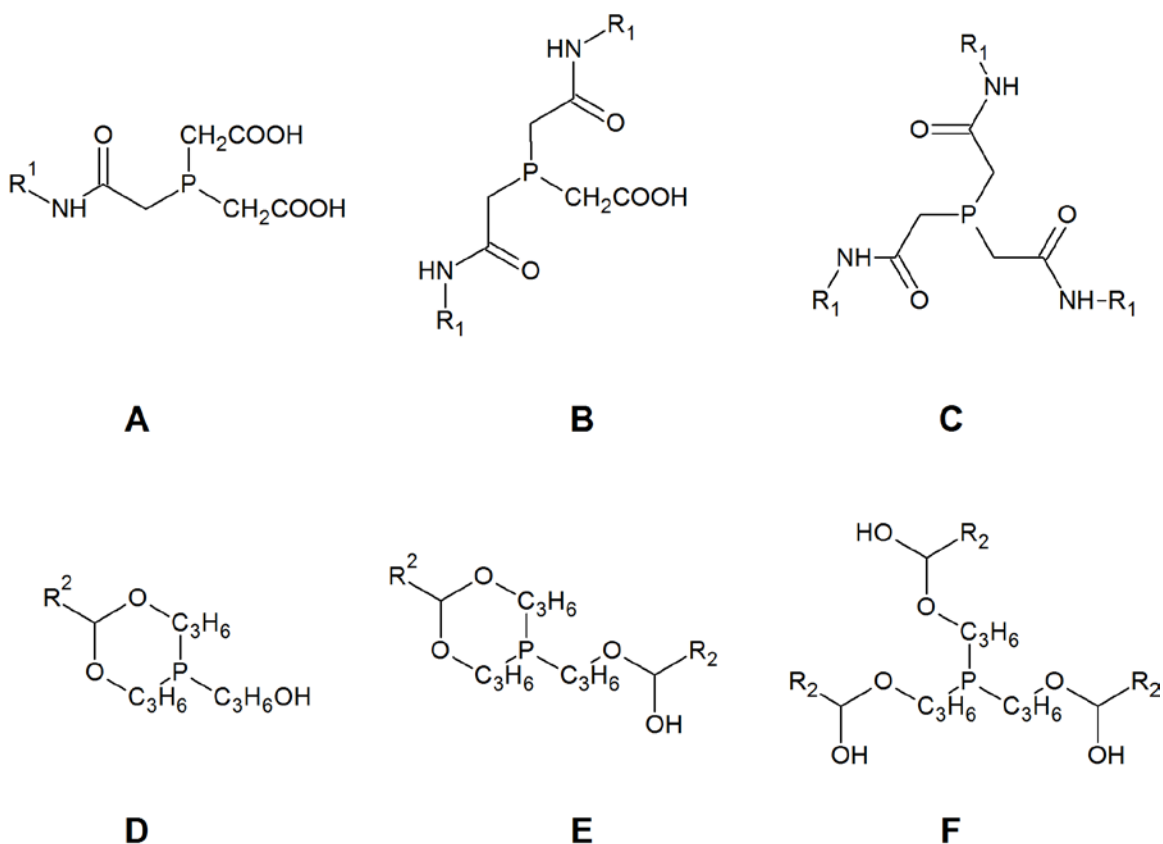
Figure 3.9. Possible conjugation arrangements for phosphine-conjugated polyacrylamide resins. (**A-C**) TCEP-acrylamide conjugation arrangements. R^1 = $CH_2CONHC_5H_{10}NHCOCH_2$-PAAm. (**D-F**) THPP-acrylamide conjugation arrangements. $R^2 = C_4H_8NHCOCH_2$-PAAm.

As discussed previously the highly-substituted monothiol resin SH-PAAm was an ineffective thiol reducing resin. However previous studies utilizing monothiol-agarose were able to achieve effective cysteine reduction [85, 100], indicating that a highly-substituted monothiol-polyacrylamide could be a viable reducing agent. Since thiol-based reductants need to have a high percentage of unprotonated thiolates at a given reaction pH in order to be effective reductants, we hypothesized that by decreasing the pK_{SH} of the monothiol-polyacrylamide we might be able to arrive at an effective monothiol reductant resin for our system.

We therefore took advantage of aldehyde-amine reactivity to generate mercaptoethylamine-conjugated resins (MEA-PAAm) (Fig. 3.1.3). We compared SH-PAAm's and MEA-PAAm's effectiveness in reducing oxidized cysteines. In parallel we added a small molar percentage of selenocysteamine (SeCys) to each reaction to see whether adding a selenol electron-relay catalyst might improve the reducing efficiencies of the monothiol resins by permitting easier access to reductant monothiols buried within the macroporous polyacrylamide resin [101]; as the polyacrylamide resin excludes molecules larger than 6,000 MW this means that any reductant monothiols in the interior of the polyacrylamide beads are inaccessible to proteins but not small molecules.

	INPUT		NC	SH-PAAm				MEA-PAAm			
0.5 mM H_2O_2	-	+	-	-	+	-	+	-	+	-	+
1 mM SeCys	-	-	-	-	-	+	+	-	-	+	+
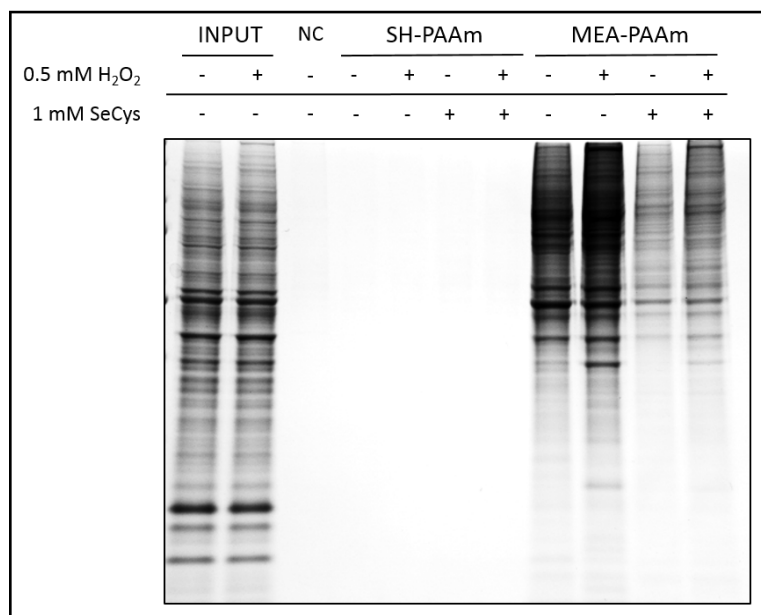
Figure 3.10. Comparison of SH-PAAm and MEA-PAAm as solid-phase reductants. BEAS-2B lysates treated with vehicle or 0.5 mM H_2O_2 were processed using the modified solid-phase reductant RAC technique previously described. Identical fractions of the same control and peroxide-treated samples were reduced with either thiopropyl-polyacrylamide (SH-PAAm) or mercaptoethylamine-polyacrylamide (MEA-PAAm) with or without selenocystamine (SeCys) addition. Lanes 1-2 (input) were loaded with 5 μg of RARC-processed whole-cell lysate from the indicated treatments, reflecting the total amount of each protein in the lysate. Lane 3 was loaded with 5 μg of whole-cell lysate which had been blocked with N-ethylmaleimide but not reduced, representing a negative control for thiopropyl-sepharose capture. Lanes 4-11 (pulldown) are eluate obtained from loading the SH-PAAm- and MEA-PAAm-reduced whole-cell lysates onto thiopropyl-sepharose to capture oxidized-cysteine containing proteins, reflecting only the amount of each protein containing reversibly-oxidized cysteines. NC indicates samples which were alkylated with N-ethylmalemide but not reduced as a negative control for thiopropyl capture. After elution from thiopropyl resin the samples were loaded onto 12% Bolt gels, electrophoresed using Bis-Tris, and visualized after electrophoresis using Coomassie G-250.

As predicted MEA-PAAm was far more effective than SH-PAAm as a reducing

agent in all scenarios tested (Fig. 3.10). Whereas SH-PAAm caused little to no reduction

of oxidized cysteines in our system, MEA-PAAm exhibited reduction capacities similar

to that seen with THPP-PAAm. Interestingly though the addition of SeCys to the system

decreased the amount of reduced cysteine for MEA-PAAm, although it did preserve the difference between control and peroxide-treated samples. This could be due to SeCys not acting as a relay catalyst between monothiol reductants within the interior of the reducing resin, but instead competing with oxidized protein cysteines for reduction.

Conclusions

The major limitation to a precipitation-free RAC technique is the need to remove the reductant from the system following cysteine reduction. Any remaining reductant, whether thiol or phosphine, would interfere with the downstream capture of previously-oxidized cysteines by thiopropyl-sepharose. This could be avoided by the use of a solid-phase reductant instead, as the sample could be separated from the reducing agent by simply removing the supernatant from the resin through centrifugation. Replacement of DTT as the reducing agent in the RAC technique with a solid-phase reductant would simplify and speed up the technique by avoiding time-consuming, user-intensive, and potential risky reductant removal.

Unfortunately due to the limitations of the RAC technique a viable solid-phase reductant resin did not previously exist. While there are commercially-available reducing resins, the capacity of these resins is far lower than what is needed for spin-column reduction of RAC samples. Highly-substituted monothiol-agarose as a reducing agent was possible, but the described substitution rates needed for the agarose are difficult to achieve through the epoxide-based synthesis route.

We therefore sought to develop polyacrylamide-based reducing resins, since

PAAm provided both the conjugation rate necessary as well as versatility in the

conjugated resin desired through PAAm-glutaraldehyde conjugation. After determining

the optimal reaction conditions for PAAm-glutaraldehyde conjugation, we developed a

range of solid-phase reductant resins based on this activated-aldehyde resin. Several of

these resins worked as well as if not better than DTT when substituted into the RAC

workflow; DTT-PAAm showed cysteine reduction levels similar to soluble DTT, while

both THPP-PAAm and MEA-PAAm showed higher cysteine reduction that DTT.

The use of these resins in a *Resin-Assisted Reduction and Capture* (RARC)

technique allowed the streamlining of the procedure by avoiding the aforementioned

precipitation steps. Therefore we were able to accomplish the entire RARC processing

from sample lysis through to electrophoresis and staining in a single 8-hour workday.

This is a significant reduction in the processing time needed as compared to the

conventional RAC technique, with no perceivable loss in signal fidelity. Additionally the

synthesis of all required compounds to accomplish RARC can be easily carried out in a

conventional biology lab setting, since the resin uses only commonly-available materials

and equipment. We therefore anticipate that RARC will become a useful technique for

the study of reversible cysteine oxidation in signaling and disease in the future.

Chapter 4 : APPLICATION OF THE OPTIMIZED RESIN-ASSISTED REDUCTION AND CAPTURE METHOD FOR THE STUDY OF METAL-INDUCED CYSTEINE OXIDATION.

Background

Heavy Metal Induced Oxidative Stress

Oxidative stress is a disease state caused an imbalance between reactive oxygen species (ROS) or reactive nitrogen species (RNS) and antioxidants within the cell. This can be caused either by an increase in production of ROS and RNS, or by a decrease in the amount or activity of antioxidant compounds or enzymes. ROS and RNS production in the cell occurs naturally due to cell processes, such as metabolism, innate immunity, and cell signaling. In order to prevent these ROS and RNS from damaging the cell, cellular antioxidants are present to react with and detoxify these reactive species. In the absence of cellular antioxidants, however, ROS and RNS can react with cellular proteins, lipids, and nucleotides, inducing oxidative damage. This damage can include lipid peroxidation, protein oxidation, and DNA oxidative damage and mutation.

The transition metals arsenic, cadmium, and chromium have been shown to induce cellular oxidative stress. The mechanisms for metal-induced oxidative stress can be categorized as either *redox-active* or *redox-inactive*. Redox-active mechanisms involve the generation of ROS directly through metal-catalyzed reactions, whereas redox-inactive mechanisms involve the inhibition or inactivation of cellular antioxidants.

Haber-Weiss-like reactions are two-step reactions which generate hydroxyl

radical from superoxide and hydrogen peroxide. In the first step, a metal M^n is reduced

by superoxide [Eq. 1]. This reduced metal M^{n-1} is then oxidized by hydrogen peroxide to

generate a hydroxide ion and hydroxyl radical, as well as regenerating the original metal

valence in a Fenton-like reaction [Eq. 2]. The net reaction from these two steps is the

generation of hydroxide ion and hydroxyl radical from superoxide and hydrogen peroxide

through a catalytic metal redox-shuttling [Eq. 3].

[1] $\quad M^n + \cdot O_2^- \rightarrow M^{n-1} + O_2$

[2] $\quad M^{n-1} + H_2O_2 \rightarrow \cdot OH + OH^-$

[3] $\quad \cdot O_2^- + H_2O_2 \rightarrow \cdot OH + OH^- + O_2$
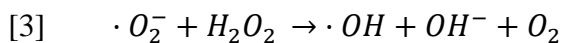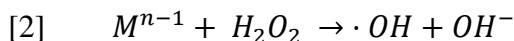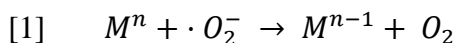
The requirement for a metal to be a Haber-Weiss-like catalyst is the existence of multiple

stable non-zero valence states for that metal. Thus chromium, which has the valence

states (II), (III), (IV), (V), and (VI), is an excellent Haber-Weiss-like catalyst [102].

Additionally arsenic, which has the stable valence states (III) and (V), can also generate

hydroxyl radicals through a Haber-Weiss-like reaction.

In addition to the Haber-Weiss-like reaction, metals which only have one stable

non-zero valence state such as cadmium can generate radicals through a non-Fenton-like

disproportionation reaction [103]. In this multistep reaction an H_2O molecule in the

metal-aqua complex is substituted for H_2O_2 [Eq. 4], the coordinated H_2O_2 undergoes

protolysis to generate a hydronium ion [Eq. 5], a second H_2O_2 substitution [Eq. 6], and

peroxide bond cleavage [Eq. 7], followed by rehydration of the complex [Eq. 8-9]. The

net reaction from these steps is to generate a hydroxyl and peroxyl radical from hydrogen peroxide [Eq. 10].

[4] $\quad [M(H_2O)_n]^{2+} + H_2O_2 \xrightarrow{-H_2O} [M(H_2O)_{n-1}(H_2O_2)]^{2+}$

[5] $\quad [M(H_2O)_{n-1}(H_2O_2)]^{2+} + H_2O \xrightarrow{-H_3O^+} [M(H_2O)_{n-1}(OOH)]^+$

[6] $\quad [M(H_2O)_{n-1}(OOH)]^+ + H_2O_2 \xrightarrow{-(m-1)H_2O} [M(H_2O)_{(n-m)}(H_2O_2)(OOH)]^+$

[7] $\quad [M(H_2O)_{(n-m)}(H_2O_2)(OOH)]^+ \rightarrow [M(H_2O)_{(n-m)}(OH)(\cdot OOH)]^+ + \cdot OH$

[8] $\quad [M(H_2O)_{(n-m)}(OH)(\cdot OOH)]^+ \rightarrow [M(H_2O)_{(n-m)}(OH)]^+ + \cdot OOH$

[9] $\quad [M(H_2O)_{(n-m)}(OH)]^+ + H_3O^+ + (m-2)H_2O \rightarrow [M(H_2O)_n]^{2+}$

[10] $\quad [M(H_2O)_n]^{2+} + 2H_2O_2 \rightarrow [M(H_2O)_n]^{2+} + \cdot OH + \cdot OOH$
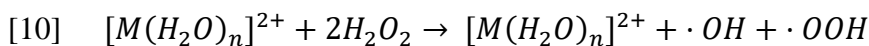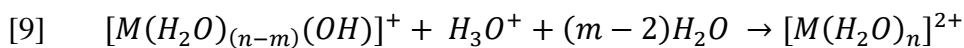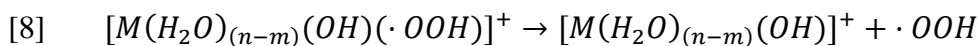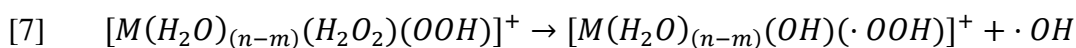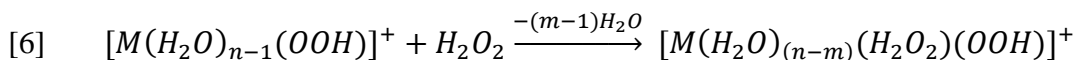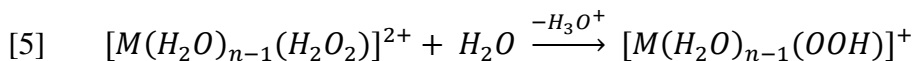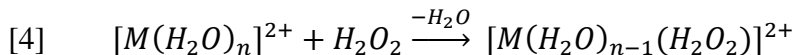
In addition to these redox-active mechanisms, arsenic, cadmium, and chromium also have redox-inactive mechanisms for inducing oxidative stress. These metals induce the generation of ROS indirectly by stimulating NADPH oxidase (NOX) activity. NOXs are a primary source of endogenous ROS; As their name suggests they oxidize NAPDH to generate superoxide radicals, which undergo dismutation to form hydrogen peroxide. As(III), Cr(VI), and Cd(II) have all been shown to upregulate both NOX expression and activity, leading to an increase in NOX-catalyzed ROS production [104-108].

Metal-induced cysteine oxidation can also occur through non-ROS-mediated pathways. All three metals have also been shown to directly interact with cysteine thiols through the formation of metal-thiolate complexes. As(III) and Cd(II) have both been

shown to preferentially displace zinc from zinc-binding motifs such as ZNF domains due to the increased affinity these metals have for thiolates [109]. Under physiological conditions Cd(II) interacts with cysteine at a 1:1 or 1:2 Cd(II):Cys molar ratio, although higher molar ratios have been observed at high cysteine:Cd(II) ratios and alkaline pH [110-113]. As(III) can bind to cysteine at up to a 1:3 molar ratio, giving a potential range of thiolate complexes from As(SCys) to As(SCys)$_3$ [114]. Cr(VI) forms Cr(VI)-thioester groups with cysteine [115] alone or in concert with adjacent carboxylic acids [116]. Additionally trivalent chromium (Cr(III)) generated through chromate reduction *in vitro* has been shown to form Cr(III)-Cys-DNA adducts [117-119].

In addition to metal-thiolate complex formation, these heavy metals can also induce cysteine oxidation directly through metal-cysteine binding. Both arsenic and cadmium form disulfide bonds between vicinal thiols, which has been used experimentally to block enzyme active-site cysteines [120, 121].

Metal-Thiol Interactions

Given the significant interaction between As(III), Cr(VI), and Cd(II) and thiols by both ROS-mediated oxidation and direct metal-thiol binding, it would stand to reason that cysteine oxidation plays a role in cellular toxicity induced by these metals.

Arsenic

As mentioned previously arsenite binds to vicinal dithiols to form either a thiolate complex or a disulfide through a redox reaction. Studies using the immobilized arsenite-containing resin *p*-aminophenylarsine oxide-sepharose to isolate proteins which bind to arsenic via metal thiolate formation found that calcineurin (CAN), heat shock protein 27

(HSP27), galectin-1 (GAL1), triose phosphate isomerase (TPI), thioredoxin (Trx), protein phosphatase 2A (PP2A), and glutathione s-transferase P1 (GSTP1) all bound to arsenite [120-123]. Additionally *in vitro* studies found that arsenic either bound directly to or oxidized multiple proteins, including metabolic proteins like pyruvate kinase M2 (PKM2), DNA repair proteins like PARP1, heat shock factors like heat shock 70 kDa protein 9 (HSPA9), and translation machinery including 60S acidic ribosomal protein P0 [124-126].

Chromium

Chromium has been shown to oxidize several antioxidant proteins *in vitro*. These include peroxiredoxins (PRXs), thioredoxins (TRXs), and the thioredoxin-reducing enzyme thioredoxin reductase (TxR) [127-129]. As mentioned previously Cr(VI) has been shown to generate Cr(VI)-Cys-DNA complexes.

Cadmium

Cadmium has been shown to oxidize TRXs *in vitro* [130]. Redoxomic studies of both cytotoxic and noncytotoxic cadmium concentrations using isotope-coded affinity tagging (ICAT) experiments have shown that cadmium has several protein cysteine oxidative targets both *in vivo* and *in vitro*. These targets include metabolic proteins, primarily those involved in amino acid and lipid metabolism [131], as well as proteins involved in translation, stress response, and the actin cytoskeleton [132].

Despite this evidence for cysteine oxidation by As(III), Cr(VI), and Cd(II), to date no studies have compared the three metals to determine similarities and differences between their oxidative targets. Given the significant overlap in protein interaction for

these metals, we would expect that all three metals would share a common pool of cysteine oxidative targets with some possible variability between them due to differences in ROS generation and direct thiol conjugation. As such we felt that investigating metal-induced cysteine oxidation *in vitro* would be an excellent test of the resin-assisted reduction and capture method's ability to study complex cysteine oxidants in a cellular environment.

Materials and Methods

Materials. Cell culture medium (Gibco DMEM+GlutaMAX, Gibco 10569), HBSS pH 7.4 (Gibco 14025), PBS pH 7.4 (Gibco 10010), screw cap microcentrifuge spin columns (Pierce 69705), and Hypersep C18 micropipettes (Thermo Scientific 60109-209) were purchased from Thermo Fisher Scientific (Waltham, MA). Trypsin Gold was from Promega (Madison, WI). Thiopropyl-sepharose 6B, mercaptoethylamine-polyacrylamide, and tris(hydroxypropyl)phosphine-polyacrylamide resins were synthesized as described previously using sepharose 6B (Aldrich 6B100, Lot# MKCG3369) (Millipore Sigma, St. Louis, MO) and Bio-Gel P6DG (Bio-Rad 150-0738 Lot# 64053706) (Bio-Rad, Hercules, CA). 0.1M sodium arsenite solution (RICCA 714232 Lot# 4603949) and cadmium chloride (Aldrich 202908 Lot# 11026JH) were purchased from Millipore Sigma (St. Louis, MO). DMPO (5,5-dimethyl-1-pyrroline n-oxide, TCI D2362 Lot# YPZIA-CG), MTT (VWR 0793 Lot# 0646C193), and N-ethylmaleimide (Alfa Aesar 40526 Lot# P290042), and sodium chromate (Alfa Aesar A10547 Lot# 10161596) were from VWR (Radnor, PA).

The following antibodies used were from Santa Cruz Biotechnology (Santa Cruz, CA): mouse anti-eEF2 (C-9), mouse anti-SOD1 (G-11), mouse anti-NNMT (G-4), mouse anti-vimentin (V-9), and mouse anti-PRDX5 (H-5). The following antibodies used were from Cell Signaling Technology (Danvers, MA): rabbit anti-GAPDH (D16H11), rabbit anti-PKM1/2 (C103A3). Rabbit anti-DJ1/PARK7 (EP2815Y) was from Abcam (Cambridge, MA). Mouse anti-β-actin (AC-15) was from Millipore Sigma. Anti-mouse and anti-rabbit near-IR secondary antibodies were from Azure Biosystems (Dublin, CA).

Cell Culture. The immortalized human bronchial epithelial cell line BEAS-2B (ATCC CRL-9609) was cultured in DMEM with 10% FBS, 1% Pen-Strep at 37°C, 5% CO_2 in a humidified incubator. Cells were subcultured prior to confluence and seeded at 3000 cells/cm^2. For experiments the cells were treated at 60-80% confluence, and treated with the concentrations of metals described in the figures or deionized water as a vehicle control.

Electron Spin Resonance. BEAS-2B cells were trypsinized, pelleted, washed with charcoal-stripped PBS twice, and resuspended into 0.5 ml CS-PBS at a concentration of $2x10^6$ cells/ml in a microcentrifuge tube. 200 mM DMPO and treatment metals (or PBS as vehicle) were added to the cell suspension, which was then sealed and incubated at 37°C for 10 minutes. Following incubation the cell suspension was transferred to a flat cell and placed in the chamber of an EMXplus (Bruker, MA). Instrument settings were: 40 mW power, 1G modulation amplitude, $6.32 \cdot 10^4$ gain, 40.96s conversion time, 9.76 GHz frequency, 100G scan width, 3505G static field, 100 kHz modulation frequency, 42s scan time, scan number of 9.

Cell Viability Assay. BEAS-2B cells were trypsinized, counted, and plated into 96-well plates at $8 \cdot 10^3$ cells/well in 100 µl cell culture medium and allowed to attach overnight. The medium was aspirated and replaced with DMEM containing the indicated concentrations of FBS; DMEM was added to an additional triplicate set of wells without cells to determine background values. Metals were added to triplicate wells at the indicated concentrations, with PBS used as the vehicle, for a final well volume of 100 µl. The plates were incubated at 37°C, 5% CO_2 for 24-hours, after which 10 µl of MTT solution (5 mg/ml in PBS) was added to each well. The plates were incubated for 2 hours, after which 100 µl solubilization solution (40% DMF, 16% SDS, 2% acetic acid) was added to each well. The plate was mixed by rotational agitation on a plate shaker until formazan crystals were fully dissolved. Absorbance was measured at 570 nm using a BioTek EX800 spectrophotometer.

Prelysis Quenching. Following treatment the cell culture medium was exchanged with HBSS containing NEM (50 mM unless otherwise noted) and incubated briefly. After incubation the HBSS + NEM was removed, the plates were washed 3x with HBSS, the cells were detached from the plate with a cell lifter, collected into 1.5ml tubes, pelleted, and resuspended in degassed lysis buffer.

Lysate Alkylation and Reduction. BEAS-2B cells were lysed in 400 µl of degassed lysis buffer containing 20 mM NEM in opaque 2-ml microcentrifuge tubes. The samples were incubated for 2 hours at RT with gentle end-over-end mixing. 20 mM mercaptoethylamine was then added to the samples to quench the NEM. After quenching for 5 minutes 50 mM DTT was added to reduce oxidized cysteines. After a one-hour

incubation the samples were again precipitated with cold acetone, allowed to incubate

overnight at -20°C, and washed 3x with cold 80% acetone before resuspension for RAC.

Resin-Assisted Reduction and Capture (RARC). Sample pellets were lysed, alkylated, and

quenched for 5 minutes with an equimolar amount of mercaptoethylamine (MEA).

Following quenching the samples were loaded into spin columns containing 35 mg of

buffer-equilibrated MEA-PAAm resin. The columns were sealed and rotated end-over-

end for one hour in the dark at RT. After incubation the columns were unsealed, placed

into clean microcentrifuge tubes, and centrifuged at $13,200 \times g$ for 5 minutes to remove the

sample from the reductant. Samples were then loaded into thiopropyl-resin spin columns

for resin-assisted capture.

On-Resin Digestion and Sample Cleanup. Following protein capture onto thiopropyl-

sepharose, columns were unsealed, placed into receiving tubes, and the nonbound fraction

was eluted by centrifugation at $1,500g$ for 30s and discarded. The columns were then

washed by 3x5 column volumes (CV) of 1% SDS, then 7x5 CV of PBS, 5x5 CV of 30%

acetonitrile (ACN), 0.1% TFA, and 5x5 CV of 30% ACN, 50 mM $NaHCO_3$; the columns

were centrifuged at $1,500g$ for 30s for each wash and the eluate was discarded. After the

last wash the bottom plugs were replaced and 150 µl of 30% ACN, 50 mM $NaHCO_3$

containing 5 ug of trypsin gold (Promega, Madison, WI) was added to each column. The

columns were sealed and allowed to digest overnight at 37°C with end-over-end digestion.

After digestion the columns were unsealed, placed into receiving tubes, and nonbound

peptides and trypsin were eluted and discarded. Columns were washed following the above

sequence. Following the last wash 100 µl of elution buffer (25 mM DTT, 50 mM $NaHCO_3$)

was added to each column. The columns were resealed and incubated for 30 minutes at

RT with rotational agitation, after which the columns were unsealed, placed into methanol-cleaned microcentrifuge tubes, and centrifuged to capture the eluate. This elution procedure was repeated 3x for a final eluate volume of 400 µl. A sufficient volume of IAM was added to each eluate tube to bring the final concentration of IAM to 60 mM. The samples were incubated for 1 hr in the dark at RT to alkylate any free thiols. The eluate was then evaporated by rotary evaporation on a SpeedVac (Savant/Thermo Fisher Scientific, Carlsbad, CA) and the peptide pellet was resuspended in 30 ul of 0.5% formic acid. Peptide samples were cleaned up by Hypersep C18 pipette tips (Thermo Fisher Scientific, Carlsbad, CA) following manufacturer guidelines. Cleaned-up peptide samples were again evaporated using rotary evaporation and resuspended in 10 µl of 0.5% formic acid for LC-ESI-MS/MS injection.

Liquid chromatography-electrospray ionization-tandem mass spectrometry (LC-ESI-MS/MS) Analysis. All mass spectra reported in this study were acquired by the University of Kentucky Proteomics Core Facility. The tryptic peptides were subjected to shot-gun proteomics analysis as previously described in Yang et al. [133]. LC-MS/MS analysis was performed using an LTQ-Orbitrap mass spectrometer (Thermo Fisher Scientific, Waltham, MA) coupled with an Eksigent Nanoflex cHiPLC™ system (Eksigent , Dublin, CA) through a nano-electrospray ionization source. The peptide samples were separated with a reversed phase cHiPLC column (75 µm x 150 mm) at a flow rate of 300 nL/min. Mobile phase A was water with 0.1% (*v/v*) formic acid while B was acetonitrile with 0.1% (*v/v*) formic acid. A 50 min gradient condition was applied: initial 3% mobile phase B was increased linearly to 40% in 24 min and further to 85% and 95% for 5 min each before it was decreased to 3% and re-equilibrated. The mass analysis method consisted of one

segment with eight scan events. The 1st scan event was an Orbitrap MS scan (300-1800 m/z) with 60,000 resolution for parent ions followed by data dependent MS/MS for fragmentation of the 7 most intense multiple charged ions with collision induced dissociation (CID) method.

MS/MS Protein Identification. The LC-MS/MS data were submitted to a local mascot server for MS/MS protein identification via Proteome Discoverer (version 1.3, Thermo Fisher Scientific, Waltham, MA) against a custom database of Homo sapiens (Human) proteins downloaded from Uniprot (number of sequences after taxonomy: 20218). Typical parameters used in the MASCOT MS/MS ion search were: trypsin digestion with a maximum of two miscleavages, cysteine carbamidomethylation, cysteine N-Ethylmaleimide (NEM) modification, cysteine oxidations, methionine oxidation, 10 ppm precursor ion and 0.8 Da fragment ion mass tolerances. A decoy database was built and searched. Filter settings that determine false discovery rates (FDR) are used to distribute the confidence indicators for the peptide matches. Peptide matches that pass the filter associated with the FDR rate of 1% and 5% are assigned as high and medium confident peptides, respectively.

SDS-PAGE. Following metal treatment cell cultures were processed by RARC as described above. Captured samples were eluted in 1x LDS sample buffer (Life Technologies, CA) + 50 mM TCEP, pH 7.0. Eluted pulldown samples and input fractions were loaded onto a Bolt Bis-Tris SDS-PAGE gel (Life Technologies, CA) and electrophoresed in MOPS running buffer at 200V. Once the dye front reached the bottom of the gel cassette the run was stopped.

Western Blotting. Electrophoresed gels were removed from their gel cassette and assembled into a transfer sandwich with 0.45 µm nitrocellulose (Bio-Rad, CA). The transfer sandwiches were rolled out to remove bubbles and loaded into a Hoefer TE-22 tank transfer apparatus (Hoefer) containing Towbin transfer buffer (25 mM Tris, 192 mM glycine, 10% ethanol). The gels were transferred for 1 hour at 400 mA with regenerative cooling. Following transfer the membranes were removed and washed briefly with deionized water, then dried for at least one hour. Membranes were then rehydrated in deionized water, blocked for 1 hour with 5% milk-PBS, washed 3x with PBS+0.1% NP-40 (PBSN), and incubated for 3 hours at RT with primary antibodies in 5% milk-PBSN. The membranes were then washed 3x with PBSN for 5 minutes each, then incubated for 1hour in the dark at RT with NIR-fluorophore secondary antibodies. The membranes were washed 3x with PBSN for 5 minutes each, then washed 3x with PBS. Membranes were imaged at 680 nm and 790 nm using an Azure Biosystems C600 imager. Blot images were converted from multichannel to grayscale using AzureSpot software.

Results and Discussion

Our lab and others have previously demonstrated ROS generation by As(III), Cr(VI), and Cd(II) using ESR in both cell-free and *in vitro* systems. Most EPR measurements for these metals have been conducted using relatively high concentrations of metals (0.1-1 mM), which would far exceed the concentration used for biological studies; these doses would easily overwhelm biological antioxidant systems, and therefore are not necessarily indicative of the metals' capacity to generate ROS in a biologically-relevant system. Therefore we wanted to confirm that measureable ROS

production was observed under lower, biologically-relevant concentrations of metals used in 24-hour toxicity studies.

We measured ROS generation *in vitro* using BEAS-2B cells which had been treated with As(III), Cr(VI), or Cd(II) using electron spin resonance (ESR) spin trapping. This method involves the addition-type reaction of a short-lived radical such as hydroxyl radical with a non-paramagnetic compound (spin trap) to form a relative long-lived resonance-stabilized paramagnetic product (spin adduct) which can be studied using ESR. For our analysis we used the spin trap 5,5-dimethyl-1-pyrroline N-oxide (DMPO). DMPO is a nitrone-containing compound which reacts with hydroxyl radical to form a resonance-stabilized product DMPO-·OH. While DMPO is non-paramagnetic, DMPO-·OH is a paramagnetic compound which is detectable via ESR; therefore measurement of DMPO-·OH by ESR can be used to measure relative hydroxyl radical levels in the sample.

We treated BEAS-2B cells with As(III), Cr(VI), and Cd(II) for 10 minutes in the presence of DMPO, then measured the resulting levels of the DMPO-·OH spin adduct using ESR. The results of this experiment are in Fig. 4.1. Arsenic did not generate detectable levels of hydroxyl radical after a 10-minute incubation. Cadmium caused a small increase in hydroxyl radical as compared to BEAS-2B. Chromium generated significantly more hydroxyl radical, an approximate doubling of the DMPO-·OH signal as compared to BEAS-2B.
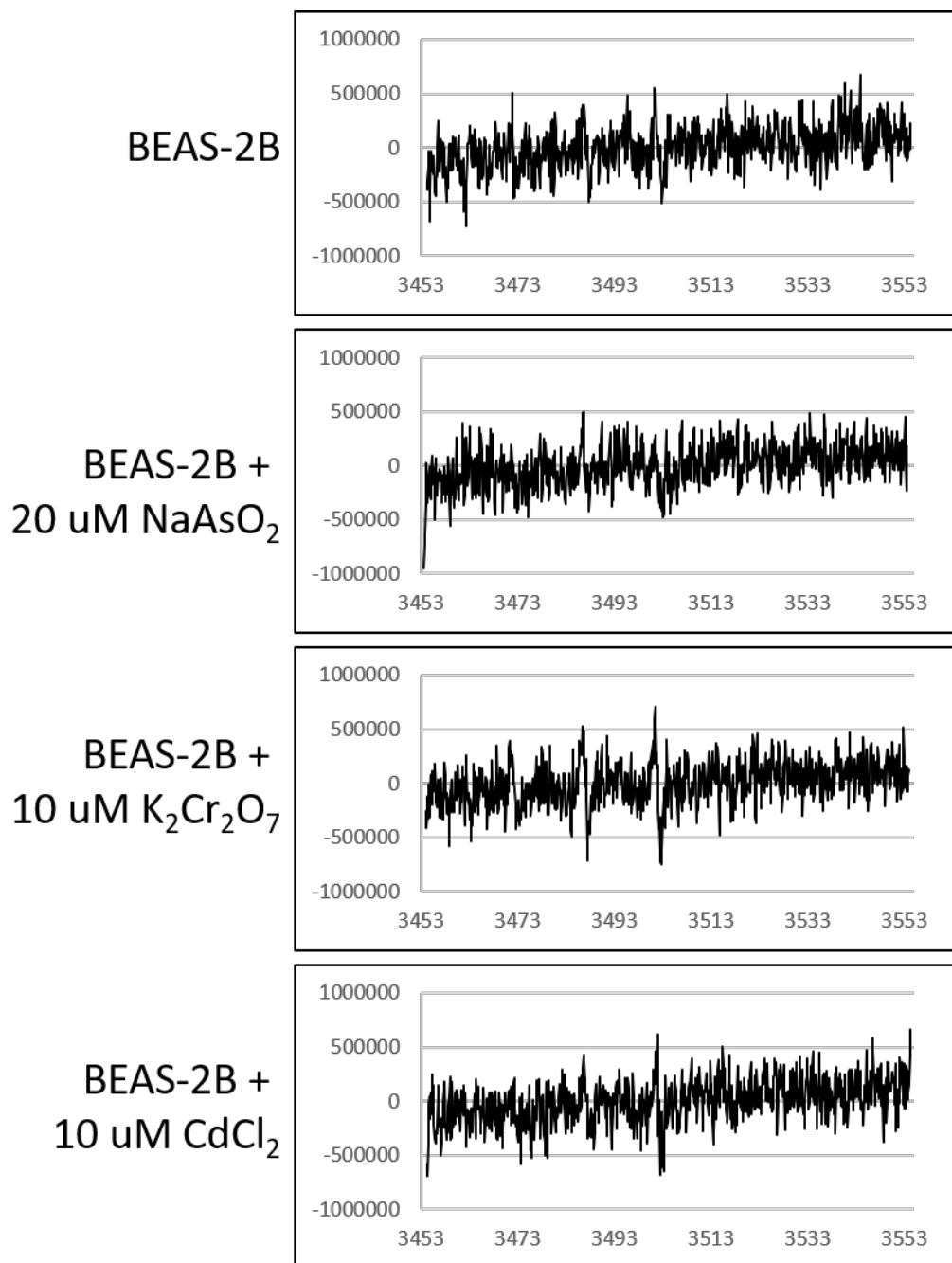
Figure 4.1. Cr(VI) and Cd(II) generate hydroxyl radicals in BEAS-2B cells as measured by electron spin resonance (ESR). BEAS-2 cells were trypsinized, counted, and pelleted, and $1 \cdot 10^6$ cells were resuspended into 0.5 ml of charcoal-stripped PBS in microcentrifuge tubes. The indicated concentrations of NaAsO$_2$, K$_2$Cr$_2$O$_7$, and CdCl$_2$ (or PBS as vehicle) and 200 mM 5,5-dimethyl-1-pyrroline N-oxide (DMPO) spin trap were added to the BEAS-2B suspensions and incubated for 10 min at 37° C. DMPO reacted with hydroxyl radicals in the suspension to form the resonance-stabilized paramagnetic product DMPO-·OH. The cell suspensions were then transferred to a quartz flat cell and ESR spectra was measured using a Bruker EMXplus. Instrument settings were: 40 mW power, 1G

modulation amplitude, $6.32 \cdot 10^4$ gain, 40.96s conversion time, 9.76 GHz frequency, 100G scan width, 3505G static field, 100 kHz modulation frequency, 42s scan time, scan number of 9.

Metal LD_{50} Determination in FBS-Containing Culture Medium. Most previous studies have used similar concentrations of both arsenite and chromate in 24-hour acute-toxicity studies with 20 μM As(III) and 20 μM Cr(VI) being commonly used as the LD_{50} for these metals. However the concentrations of cadmium used have varied widely between different research studies, with anywhere from 10-50 μM Cd(II) being used as an LD_{50} in 24-hour exposure studies [134, 135]. This discrepancy between reported *in vitro* LD_{50} can be partly explained by different studied cell lines and varying media compositions. As such it was important to reconfirm or determine the dose-dependent response to these metals in the BEAS-2B immortalized human bronchial epithelial cell line.

Additionally the prior studies had utilized serum-starvation conditions during metal treatment. Serum-starvation is known to generate oxidative stress [136]. Since starvation-induced oxidative stress could raise background cysteine oxidation levels, we wanted to avoid this by treating BEAS-2B cultures under normal culture conditions to avoid exogenous stressors. As such we conducted a viability assay to determine the 24-hour LD_{50} for As(III), Cr(VI), and Cd(II) under differing medium serum compositions.

The results of this experiment are in Fig. 4.2. Both arsenic and chromium showed a fairly consistent toxicity profile independent of the presence of serum in the medium, with As(III) and Cr(VI) LD_{50}s of 25.8 μM and 20 μM respectively. However cadmium toxicity was highly dependent upon medium serum concentration, with the LD_{50} for Cd(II) ranging from ~24.5 μM in serum-free DMEM to 53.9 μM in 10% FBS-DMEM.

Since cadmium uptake intracellularly has been previously found to be serum-dependent in *in vitro* cell cultures [137-139], we would expect some variance in cadmium-induced cell toxicity due to the presence of serum components since albumins and metallothioneins contained in FBS may be binding to and preventing Cd(II) uptake by BEAS-2B cells.

However both 5% FBS and 10% FBS showed similar toxicity profiles indicating that this difference is not solely due to serum protein binding or chelation of cadmium, as presumably the increased concentration of serum proteins at 10% FBS would cause a further decrease in cadmium concentration available for cellular uptake. Since this inhibitory effect is not solely due to serum protein concentrations, it is most likely due to a combination of the presence of Cd(II)-binding serum proteins and to serum-induced cell signaling effects influencing cellular uptake of Cd(II).

Given the 24-hour viability results, we chose to use 5% FBS-DMEM for all following treatments. This would, as mentioned previously, reduce or eliminate exogenous stressor-induced oxidative stress. Additionally it would prevent cadmium-induced toxicity caused by serum-starvation induced cell signaling pathway disruptions.
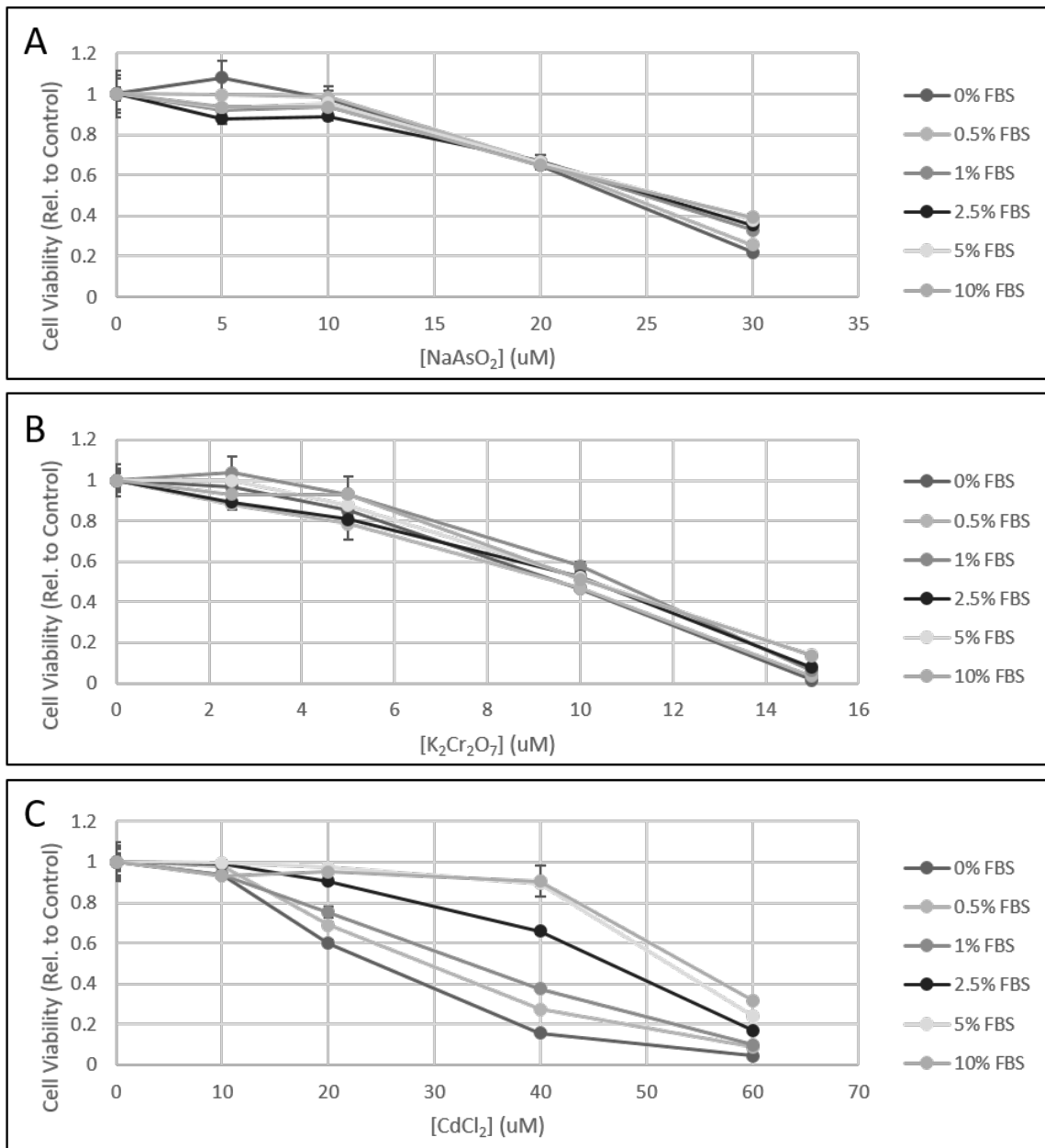
Figure 4.2. 24-hour cell viability measurement for dose-course exposures to As(III), Cr(VI), and Cd(II). BEAS-2B cells in triplicate wells were treated with the indicated concentrations of NaAsO2 (**A**), $K_2Cr_2O_7$ (**B**), $CdCl_2$ (**C**) or PBS vehicle with or without the indicated concentrations of FBS and incubated for 24 hrs. Cell viability following treatment was determined using the MTT assay as described above. Relative cell viability was determined by dividing the average OD_{562} for each treatment concentration by the OD_{562} of the corresponding non-treated vehicle controls. Statistical analysis was performed using Microsoft Excel. Data points represent average relative viability, n=3.

Measurement of Reversible Cysteine Oxidation Caused by Metal Exposure. Having

determined both the generation of ROS by As(III), Cr(VI), and Cd(II), as well as their

$LD_{50}s$ for BEAS-2B in serum-containing medium, we wanted to determine whether these

metals could induce significant reversible cysteine oxidation *in vitro*. Furthermore we

wanted to investigate the RARC methodology's utility in detecting cysteine oxidation

caused by complex oxidants in an experimental setting.

We treated BEAS-2B cultures with metals for 24 hrs and used the RARC method

to measure the resulting levels of reversible cysteine oxidation. The results of this

experiment are in Fig. 4.3. Reversible cysteine oxidation increased in a dose-dependent

manner for all three metals. Since arsenic and cadmium generated lower levels of

hydroxyl radical than chromium in our EPR measurements, we would expect that

cysteine oxidation would be higher for chromium than either of the other two metals were

cysteine oxidation be primarily ROS-driven. However the observed increase was more

pronounced for both arsenic and cadmium than chromium.

Since both arsenic and cadmium can form metal-catalyzed disulfide bridges, this

would be consistent with the observed increases caused by these metals. Therefore the

cysteine oxidation caused by these metals occurs through at least two distinct paths: a

hydroxyl-mediated cysteine oxidation favored by chromium, and a metal-catalyzed

disulfide formation favored by arsenic and cadmium.
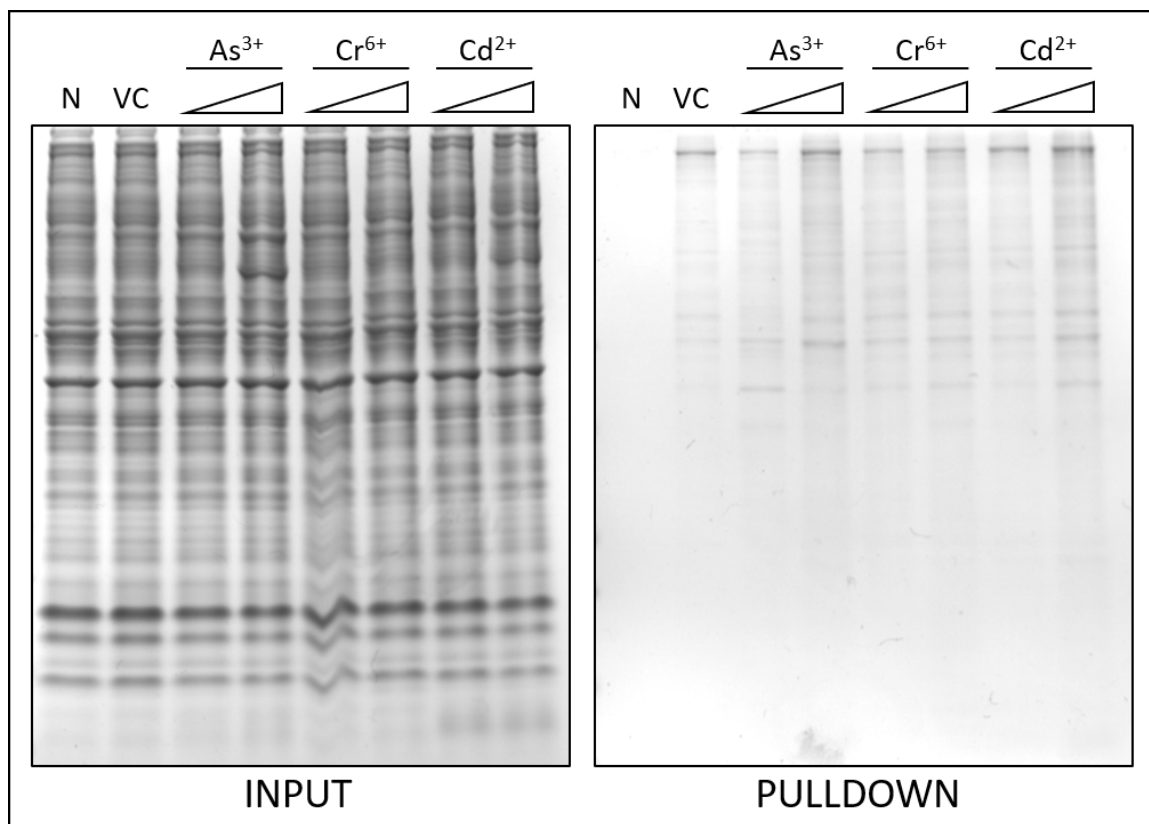
Figure 4.3. The heavy metals As(III), Cr(VI), and Cd(II) induce cysteine oxidation after 24hr treatment. BEAS-2B cultures were treated with sublethal and lethal doses of NaAsO$_2$ (5 or 20 µM), K$_2$Cr$_2$O$_7$ (2.5 or 10 µM), or CdCl$_2$ (40 or 60 µM) for 24 hrs in 5% FBS-DMEM at 37 °C, 5% CO$_2$. Following treatment the cultures were prelysis quenched and processed for RARC as described in the Methods section. Equivalent amounts of reduced whole cell lysates as determined by bicinchoninic acid assay were loaded onto thiopropyl-sepharose columns to capture oxidized proteins, washed, and eluted (RAC pulldown). The lanes on the left side of the figure were loaded with 5 µg of reduced whole cell lysate (INPUT), and the lanes on the right side of the figure were loaded with 20 µl of eluate (PULLDOWN) containing only oxidized proteins from each treatment. N indicates samples which were alkylated with N-ethylmalemide but not reduced as a negative control for thiopropyl capture. Both input and pulldown fractions were loaded onto a 12% Bolt bis-tris gel and electrophoresed using MOPS buffer. The gels were fixed in 10% acetic acid, 50% methanol for 10 minutes, then stained with 0.01% Coomassie G-250 in 10% acetic acid for 30 minutes. Following extensive destaining with deionized water, the gels were imaged using an Azure C600.

Proteomic Analysis of Metal-Induced Reversible Cysteine Oxidation.

While this experiment further reinforced the utility of the RARC method in measuring cysteine oxidation, it did not elucidate what fraction of observed oxidation was caused by ROS or metal catalyzed oxidation. Additionally the identity of the proteins oxidized by these metals was still unknown. Fortunately the RARC method could be adapted to a proteomic workflow by utilizing on-resin trypsin digestion prior to sample elution and cleanup from capture resin; proteomic analysis of the resulting cysteine-containing peptides would tell not only the protein identity, but the exact cysteines oxidized on each protein.

Quadruplicate sets of metal-treated BEAS-2B lysates were processed via RARC and digested on-resin, washed, and eluted for cleanup and proteomic analysis using label-free proteomics. The resulting peptide lists were cleaned up using a peptide ion score cutoff of ≥ 25. These protein lists were collated across the quadruplicate sets, and only proteins which were detected in *at least* three of the four sets were retained. From this collated set a list of proteins which were present in metal-treated samples but not the vehicle control samples was generated (Table 3.1), along with the cysteines oxidized on the proteins by each metal.

Consistent with the results observed in Fig. 4.3, more proteins were oxidized by arsenic and cadmium than chromium. Two sets of proteins were observed between the groups: proteins oxidized by all three metals, and proteins oxidized by arsenic, cadmium, or a combination of these two metals. No proteins were observed to be oxidized by

chromium but neither of the other two metals consistent with the decreased cysteine oxidation by Cr(VI) compared to As(III) and Cd(II).

Metabolic, protein synthesis, and antioxidant proteins were significantly enriched in the metal-oxidized groups. Several of the cysteines identified were known to be ROS-sensitive, as with GAPDH, vimentin, and peroxiredoxins, or metal-binding cysteines, such as metallothionien-2; furthermore several of the identified cysteines are in enzymatic active sites, which would indicate that these metals may be inhibiting enzymatic function through cysteine oxidation. These results indicate that cysteine oxidation may play a role in metal-induced toxicity for As(III), Cr(VI), and Cd(II).

Table 4.1. List of Reversibly-Oxidized Proteins and Specific Cysteines Oxidized by As(III), Cr(VI), Cd(II) by Triplicate Inclusion Criteria

Protein Name	GN	Oxidized Cysteines*		
		Arsenic	**Chromium**	**Cadmium**
Glyceraldehyde-3-Phosphate Dehydrogenase	GAPDH	C152 C156 *C247*	C152 C156 *C247*	C152 C156 *C247*
Elongation Factor 2	EEF2	C41 C466 *C728*	*C41* *C466* C728	C466 C728
Peroxiredoxin-5, Mitochondrial	PRDX5	C204	C204 *C100*	C204 *C100*
60S Ribosomal Protein L30	RPL30	C52 *C92*	C52	C52 *C92*
Vimentin	VIM	C328	C328	C328
Cation-independent mannose-6-phosphate receptor	IGF2R	C134		C134
Peptidyl-prolyl cis-trans isomerase A	PPIA/CyPA	C161 *C62*		C161 *C62* C115
Heat Shock 70 kDa Protein 6	HSPA6	C624 C605		*C308* *C605* *C624*
Metallothionein-2	MT2A	C33 C34 C36 C37 C41 C44 C48 C50		C33 C34 C36 C37 C41 C44 C48 C50
Filamin-A	FLNA	C205 *C1018*		C2543 *C1018*
Superoxide Dismutase [Cu-Zn]	SOD1	C147		C147
Cell Surface Glycoprotein MUC18	MCAM	C161 *C499*		C161
Heat Shock Protein 105 kDa	HSPH1	C34 *C167*		
ADP-Dependent Glucokinase	ADPGK	C415		
60 kDa Heat Shock Protein, Mitochondrial	HSPD1	C442		
Lysosomal Alpha-Mannosidase	MAN2B1	C472		
Complement Component 1 Q Subcomponent-Binding Protein, Mitochondrial	C1QBP	C186		
60S Ribosomal Protein L18	RPL18	C134		
Protein Disulfide-Isomerase A3	PDIA3	C85 C92		
Leucine-Rich Repeat-Containing Protein 59	LRRC59	C277		
Thioredoxin-Domain Containing Protein 5	TXNDC5			C247 *C121*

Specific Cysteines Identified in Fewer Than 3 Replicate Proteomic Runs are Indicated by Italicized Font.

Loosening the inclusion criteria to include all proteins that were identified in duplicate

sets understandably altered the list of proteins oxidized by metals (Table 3.2). While

loosening the criteria would be assumed to just increase the number of proteins identified

across the board, the result was more nuanced. The proteins identified did increase from

21 to 30 in total, but several proteins moved from categories or were omitted under the

revised criteria. PPIA/CyPA and FLNA were reidentified as oxidized by all three metals,

while HSPH1 was oxidized by both As(III) and Cd(II). Several proteins, including

IGF2R, MT2A, SOD1, and ADPGK were excluded from the list of oxidized proteins due

to their identification in two of the four control sets.

For proteins like GAPDH, EEF2, and VIM which were included in the oxidized

set under both criteria, this further reinforced that they should be significantly oxidized

by metals. This is because these proteins showed up in *at least* 3 of the 4 metal-treated

sets, and yet did not show up in 2 of the control sets. Additionally conditionally-

excluded proteins should not be discounted entirely due to their appearance in the control

sets, since the data suggests that they are more likely to be oxidized due to metal

treatment.

Table 4.2. List of Reversibly-Oxidized Proteins Identified by Both Triplicate- and Duplicate-Inclusion Criteria.

Protein Name	GN	Protein Name	GN
Triplicate		Duplicate	
Common to All Metals			
Glyceraldehyde-3-Phosphate Dehydrogenase	GAPDH	Glyceraldehyde-3-Phosphate Dehydrogenase	GAPDH
Elongation Factor 2	EEF2	Elongation Factor 2	EEF2
Peroxiredoxin-5, Mitochondrial	PRDX5	Peroxiredoxin-5, Mitochondrial	PRDX5
60S Ribosomal Protein L30	RPL30	60S Ribosomal Protein L30	RPL30
Vimentin	VIM	Vimentin	VIM
		Peptidyl-prolyl cis-trans isomerase A	PPIA/CyPA
		Calnexin	CANX
		Filamin-A	FLNA
Common to As/Cd			
Cation-independent mannose-6-phosphate receptor	IGF2R		
Peptidyl-prolyl cis-trans isomerase A	PPIA/CyPA		
Heat Shock 70 kDa Protein 6	HSPA6	Heat Shock 70 kDa Protein 6	HSPA6
Metallothionein-2	MT2A		
Filamin-A	FLNA		
Superoxide Dismutase [Cu-Zn]	SOD1		
Cell Surface Glycoprotein MUC18	MCAM	Cell Surface Glycoprotein MUC18	MCAM
		Heat Shock Protein 105 kDa	HSPH1
		Heat Shock Protein 70 kDa 1A	HSPA1A
As Only			
Heat Shock Protein 105 kDa	HSPH1		
ADP-Dependent Glucokinase	ADPGK		
60 kDa Heat Shock Protein, Mitochondrial	HSPD1	60 kDa Heat Shock Protein, Mitochondrial	HSPD1
Lysosomal Alpha-Mannosidase	MAN2B1		
Complement Component 1 Q Subcomponent-Binding Protein, Mitochondrial	C1QBP		
60S Ribosomal Protein L18	RPL18	60S Ribosomal Protein L18	RPL18
Protein Disulfide-Isomerase A3	PDIA3	Protein Disulfide-Isomerase A3	PDIA3

Leucine-Rich Repeat-Containing Protein 59	LRRC59	Leucine-Rich Repeat-Containing Protein 59	LRRC59
Cd Only			
Thioredoxin-Domain Containing Protein 5	TXNDC5		
		Putative Heat Shock 70 kDa Protein 7	HSPA7
		Torsin-1A-Interacting Protein 1	TOR1AIP1
		Myosin-9	MYH9
		Thrombospondin-1	THBS1

We compared the proteomic results for proteins that were identified in both the triplicate and duplicate analyses to both the UniProt Knowledgebase (UniProtKB) and RedoxDB databases, as well as the literature, to determine whether the identified cysteines were known oxidative targets (Table 3.3). We found that many of the cysteines we identified as being oxidized by metals have been previously reported to be oxidized by ROS, further validating our results. We additionally identified several cysteines, including eukaryotic elongation factor 2 (eEF2) C466, 60S ribosomal protein L30 (RPL30) C52 and C92, peptidyl prolyl cis-trans isomerase A (PPIA/CyPA) C161, heat shock 70 kDa protein 6 (HSPA6) C605 and C624, and leucine-rich repeat-containing protein 59 (LRRC59) C277, which have not been previously identified as reactive.

For the known cysteines, several of them have been shown to be involved in ROS-mediated cell signaling or oxidative stress. GAPDH C152 is the active-site thiolate, while mutational studies have shown that C156 facilitates C152 oxidation by ROS through a proton relay; C156S mutants are significantly more resistant to ROS than wildtype [140]. Vimentin C328 acts as an oxidant sensor, reorganizing vimentin cytoskeletal networks in response to oxidative stress [141]. C41 of eukaryotic elongation factor has been previously shown to be hypersensitive to a variety of oxidants [142-144].

Table 4.3. List of oxidized cysteines identified by both triplicate- and duplicate-inclusion analysis and references for known reactive cysteines.

Protein Name	GN	Oxidized Cysteines*	Known Cysteines and References
Glyceraldehyde-3-Phosphate Dehydrogenase	GAPDH	C152 C156	C152, C156: [140]
Elongation Factor 2	EEF2	C41 C466	C41: [142-145]
Peroxiredoxin-5, Mitochondrial	PRDX5	C204	[146, 147]
60S Ribosomal Protein L30	RPL30	C52 *C92*	
Vimentin	VIM	C328	[141]
Peptidyl-prolyl cis-trans isomerase A	PPIA/CyPA	C161	
Heat Shock 70 kDa Protein 6	HSPA6	C308 C624 C605	C308: [145]
Cell Surface Glycoprotein MUC18	MCAM	C161	UniProt Manual Curation
60 kDa Heat Shock Protein, Mitochondrial	HSPD1	C442	[148]
60S Ribosomal Protein L18	RPL18	C134	[145]
Protein Disulfide-Isomerase A3	PDIA3	C85 C92	[149] (Disulfide)
Leucine-Rich Repeat-Containing Protein 59	LRRC59	C277	

Western Blot Validation of Proteomic Results. We selected several of the proteins identified to validate the proteomic results (Fig. 3.4A-D). Consistent with the proteomic results GAPDH, PRDX5, EEF2, and VIM were all increased in metal-treated groups. PRDX5 oxidation was relatively similar between all three metals (Fig. 3.4A). EEF2 was more oxidized by As(III) and Cd(II) than Cr(VI) (Fig. 3.4B), while GAPDH was more oxidized by Cr(VI) than either of the other two metals (Fig. 3.4C). Vimentin was oxidized at low levels by As(III) and Cr(VI) but was strongly oxidized by Cd(II) (Fig. 3.4D).
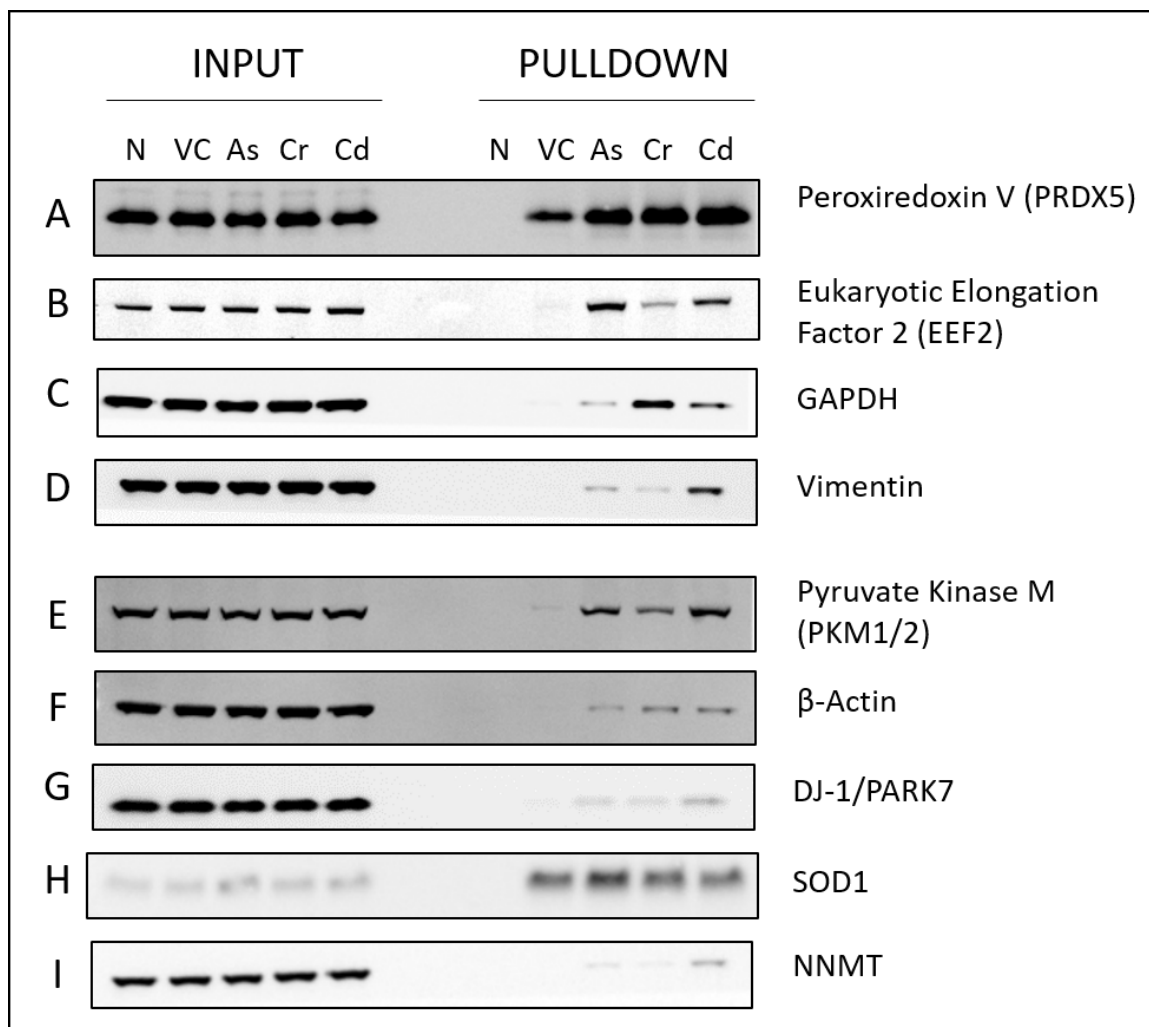
Figure 4.4. Western blot analysis of metal-induced protein cysteine oxidation. BEAS-2B cells were treated with 20 µM NaAsO$_2$, 10 µM K$_2$Cr$_2$O$_7$, or 60 µM CdCl$_2$ for 24 hrs, then quenched, captured via RARC, and immunoblotted as described in the methods. Equivalent amounts of reduced whole cell lysates as determined by bicinchoninic acid assay were loaded onto thiopropyl-sepharose columns to capture oxidized proteins, washed, and eluted (RAC pulldown). The lanes on the left side of the figure were loaded with 5 µg of reduced whole cell lysate (INPUT), and the lanes on the right side of the figure were loaded with 20 µl of eluate (PULLDOWN) containing only oxidized proteins from each treatment. N indicates samples which were alkylated with N-ethylmalemide but not reduced as a negative control for thiopropyl capture. Following SDS-PAGE electrophoresis the gels were transferred to nitrocellulose, blocked with nonfat milk, and probed with antibodies. Near-IR secondary antibodies were used for detection on an Azure C600 using fluorescence. The experiment was done in triplicate.

In addition to the proteins determined to be consistently oxidized by As(III), Cr(VI), and Cd(II), we wanted to probe against some other identified targets that were excluded from the final proteomic results for a variety of reasons. Pyruvate kinase M has been previously shown to be oxidized by arsenite [124]. PKM was identified by our proteomic analysis, but it was present in both control and treatment groups. As seen in Fig. 3.4E, PKM is significantly oxidized by all three metals. Likewise β-actin was significantly oxidized by all three metals (Fig. 3.4F); in this case β-actin *was* identified as being oxidized by the proteomic analysis, but was excluded because the identified peptide was not unique to an individual actin.

As mentioned previously, SOD1 was identified as being oxidized by As(III) and Cd(II) using triplicate-inclusion criteria (Table 3.1) but when duplicate-inclusion criteria was used it was omitted from the list of metal-oxidized proteins(Table 3.2). We therefore wanted to see whether SOD1 was in fact oxidized by As(III) and Cd(II). SOD1 was found to be oxidized in both control and treatment groups, with some increase caused by As(III) (Fig. 3.4H). SOD1 oxidation in the control sample is most likely due to the presence of intramolecular disulfide bridges; this would explain why SOD1 was excluded from the proteomic results once the stringency of analysis was loosened.

Additionally DJ-1/PARK7, a known oxidant-response protein, and nicotinamide n-methyltransferase were identified in a single proteomic run per metal. As seen in Fig. 3.4G and Fig. 3.4I, both proteins were oxidized by As(III), Cr(VI), and Cd(II). Since proteomic analysis by LC-MS/MS has a higher lower limit for detection than western blotting, it is understandable that western blotting can detect lower levels of protein

enrichment than proteomic analysis, at the cost of more time and resources spent probing against single targets.

Conclusions

As(III), Cr(VI), and Cd(II) are cytotoxic heavy metals which cause oxidative stress *in vitro* and *in vivo*.

We used the resin-assisted reduction and capture (RARC) to determine whether metals induced whole-proteome cysteine oxidation *in vitro*, and to identify the proteins oxidized. We found that arsenic, chromium, and cadmium all induced cysteine oxidation with arsenic and cadmium increasing cysteine oxidation more than chromium. Label-free proteomic analysis was used with on-resin digestion to isolate peptides containing reversibly-oxidized cysteines, allowing us to identify both the proteins and specific cysteines involved. Proteomic results, confirmed by western blotting, showed that the metals oxidized oxidoreductase proteins involved in oxidative stress, cellular metabolism, and protein folding and translation.

These results both confirm that RARC can be used to identify reversibly-oxidized cysteines as well as directions for further improvements and future research directions. A label-free proteomic approach was selected for its accessibility, with a simple inclusion-exclusion screen used to identify proteins that were oxidized at a high enough level to be detected reliably in metal-treated samples but not control samples. This approach did not require comparative analysis of peptide levels between treatment groups, which

simplified data reduction by naturally excluding samples which were present in both control and treatment groups at different concentrations.

Unfortunately the relatively high lower limit for LC-MS/MS peptide detection resulted in several oxidized proteins not being reliably identified via proteomic analysis. The lack of sample complexity for the proteomic input resulted in single peptides being identified for several proteins, as would be expected for proteins with a single oxidized cysteine. For some proteins, such as β-actin, this resulted in the identified peptide being flagged as non-unique since the sequence was shared between ACTB and ACTG1.

Based on these results, RARC has been demonstrated to be useful technique for isolating and enriching proteins containing reversibly-oxidized cysteines in a rapid and reproducible manner. Coupling RARC with western blotting allows for comparative analysis of protein oxidation caused by treatments for known targets, while coupling RARC to label-free or labeled proteomic analysis allows for the discovery of new oxidative targets. Future improvements to the method would include developing a spike-in standard methodology that was compatible with RARC and on-resin digestion to facilitate quantitative proteomics for peptides detected in both control and treatment sets, and utilizing more sensitive proteomic techniques like MudPIT [150] to decrease the threshold for proteomic detection of oxidized peptides towards that of western blotting.

Despite this room for improvement, this project has both established the utility of the RARC method for discovering cysteine modifications and analyzing qualitative differences in cysteine oxidation between treatments. By utilizing RARC we have been able to confirm cysteine oxidation on several proteins previously reported to be oxidized

by As(III) and Cd(II), such as vimentin, β-actin, and pyruvate kinase. Additionally we have identified several oxidized proteins which were previously not known to be oxidized by metals, as well as several novel reactive cysteines. While the relative oxidation levels caused by As(III), Cr(VI), and Cd(II) varied depending on the protein, the overall trend is that these three metals share similar oxidative targets. These results will allow us to further understand the role that cysteine oxidation plays in metal-induced oxidative stress and cytotoxicity.

Chapter 5 : DISCUSSION

The role of cysteine oxidation in cellular signaling pathways and oxidative stress is an emerging field of interest in cell biology. Cysteine oxidation as a post-translational modification is difficult to detect using molecular biology methods, a problem only exacerbated by the tendency of cysteines to auto-oxidize upon lysis. This hampers discovery of oxidized cysteines by high-throughput proteomic methods.

Approaches to studying reversibly cysteine oxidation have improved in the past two decades but are still laborious. The current state of the art for isolating and enriching proteins containing reversibly-oxidized cysteines, the resin-assisted capture (RAC) method, still requires several protein precipitation and transfer steps, each of which increases user handling and risks sample contamination or loss; sample losses due to precipitation and resuspension could exceed 30% of the original lysate, while either incomplete drying or overdrying the protein pellet following precipitation could result in the complete insolubility of the pellet. The losses incurred to these steps are not only frustrating but also result in a lysate composition at the end of the alkylation and reduction steps which may no longer resemble the initial starting lysate, muddying the real-world conclusions which could be drawn from these experiments.

Additionally the complicated nature of this methodology poses a high barrier of entry for investigators wishing to study reversible cysteine oxidation in cell signaling and cellular functions. Given the key role that cysteine plays in enzymatic function, oxidative cell signaling, and stress response it is critical that a reliable, simple method exists for the study of reversible cysteine oxidation caused by cellular oxidants.

We sought to improve upon the current RAC methodology with a focus on eliminating the precipitation steps required, thus both reducing the time required to isolate reversibly-oxidized fractions for downstream analysis and decreasing loss and variability between samples. The three precipitation steps were at the initial point of lysis by trichloroacetic acid-mediated disulfide exchange quenching and precipitation, as well as two organic solvent precipitation steps between alkylation-reduction and reduction-capture steps using ice-cold acetone.

Trichloroacetic acid-mediated disulfide exchange had been questioned before we undertook our examination, as prior studies had indicated that it may not be sufficient to stop cysteine oxidation by the oxidant diamide. Since our lab studies ROS-generating heavy metals, we were concerned that not only would these metals be insufficiently quenched by trichloroacetic acid, but more powerful oxidizing species such as chromic acid could be formed by protonation of the metals at low pH; therefore even trace amounts of these metals, whether residual amounts left after washing a metal-treated cell culture or trace contamination of PBS or other wash buffers, could cause artefactual oxidation of protein cysteines during the disulfide exchange step.

We found that trichloroacetic acid did cause chromate oxidation of protein cysteines through chromic acid production. However treatment of the cell culture with the cysteine alkylant N-ethylmaleimide (NEM) prior to lysis and disulfide quenching significantly reduced cysteine oxidation by chromic acid. Furthermore we found that by optimizing our NEM pre-lysis alkylation of protein cysteines we could omit the need for trichloroacetic acid disulfide quenching and replace it with a simple 5 minute pre-lysis incubation with NEM. This eliminated a time-consuming precipitation step as well as

any acid-induced post-lysis metal oxidation of protein cysteines, although these benefits extend beyond just metal contamination. The elimination of free protein cysteine thiols through NEM alkylation prior to lysis means that post-lysis cysteine oxidation caused by residual amounts of treatment oxidants would be severely reduced, increasing confidence that the oxidative modifications detected were caused by specific cysteine oxidation and not just stochastic lysis- and denaturation-induced oxidation caused by contaminants.

When it came to investigating the organic solvent protein precipitation between alkylation and reduction, our starting point was a comparison between the standard RAC method and a variant known as purification of reversibly-oxidized proteins (PROP). The PROP method had omitted the precipitation step between the alkylation and reduction phases, instead adding an 2.5-fold molar excess of dithiothreitol (DTT) to the NEM-containing lysate with the intention that the DTT would be alkylated by any free NEM, thereby removing inactivating residual NEM, while simultaneously reducing oxidized cysteines. To our knowledge no studies had compared the standard RAC protocol to the PROP protocol to see whether the PROP modifications affected the quality of cysteine reduction and capture.

We found that PROP as originally designed resulted in decreased changes in protein oxidation detected between control and peroxide-treated BEAS-2B cells when compared to the conventional RAC method. Dithiol compounds like DTT were found to be poor NEM quenching reagents, while monothiol compounds like β-mercaptoethanol, l-cysteine, and mercaptoethylamine were efficient NEM quenching reagents. We separated NEM-quenching and reduction into two distinct steps, first adding an equimolar concentration of mercaptoethylamine to our NEM-containing lysates to

eliminate free NEM prior to the addition of thiol reductant, facilitating cysteine reduction without fear of NEM alkylating the newly-reduced cysteines.

These simple modifications, NEM pre-lysis treatment and NEM quenching, allowed us to detect protein oxidation changes induced by hydrogen peroxide at efficacies rivaling that of RAC-processed samples. Furthermore our optimized RAC method reduced the time needed to complete the RAC method by a day through the elimination of two precipitation steps, while it also eliminated post-lysis acid-induced cysteine oxidation caused by trace metal contaminants through the elimination of trichloroacetic acid quenching and reduced protein loss and contamination risk by eliminating an organic solvent precipitation step. These modifications are extremely simple to incorporate into a RAC workflow, with the only additional reagent needed being the inexpensive monothiol mercaptoethylamine.

Beyond our analysis of total protein cysteine oxidation, our modified, optimized method can also be used for the study of specific reversible cysteine oxidants such as nitrosothiols and sulfenic acids. An RAC workflow for the capture of nitrosothiols or sulfenic acids relies on alkylation of free cysteine thiols with NEM, followed by precipitation and resuspension into a buffer containing species specific reductants such as sinapinic acid for nitrosothiols or sodium arsenite for sulfenic acids. Neither of these reductants are capable of reducing disulfide bridges, allowing simultaneous reduction and capture of proteins. The incorporation of an NEM-quenching step would eliminate the need for precipitation, allowing the lysates to be directly added into a thiopropyl-sepharose capture column for reduction and capture.

The elimination of the precipitation step between reduction and capture proved a greater challenge, since the second precipitation was intended to remove any excess reductant from the samples prior to cysteine capture. Failure to properly remove the reductant would decrease or altogether eliminate cysteine capture. In order to address this we wanted to avoid the need to precipitate samples by incorporating an immobilized reducing resin; following reduction the samples could be eluted from the immobilized reductant by centrifugation, allowing the immediate capture of the newly-reduced lysates without needing a precipitation step.

However commercially-available immobilized reductant resins were incompatible with our method, being low-capacity and based on highly macroporous sepharose beads. We addressed this by developing a class of high-capacity reducing resins based on aldehyde-activation of polyacrylamide desalting resins. We used this activated aldehyde to generate both solid-phase thiol- and non-thiol reductants and utilized these reducing resins in place of soluble reductants for the reduction of reversibly-oxidized cysteines.

This modified RAC technique, resin-assisted *reduction* and capture (RARC), achieved cysteine capture fidelity similar to or greater than that of RAC. At the same time a total RARC workflow, from cell lysis to electrophoresis and transfer, could easily be performed in a single workday. Additionally because RARC did not require trichloroacetic acid or organic solvent precipitation, RARC-processed samples did not have precipitation-induced sample loss or acid-induced artefactual oxidation and greatly decreased risk of contamination. The use of immobilized reductants which were effective at acidic pH, such as mercaptoethylamine-polyacrylamide and the phosphine

reagent tris(hydroxypropyl)phosphine-polyacrylamide, allowed us to conduct the entire processing at mildly acidic pH. Decreasing pH causes the protonation of protein thiolates, helping to further reduce disulfide exchange prior to and during NEM alkylation, as well as preventing anti-Michael addition of alkylated NEM; however since DTT is only marginally effective below pH 7, prior RAC workflows have been limited to using alkylation and reduction buffers at neutral or basic pH. The incorporation of our high-capacity reducing resins eliminates this need to accommodate DTT's reducing capacity when selecting buffer pH, resulting in capture efficacies for oxidized cysteines at pH 6.5 which are higher than a conventional RAC conducted at pH 7.2.

We used RARC to study cysteine oxidation caused by the thiol-reactive and ROS-generating metals trivalent arsenic (As(III)), hexavalent chromium (Cr(VI)), and divalent cadmium (Cd(II)). We found that all three metals caused cysteine oxidation. We used label-free LC-MS/MS proteomic analysis downstream of RARC processing to identify proteins oxidized by these metals, as well as the specific cysteines oxidized. Proteomic analysis found that all three metals caused oxidation of several proteins, including the translation enzyme eukaryotic elongation factor 2, the cytoskeletal protein vimentin, the antioxidant oxidoreductase peroxiredoxin 5, and the glycolytic enzyme glyceraldehyde 3-phosphate dehydrogenase, results which were confirmed by western blot analysis. We also found that the glycolytic enzyme pyruvate kinase M1/2, the cytoskeletal protein β-actin, the redox sensor DJ-1/PARK7, and the xenobiotic metabolism enzyme nicotinamide N-methyltransferase were oxidized by all three metals.

While these results are interesting in themselves, they also allow us to identify targets for future research into metal-induced protein oxidation and its inactivation or

activation of downstream signaling. Having identified oxidized cysteines on these

proteins, we can now use site-directed mutagenesis to determine whether these cysteines

are both necessary for protein function as well as how oxidation of these cysteines

contributes to metal-induced toxicity. We can also use the RARC method to identify and

track time- and dose-dependent changes in metal-induced protein oxidation; label free

proteomic analysis of RARC-processed lysates from different time points and metal

concentrations will allow us to determine differential oxidative products caused by

differing exposures to reactive metals.

This project has demonstrated the utility of RARC. However, as with its

immediate predecessor, RAC, improvements can and should still be made to the RARC

workflow. The stable of immobilized reductants needs to be expanded. For example, the

steric hindrance of the immobilized TCEP-PAAm from being an effective reductant can

be addressed through the use of uronium compounds such as HATU or HBTU for amide

synthesis instead of the carbodiimide EDC. Since TCEP is a commonly-used laboratory

reductant, developing an easily synthesized and effective TCEP-based resin would allow

for easier adoption of the RARC method.

Additional improvements to the solid-phase portions of the technique could

further reduce the time needed to perform RARC by combining the reduction and capture

phases; since both reduction and capture are accomplished via immobilized resins,

physically separating the reducing and capturing components within a single column and

allowing lysate to move freely between them would allow immediate capture of newly-

reduced cysteine thiols. This could be accomplished by synthesizing a bimodal resin

which features both reducing and capturing derivitizations physically separated from each

other, say with the reducing components on the exterior of the resin beads and the capturing components on the interior. Alternatively a mixed-resin bed combining both immobilized reductant-polyacrylamide and thiopropyl-sepharose could be examined. This would further streamline and improve the RARC methodology.

The development of a protocol for spike-in incorporation into cysteine redox proteomics, whether via RAC and RARC, is also sorely needed. The necessity of using inclusion/exclusion criteria for our proteomic analysis of metal-induced cysteine oxidation was caused by not having an effective means for quantitating relative amounts of the LC-MS/MS-detected proteins between samples. Spike-in standards have been commonly used for quantitative proteomics before, providing a known amount of a standard which can be used to quantitate the amounts of protein peptides detected via LC-MS/MS. However no studies have addressed the incorporation of spike-in standards for redox proteomics, specifically the what, when, and where or spiking in. Since cysteine redox proteomics refines and simplifies the proteome based on cysteine capture and elution, spiking in a non-cysteine-containing standard at the beginning of an experiment, or even during capture, would mean that all of that standard would be washed out prior to elution. However, spiking in a standard following elution and during peptide cleanup may not provide an accurate relative quantitation of the samples since the spiked standard has not undergone the some processing steps as the rest of the sample.

Therefore it is critical to address this need, determining what spike-in standards are useful for RARC-mediated cysteine redox proteomics as well as when and where to add the standard into the lysates. If properly addressed, label-free cysteine redox proteomics would be able to reliably determine more subtle changes in cysteine oxidation

between proteins which were identified in both control and treatment samples, something which we had to rely upon western blotting to accomplish.

Additionally new and more effective alkylants are always needed within the field. While we determined that NEM was the most efficient alkylant for our method to date, NEM is, as mentioned previously, not without its drawbacks. While NEM is highly specific for cysteine, NEM can still cause trace misalkylation of amino acids other than cysteine. NEM can also undergo retro-Michael addition, potentially regenerating free thiols from NEM-alkylated cysteines. While both of these concerns can be and have been ameliorated by reducing reaction pH to below neutral, these only highlight the need for better, more specific and irreversible cysteine alkylants in addition to optimized reaction conditions.

Despite this room for improvement, the RARC technique is a simple and highly effective modification to the existing RAC methodology. The high-capacity resins developed can be synthesized inexpensively using common lab equipment, lowering the barrier to entry for researchers interested in studying cysteine oxidation caused by cellular oxidants and ROS-generating toxicants. Additionally RARC allows for a single-day experiment to probe for cysteine oxidation, while both capturing more oxidized proteins and eliminating size exclusion- or precipitation-induced sample loss and contamination. Since RARC is based on sample separation from an immobilized resin, it could be easily adapted from our spin-column format to a vacuum manifold system to speed up washes, or a spin-plate to allow high-throughput processing and potentially automation of cysteine oxidation analysis.

Given the increased speed and efficiency of RARC versus the older RAC technique, we see RARC as a useful new addition to the quiver of available methods to study reversible cysteine oxidation. RARC can be used to identify cysteine oxidation caused by oxidants in a rapid, medium-to-high throughput. This will enable the discovery of new cysteine oxidative targets for oxidants, as well as antioxidant and drug discovery, allow the routine analysis of cysteine redox signaling pathways during normal cell function or cell pathology, and enhance our understanding of the role that cysteines play within the proteome, metabolome, and beyond.

APPENDICES

Appendix I.

PROTOCOL FOR RESIN-ASSISTED REDUCTION AND CAPTURE (RARC) OF REVERSIBLY-OXIDIZED PROTEINS

Treatment and Prelysis Quenching of Protein Samples

1. Culture adherent cells to 60-90% confluency in complete culture medium in 10 cm^2 cell culture dishes.

2. Remove culture medium and replace with medium containing either vehicle or treatment compound. Incubate for desired exposure time.

3. Remove the treatment medium, wash once with PBS, then replace the medium with serum-free medium containing 50 mM NEM. Incubate the cells at 37°C for 15 minutes.

4. Remove quenching medium, then wash the cells carefully with PBS. Aspirate. Repeat this step once.

5. Detach the cells from the plate using a cell lifter into 1 ml of PBS. Collect the cells in a 1.5-ml microcentrifuge tube and centrifuge the tube at 200g at 4°C for 5 min. Aspirate the PBS from the cell pellet.
   PAUSE/STORAGE: Cell pellets may be stored overnight at -80°C.

Alkylation of Free Thiols

6. Pipette 600 μl of degassed cell lysis buffer containing 20 mM NEM into each tube. Incubate the samples in the dark at RT for 2 hours with end-over-end or rotational mixing.

7. Transfer the samples to TPX tubes for DNA shearing. Working in six-sample batches, place the samples into the carousel of a precooled BioRuptor Pico (Diagenode, Denville, NJ). Sonicate for 10 cycles of 30s/30s at 4°C.

   NOTE: Samples can be collected, lysed, and alkylated in TPX tubes in order to avoid sample transfer. If so, handle the tubes carefully since TPX is a brittle plastic and may be prone to cracking.

   NOTE: Alternative DNA shearing techniques may be used. This protocol has successfully used microtip sonication with no discernable changes in sample quality. Due to the risks of sample foaming and aspiration using a Bioruptor or other bath-type sonicator is preferred.

   NOTE: SDS in the lysis buffer may precipitate during the shearing incubation. If this occurs the SDS will redissolve as the samples are brought back to RT.

8. Centrifuge the samples at 16,000*g* for 5 minutes to pellet cellular debris. Measure protein concentration using the BCA assay.

Preparation of Reduction and Capture Resins

9. Weigh 35 mg each of MEA-polyacrylamide and thiopropyl Sepharose-6B for each sample to be enriched. Place the resins in 15-ml tubes.

   NOTE: It may be helpful to weigh out an additional sample's-worth of resins to avoid running out of rehydrated resin due to pipette retention.

10. Add deionized water to each tube to rehydrate the resins and incubate for 15 minutes at RT. A good final volume to aim for is 500 μl of water + rehydrated resin slurry per sample (ex. 5 samples would be 2.5 ml of slurry).

11. Cut the end of a 1-ml pipette tip off at an angle to make a large-bore tip. Use this large-bore tip to resuspend the resin, and transfer 500 μl of the slurry into spin column(s).

12. Place the spin column into a 2-ml receiving tube and centrifuge the tube at $1,000g$ for 30s at RT. Remove the eluted water from the receiving tube, pipette 500 μl of water to the resin, and centrifuge. Repeat this wash twice with cell lysis buffer.

13. Place the bottom plug and top cap on the column following the last wash, and store the tubes at 4°C in the dark until use.

Alkylant Quench and Sample Reduction

14. Add mercaptoethylamine to the samples to a final concentration of 20 mM. Incubate for 5 minutes with mixing at RT to quench any free NEM.

15. Transfer the samples to the spin columns containing prepared MEA-polyacrylamide resins, pipetting briefly up and down to break up and mix the resin into a slurry. After making sure that the bottom plug and top cap are sealed properly, incubate the samples for 1 hour in the dark at RT with end-over-end mixing.

16. Remove the bottom plug, loosen the top cap, and place the column into a clean 2-ml microcentrifuge tube. Centrifuge the columns at $3,000g$ for 5 min at RT to elute the reduced lysate.

Enrichment of Previously-Oxidized Proteins

17. Transfer equal amounts of protein (~350 ug) from each sample into spin columns containing prepared thiopropyl Sepharose-6B. After sealing both bottom plug and top cap, incubate the samples for 30 minutes in the dark at RT with rotational agitation at 800 rpm.

18. Remove the bottom plug, loosen the top cap, and place the column into a 2-ml microcentrifuge tube. Centrifuge the columns at 1,000g for 30s at RT to remove all nonbound proteins. Remove the top cap.

19. Wash the resin 3 times with 1% SDS, 7 times with diH$_2$O, 5 times with 30% acetonitrile/0.1% trifluoroacetic acid, and 5 times with 30% acetonitrile, 50 mM NaHCO$_3$. Use 5 column volumes (500 µl) for each wash for a total of 100 CVs of wash. After the last wash replace the bottom plug.

    NOTE: If total protein eluate is desired for downstream applications (ex. western blotting), skip on-resin digestion and proceed to Step 23.

On-Resin Digestion

20. Add 150 µl of digestion buffer (30% acetonitrile, 50 mM NaHCO$_3$) containing 5 µg of MS-grade modified trypsin. Replace the top cap and incubate the columns overnight at 37 °C with end-over-end mixing.

21. Remove the bottom plug, loosen the top cap, and place the column into a clean microcentrifuge tube. Centrifuge the columns at 1,000g for 30s at RT to remove the non-oxidized-cysteine containing fraction.

NOTE: This fraction can be saved and used for confirmation of the proteomic results from the oxidized fraction if desired.

22. Remove the top cap and wash the columns 5 times with diH$_2$O, 5 times with 30% acetonitrile/0.1% TFA, and 5 times with 50 NaHCO$_3$ for a total of 75 CVs. After the last wash replace the bottom plug.

Elution

23. Add 120 μl of elution buffer (50 mM NaHCO$_3$, 25 mM IAM) to the columns. Replace the top cap and incubate columns for 30 min at RT with rotational agitation.
NOTE: If the intended application is western blotting, replace the elution buffer with 1X Laemmli sample buffer containing 25 mM TCEP.

24. Remove the bottom plug, loosen the top cap, and place the column into a clean microcentrifuge tube. Centrifuge the columns at 1,000g for 30s at RT to elute the oxidized-cysteine containing peptides. After centrifugation remove the column from the receiving tube and replace the bottom plug.
NOTE: If the intended application is western blotting, one round of elution is enough to elute ~90% of captured proteins. Repeat elutions can be conducted, but sample concentration will decrease with each repeat. Eluate can be directly used at this step for SDS-PAGE.

25. Repeat steps 23 and 24 3 times, placing the column into the same microcentrifuge tube after each incubation. The receiving sample tubes will contain 480 μl of eluate at this point.

26. Add 30 μl of 1M iodoacetamide (IAM) to each microcentrifuge tube to bring the final IAM concentration to ~60 mM. Incubate the tubes for 1 hr at RT in the dark.

27. Open the tubes and place them in a rotary evaporator. Dry the tubes. Resuspend the peptide pellets in 30 μl 0.5% formic acid.

28. Clean up the peptide samples with C18 pipette tips. Condition the tips following manufacturer instructions. Load the samples by 10-50 cycles of sample aspiration and dispensing. Wash the samples 5 times with 5% acetonitrile, 0.1% formic disposing of the wash each time. Elute samples with 10 μl 80% acetonitrile, 0.1% formic acid. Repeat elution step 2 times for a total of 30 μl eluate. Dry down the cleaned samples using a rotary evaporator and resuspend in 10 μl of 0.1% formic acid. Samples are now ready for LC-MS/MS analysis.

REFERENCES

1.   Brooks, D.J. and J.R. Fresco, *Increased frequency of cysteine, tyrosine, and phenylalanine residues since the last universal ancestor.* Mol Cell Proteomics, 2002. **1**(2): p. 125-31.

2.   Brooks, D.J., J.R. Fresco, A.M. Lesk, and M. Singh, *Evolution of amino acid frequencies in proteins over deep time: inferred order of introduction of amino acids into the genetic code.* Mol Biol Evol, 2002. **19**(10): p. 1645-55.

3.   Dixon, M. and H.E. Tunnicliffe, *On the Reducing Power of Glutathione and Cysteine.* Biochem J, 1927. **21**(4): p. 844-51.

4.   Toennies, G., *Oxidation of Cysteine in Non-Aqueous Media: The "Sulfenic Acid" as the Primary Oxidation Product.* Journal of Biological Chemistry, 1937. **122**(1): p. 27-49.

5.   Benesch, R.E.B., R., *The acid strength of the -SH group in cysteine and related compounds.* J Am Chem Soc, 1955. **77**(22): p. 5877-5881.

6.   Thurlkill, R.L., G.R. Grimsley, J.M. Scholtz, and C.N. Pace, *pK values of the ionizable groups of proteins.* Protein Sci, 2006. **15**(5): p. 1214-8.

7.   Pace, C.N., G.R. Grimsley, and J.M. Scholtz, *Protein ionizable groups: pK values and their contribution to protein stability and solubility.* J Biol Chem, 2009. **284**(20): p. 13285-9.

8.   Winterbourn, C.C. and D. Metodiewa, *Reactivity of biologically important thiol compounds with superoxide and hydrogen peroxide.* Free Radic Biol Med, 1999. **27**(3-4): p. 322-8.

9.   Giustarini, D., F. Galvagni, A. Tesei, A. Farolfi, M. Zanoni, S. Pignatta, A. Milzani, I.M. Marone, I. Dalle-Donne, R. Nassini, and R. Rossi, *Glutathione, glutathione disulfide, and S-glutathionylated proteins in cell cultures.* Free Radic Biol Med, 2015. **89**: p. 972-81.

10.   Woo, H.A., W. Jeong, T.S. Chang, K.J. Park, S.J. Park, J.S. Yang, and S.G. Rhee, *Reduction of cysteine sulfinic acid by sulfiredoxin is specific to 2-cys peroxiredoxins.* J Biol Chem, 2005. **280**(5): p. 3125-8.

11.   Chang, T.S., W. Jeong, H.A. Woo, S.M. Lee, S. Park, and S.G. Rhee, *Characterization of mammalian sulfiredoxin and its reactivation of hyperoxidized peroxiredoxin through reduction of cysteine sulfinic acid in the active site to cysteine.* J Biol Chem, 2004. **279**(49): p. 50994-1001.

12.   Rodriguez, C.E., J.M. Fukuto, K. Taguchi, J. Froines, and A.K. Cho, *The interactions of 9,10-phenanthrenequinone with glyceraldehyde-3-phosphate dehydrogenase (GAPDH), a potential site for toxic actions.* Chem Biol Interact, 2005. **155**(1-2): p. 97-110.

13.   Lopez, B.E., D.A. Wink, and J.M. Fukuto, *The inhibition of glyceraldehyde-3-phosphate dehydrogenase by nitroxyl (HNO).* Arch Biochem Biophys, 2007. **465**(2): p. 430-6.

14.   Blum, J. and I. Fridovich, *Inactivation of glutathione peroxidase by superoxide radical.* Arch Biochem Biophys, 1985. **240**(2): p. 500-8.

15.   Cho, C.S., S. Lee, G.T. Lee, H.A. Woo, E.J. Choi, and S.G. Rhee, *Irreversible inactivation of glutathione peroxidase 1 and reversible inactivation of peroxiredoxin II by H2O2 in red blood cells.* Antioxid Redox Signal, 2010. **12**(11): p. 1235-46.

16.   Pigeolet, E., P. Corbisier, A. Houbion, D. Lambert, C. Michiels, M. Raes, M.D. Zachary, and J. Remacle, *Glutathione peroxidase, superoxide dismutase, and catalase inactivation by peroxides and oxygen derived free radicals.* Mech Ageing Dev, 1990. **51**(3): p. 283-97.

17.   Canet-Aviles, R.M., M.A. Wilson, D.W. Miller, R. Ahmad, C. McLendon, S. Bandyopadhyay, M.J. Baptista, D. Ringe, G.A. Petsko, and M.R. Cookson, *The*

Parkinson's disease protein DJ-1 is neuroprotective due to cysteine-sulfinic acid-driven mitochondrial localization. Proc Natl Acad Sci U S A, 2004. **101**(24): p. 9103-8.

18.   Junn, E., H. Taniguchi, B.S. Jeong, X. Zhao, H. Ichijo, and M.M. Mouradian, *Interaction of DJ-1 with Daxx inhibits apoptosis signal-regulating kinase 1 activity and cell death.* Proc Natl Acad Sci U S A, 2005. **102**(27): p. 9691-6.

19.   Im, J.Y., K.W. Lee, E. Junn, and M.M. Mouradian, *DJ-1 protects against oxidative damage by regulating the thioredoxin/ASK1 complex.* Neurosci Res, 2010. **67**(3): p. 203-8.

20.   Mo, J.S., M.Y. Kim, E.J. Ann, J.A. Hong, and H.S. Park, *DJ-1 modulates UV-induced oxidative stress signaling through the suppression of MEKK1 and cell death.* Cell Death Differ, 2008. **15**(6): p. 1030-41.

21.   Kim, Y.C., H. Kitaura, T. Taira, S.M. Iguchi-Ariga, and H. Ariga, *Oxidation of DJ-1-dependent cell transformation through direct binding of DJ-1 to PTEN.* Int J Oncol, 2009. **35**(6): p. 1331-41.

22.   Kato, I., H. Maita, K. Takahashi-Niki, Y. Saito, N. Noguchi, S.M. Iguchi-Ariga, and H. Ariga, *Oxidized DJ-1 inhibits p53 by sequestering p53 from promoters in a DNA-binding affinity-dependent manner.* Mol Cell Biol, 2013. **33**(2): p. 340-59.

23.   Rehder, D.S. and C.R. Borges, *Cysteine sulfenic acid as an intermediate in disulfide bond formation and nonenzymatic protein folding.* Biochemistry, 2010. **49**(35): p. 7748-55.

24.   Salmeen, A., J.N. Andersen, M.P. Myers, T.C. Meng, J.A. Hinks, N.K. Tonks, and D. Barford, *Redox regulation of protein tyrosine phosphatase 1B involves a sulphenyl-amide intermediate.* Nature, 2003. **423**(6941): p. 769-73.

25.   Allison, W.S., *Formation and reactions of sulfenic acids in proteins.* Acc. Chem. Res., 1976. **9**(8): p. 293-299.

26.   Claiborne, A., J.I. Yeh, T.C. Mallett, J. Luba, E.J. Crane, 3rd, V. Charrier, and D. Parsonage, *Protein-sulfenic acids: diverse roles for an unlikely player in enzyme catalysis and redox regulation.* Biochemistry, 1999. **38**(47): p. 15407-16.

27.   Ishii, T., O. Sunami, H. Nakajima, H. Nishio, T. Takeuchi, and F. Hata, *Critical role of sulfenic acid formation of thiols in the inactivation of glyceraldehyde-3-phosphate dehydrogenase by nitric oxide.* Biochem Pharmacol, 1999. **58**(1): p. 133-43.

28.   Ralser, M., M.M. Wamelink, A. Kowald, B. Gerisch, G. Heeren, E.A. Struys, E. Klipp, C. Jakobs, M. Breitenbach, H. Lehrach, and S. Krobitsch, *Dynamic rerouting of the carbohydrate flux is key to counteracting oxidative stress.* J Biol, 2007. **6**(4): p. 10.

29.   Luanpitpong, S., P. Chanvorachote, C. Stehlik, W. Tse, P.S. Callery, L. Wang, and Y. Rojanasakul, *Regulation of apoptosis by Bcl-2 cysteine oxidation in human lung epithelial cells.* Mol Biol Cell, 2013. **24**(6): p. 858-69.

30.   Givol, D., F. Delorenzo, R.F. Goldberger, and C.B. Anfinsen, *Disulfide Interchange and the Three-Dimensional Structure of Proteins.* Proc Natl Acad Sci U S A, 1965. **53**: p. 676-84.

31.   Rajpal, G. and P. Arvan, *Disulfide Bond Formation*, in *Handbook of Biologically Active Peptides*, A.J. Kastin, Editor. 2013, Academic Press.

32.   Kosuri, P., J. Alegre-Cebollada, J. Feng, A. Kaplan, A. Ingles-Prieto, C.L. Badilla, B.R. Stockwell, J.M. Sanchez-Ruiz, A. Holmgren, and J.M. Fernandez, *Protein folding drives disulfide formation.* Cell, 2012. **151**(4): p. 794-806.

33.   Qin, M., W. Wang, and D. Thirumalai, *Protein folding guides disulfide bond formation.* Proc Natl Acad Sci U S A, 2015. **112**(36): p. 11241-6.

34.   Nakagawa, T., H. Zhu, N. Morishima, E. Li, J. Xu, B.A. Yankner, and J. Yuan, *Caspase-12 mediates endoplasmic-reticulum-specific apoptosis and cytotoxicity by amyloid-beta.* Nature, 2000. **403**(6765): p. 98-103.

35.   Hetz, C., M. Russelakis-Carneiro, S. Walchli, S. Carboni, E. Vial-Knecht, K. Maundrell, J. Castilla, and C. Soto, *The disulfide isomerase Grp58 is a protective factor against prion neurotoxicity.* J Neurosci, 2005. **25**(11): p. 2793-802.

36.   Scheuner, D., B. Song, E. McEwen, C. Liu, R. Laybutt, P. Gillespie, T. Saunders, S. Bonner-Weir, and R.J. Kaufman, *Translational control is required for the unfolded protein response and in vivo glucose homeostasis.* Mol Cell, 2001. **7**(6): p. 1165-76.

37.   Fourquet, S., R. Guerois, D. Biard, and M.B. Toledano, *Activation of NRF2 by nitrosative agents and H2O2 involves KEAP1 disulfide formation.* J Biol Chem, 2010. **285**(11): p. 8463-71.

38.   Biswas, S., A.S. Chida, and I. Rahman, *Redox modifications of protein-thiols: emerging roles in cell signaling.* Biochem Pharmacol, 2006. **71**(5): p. 551-64.

39.   Laurindo, F.R., L.A. Pescatore, and C. Fernandes Dde, *Protein disulfide isomerase in redox cell signaling and homeostasis.* Free Radic Biol Med, 2012. **52**(9): p. 1954-69.

40.   Lima, B., M.T. Forrester, D.T. Hess, and J.S. Stamler, *S-nitrosylation in cardiovascular signaling.* Circ Res, 2010. **106**(4): p. 633-46.

41.   Yang, L., E.S. Calay, J. Fan, A. Arduini, R.C. Kunz, S.P. Gygi, A. Yalcin, S. Fu, and G.S. Hotamisligil, *METABOLISM. S-Nitrosylation links obesity-associated inflammation to endoplasmic reticulum dysfunction.* Science, 2015. **349**(6247): p. 500-6.

42.   Yasukawa, T., E. Tokunaga, H. Ota, H. Sugita, J.A. Martyn, and M. Kaneki, *S-nitrosylation-dependent inactivation of Akt/protein kinase B in insulin resistance.* J Biol Chem, 2005. **280**(9): p. 7511-8.

43.   Seneviratne, U., A. Nott, V.B. Bhat, K.C. Ravindra, J.S. Wishnok, L.H. Tsai, and S.R. Tannenbaum, *S-nitrosation of proteins relevant to Alzheimer's disease during early stages of neurodegeneration.* Proc Natl Acad Sci U S A, 2016. **113**(15): p. 4152-7.

44.   Azad, N., V. Vallyathan, L. Wang, V. Tantishaiyakul, C. Stehlik, S.S. Leonard, and Y. Rojanasakul, *S-nitrosylation of Bcl-2 inhibits its ubiquitin-proteasomal degradation. A novel antiapoptotic mechanism that suppresses apoptosis.* J Biol Chem, 2006. **281**(45): p. 34124-34.

45.   Wright, C., A.K. Iyer, Y. Kulkarni, and N. Azad, *S-Nitrosylation of Bcl-2 Negatively Affects Autophagy in Lung Epithelial Cells.* J Cell Biochem, 2016. **117**(2): p. 521-32.

46.   Salmeen, A. and D. Barford, *Methods for preparing crystals of reversibly oxidized proteins: crystallization of protein tyrosine phosphatase 1B as an example.* Methods Mol Biol, 2008. **476**: p. 101-16.

47.   Samelson, L.E., *Diagonal gel electrophoresis.* Curr Protoc Immunol, 2001. **Chapter 8**: p. Unit 8 6.

48.   Goodson, R.J. and N.V. Katre, *Site-directed pegylation of recombinant interleukin-2 at its glycosylation site.* Biotechnology (N Y), 1990. **8**(4): p. 343-6.

49.   Jaffrey, S.R., H. Erdjument-Bromage, C.D. Ferris, P. Tempst, and S.H. Snyder, *Protein S-nitrosylation: a physiological signal for neuronal nitric oxide.* Nat Cell Biol, 2001. **3**(2): p. 193-7.

50.   Landino, L.M., M.T. Koumas, C.E. Mason, and J.A. Alston, *Ascorbic acid reduction of microtubule protein disulfides and its relevance to protein S-nitrosylation assays.* Biochem Biophys Res Commun, 2006. **340**(2): p. 347-52.

51.   Giustarini, D., I. Dalle-Donne, R. Colombo, A. Milzani, and R. Rossi, *Is ascorbate able to reduce disulfide bridges? A cautionary note.* Nitric Oxide, 2008. **19**(3): p. 252-8.

52.   Leichert, L.I. and U. Jakob, *Protein thiol modifications visualized in vivo.* PLoS Biol, 2004. **2**(11): p. e333.

53.   Egorov, T.A., A. Svenson, L. Ryden, and J. Carlsson, *A rapid and specific method for isolation of thiol-containing peptides from large proteins by thiol-disulfide exchange on a solid support.* Proc Natl Acad Sci U S A, 1975. **72**(8): p. 3029-33.

54.   Akhter, S., J.R. Green, P. Root, G.J. Thatcher, and B. Mutus, *Peroxynitrite and NO+ donors form colored nitrite adducts with sinapinic acid: potential applications.* Nitric Oxide, 2003. **8**(4): p. 214-21.

55.   Kallakunta, V.M., A. Staruch, and B. Mutus, *Sinapinic acid can replace ascorbate in the biotin switch assay.* Biochim Biophys Acta, 2010. **1800**(1): p. 23-30.

56.   Reeves, B.D., J.K. Hilmer, L. Mellmann, M. Hartzheim, K. Poffenberger, K. Johnson, N. Joshi, D.J. Singel, and P.A. Grieco, *Selective trapping of SNO-BSA and GSNO by benzenesulfinic acid sodium salt: mechanistic study of thiosulphonate formation and feasibility as a protein S-nitrosothiol detection strategy.* Tetrahedron Lett, 2013. **54**(42).

57.   Reeves, B.D., N. Joshi, G.C. Campanello, J.K. Hilmer, L. Chetia, J.A. Vance, J.N. Reinschmidt, C.G. Miller, D.P. Giedroc, E.A. Dratz, D.J. Singel, and P.A. Grieco, *Conversion of S-phenylsulfonylcysteine residues to mixed disulfides at pH 4.0: utility in protein thiol blocking and in protein-S-nitrosothiol detection.* Org Biomol Chem, 2014. **12**(40): p. 7942-56.

58.   Templeton, D.J., M.S. Aye, J. Rady, F. Xu, and J.V. Cross, *Purification of reversibly oxidized proteins (PROP) reveals a redox switch controlling p38 MAP kinase activity.* PLoS One, 2010. **5**(11): p. e15012.

59.   Kohr, M.J., J. Sun, A. Aponte, G. Wang, M. Gucek, E. Murphy, and C. Steenbergen, *Simultaneous measurement of protein oxidation and S-nitrosylation during preconditioning and ischemia/reperfusion injury with resin-assisted capture.* Circ Res, 2011. **108**(4): p. 418-26.

60.   Guo, J., M.J. Gaffrey, D. Su, T. Liu, D.G. Camp, 2nd, R.D. Smith, and W.J. Qian, *Resin-assisted enrichment of thiols as a general strategy for proteomic profiling of cysteine-based reversible modifications.* Nat Protoc, 2014. **9**(1): p. 64-75.

61.   Axen, R.D., H.; Carlsson, J., *Preparation of Modified Agarose Gels Containing Thiol Groups.* Acta Chem Scand B, 1975. **29**: p. 471-474.

62.   Matsumoto, I., Y. Mizuno, and N. Seno, *Activation of Sepharose with epichlorohydrin and subsequent immobilization of ligand for affinity adsorbent.* J Biochem, 1979. **85**(4): p. 1091-8.

63.   Meng, Q.-Q., J.-X. Wang, G.-H. Ma, and Z.-G. Su, *Lyophilization of CNBr-activated agarose beads with lactose and PEG.* Process Biochemistry, 2009. **44**: p. 562-571.

64.   Ellman, G.L., *Tissue sulfhydryl groups.* Arch Biochem Biophys, 1959. **82**(1): p. 70-7.

65.   Dietz, A.A. and H.M. Rubinstein, *Laboratory note--standardization of the Ellman reaction.* Clin Biochem, 1972. **5**(2): p. 136-8.

66.   Smith, P.K., R.I. Krohn, G.T. Hermanson, A.K. Mallia, F.H. Gartner, M.D. Provenzano, E.K. Fujimoto, N.M. Goeke, B.J. Olson, and D.C. Klenk, *Measurement of protein using bicinchoninic acid.* Anal Biochem, 1985. **150**(1): p. 76-85.

67.   Curbo, S.R., K.; Rundloef, A.-K.; Karlsson, A.; Lundberg, M., *Is trichloroacetic acid an insuffienct sample quencher of redox reactions?* Antioxid Redox Signal, 2013. **18**(7): p. 795-799.

68.   Ngo, A.N., M.J. Ezoulin, I. Youm, and B.B. Youan, *Optimal Concentration of 2,2,2-Trichloroacetic Acid for Protein Precipitation Based on Response Surface Methodology.* J Anal Bioanal Tech, 2014. **5**(4).

69.   Boutureira, O. and G.J. Bernardes, *Advances in chemical protein modification.* Chem Rev, 2015. **115**(5): p. 2174-95.

70.   Sechi, S. and B.T. Chait, *Modification of cysteine residues by alkylation. A tool in peptide mapping and protein identification.* Anal Chem, 1998. **70**(24): p. 5150-8.

71.   Turko, I.V. and S. Sechi, *Acrylamide--a cysteine alkylating reagent for quantitative proteomics.* Methods Mol Biol, 2007. **359**: p. 1-16.

72.   Bernardim, B., P.M. Cal, M.J. Matos, B.L. Oliveira, N. Martinez-Saez, I.S. Albuquerque, E. Perkins, F. Corzana, A.C. Burtoloso, G. Jimenez-Oses, and G.J. Bernardes,

Stoichiometric and irreversible cysteine-selective protein modification using carbonylacrylic reagents. Nat Commun, 2016. **7**: p. 13128.

73.   Karakosta, T.D., P.D. Tzanavaras, and D.G. Themelis, *Determination of glutathione and cysteine in yeasts by hydrophilic interaction liquid chromatography followed by on-line postcolumn derivatization.* J Sep Sci, 2013. **36**(12): p. 1877-82.

74.   Shiu, H.Y., T.C. Chan, C.M. Ho, Y. Liu, M.K. Wong, and C.M. Che, *Electron-deficient alkynes as cleavable reagents for the modification of cysteine-containing peptides in aqueous medium.* Chemistry, 2009. **15**(15): p. 3839-50.

75.   Koniev, O., G. Leriche, M. Nothisen, J.S. Remy, J.M. Strub, C. Schaeffer-Reiss, A. Van Dorsselaer, R. Baati, and A. Wagner, *Selective irreversible chemical tagging of cysteine with 3-arylpropiolonitriles.* Bioconjug Chem, 2014. **25**(2): p. 202-6.

76.   Zhang, D., N.O. Devarie-Baez, Q. Li, J.R. Lancaster, Jr., and M. Xian, *Methylsulfonyl benzothiazole (MSBT): a selective protein thiol blocking reagent.* Org Lett, 2012. **14**(13): p. 3396-9.

77.   Lyon, R.P., J.R. Setter, T.D. Bovee, S.O. Doronina, J.H. Hunter, M.E. Anderson, C.L. Balasubramanian, S.M. Duniho, C.I. Leiske, F. Li, and P.D. Senter, *Self-hydrolyzing maleimides improve the stability and pharmacological properties of antibody-drug conjugates.* Nat Biotechnol, 2014. **32**(10): p. 1059-62.

78.   Beutler, E., S.K. Srivastava, and C. West, *The reversibility of N-ethylmaleimide (NEM) alkylation of red cell glutathione.* Biochem Biophys Res Commun, 1970. **38**(2): p. 341-7.

79.   Baldwin, A.D. and K.L. Kiick, *Tunable degradation of maleimide-thiol adducts in reducing environments.* Bioconjug Chem, 2011. **22**(10): p. 1946-53.

80.   Ryan, C.P., M.E. Smith, F.F. Schumacher, D. Grohmann, D. Papaioannou, G. Waksman, F. Werner, J.R. Baker, and S. Caddick, *Tunable reagents for multi-functional bioconjugation: reversible or permanent chemical modification of proteins and peptides by control of maleimide hydrolysis.* Chem Commun (Camb), 2011. **47**(19): p. 5452-4.

81.   Shen, B.Q., K. Xu, L. Liu, H. Raab, S. Bhakta, M. Kenrick, K.L. Parsons-Reponte, J. Tien, S.F. Yu, E. Mai, D. Li, J. Tibbitts, J. Baudys, O.M. Saad, S.J. Scales, P.J. McDonald, P.E. Hass, C. Eigenbrot, T. Nguyen, W.A. Solis, R.N. Fuji, K.M. Flagella, D. Patel, S.D. Spencer, L.A. Khawli, A. Ebens, W.L. Wong, R. Vandlen, S. Kaur, M.X. Sliwkowski, R.H. Scheller, P. Polakis, and J.R. Junutula, *Conjugation site modulates the in vivo stability and therapeutic activity of antibody-drug conjugates.* Nat Biotechnol, 2012. **30**(2): p. 184-9.

82.   Paulech, J., N. Solis, and S.J. Cordwell, *Characterization of reaction conditions providing rapid and specific cysteine alkylation for peptide-based mass spectrometry.* Biochim Biophys Acta, 2013. **1834**(1): p. 372-9.

83.   Lukesh, J.C., 3rd, M.J. Palte, and R.T. Raines, *A potent, versatile disulfide-reducing agent from aspartic acid.* J Am Chem Soc, 2012. **134**(9): p. 4057-9.

84.   Gorecki, M. and A. Patchornik, *Polymer-bound dihydrolipoic acid: a new insoluble reducing agent for disulfides.* Biochim Biophys Acta, 1973. **303**(1): p. 36-43.

85.   Grazu, V., K. Ovsejevi, K. Cuadra, L. Betancor, C. Manta, and F. Batista-Viera, *Solid-phase reducing agents as alternative for reducing disulfide bonds in proteins.* Appl Biochem Biotechnol, 2003. **110**(1): p. 23-32.

86.   Axen, R., J. Porath, and S. Ernback, *Chemical coupling of peptides and proteins to polysaccharides by means of cyanogen halides.* Nature, 1967. **214**(5095): p. 1302-4.

87.   Porath, J., R. Axen, and S. Ernback, *Chemical coupling of proteins to agarose.* Nature, 1967. **215**(5109): p. 1491-2.

88.   Meng, Q.-Q., J.-X. Wang, and G.-H.S. Ma, Z-G., *Lyophilization of CNBr-activated agarose beads with lactose and PEG.* Process Biochemistry, 2009. **44**: p. 562-571.

89.   Inman, J.K. and H.M. Dintzis, *The derivatization of cross-linked polyacrylamide beads. Controlled introduction of functional groups for the preparation of special-purpose, biochemical adsorbents.* Biochemistry, 1969. **8**(10): p. 4074-82.

90.   Laboratories, B.-R., *Bio-Gel P Polyacrylamide Gel Instruction Manual*, B.-R. Laboratories, Editor., Bio-Rad: Online.

91.   Okuda, K., I. Urabe, Y. Yamada, and H. Okada, *Reaction of glutaraldehyde with amino and thiol compounds.* J. of Ferm. and Bioeng., 1991. **71**(2): p. 100-105.

92.   Weston, P.D. and S. Avrameas, *Proteins coupled to polyacrylamide beads using glutaraldehyde.* Biochem Biophys Res Commun, 1971. **45**(6): p. 1574-80.

93.   Ternynck, T. and S. Avrameas, *Polyacrylamide-protein immunoadsorbents prepared with glutaraldehyde.* FEBS Lett, 1972. **23**(1): p. 24-8.

94.   Gage, J.C., *The toxicity of epichlorhydrin vapour.* Br J Ind Med, 1959. **16**(1): p. 11-4.

95.   Lawrence, W.H., M. Malik, J.E. Turner, and J. Autian, *Toxicity profile of epichlorohydrin.* J Pharm Sci, 1972. **61**(11): p. 1712-6.

96.   Fishbein, L., *Industrial mutagens and potential mutagens I. Halogenated aliphatic derivatives.* Mutat Res, 1976. **32**(3-4): p. 267-307.

97.   Yang, R.S., R.H. Garman, R.R. Maronpot, J.A. McKelvey, C.S. Weil, and M.D. Woodside, *Acute and subchronic toxicity of ethylenediamine in laboratory animals.* Fundam Appl Toxicol, 1983. **3**(6): p. 512-20.

98.   Burns, J.A., J.C. Butler, J. Moran, and G.M. Whitesides, *Selective reduction of disulfides by tris(2-carboxyethyl)phosphine.* J. Org. Chem., 1991. **56**: p. 2648-2650.

99.   Shafer, D.E., J.K. Inman, and A. Lees, *Reaction of Tris(2-carboxyethyl)phosphine (TCEP) with maleimide and alpha-haloacyl groups: anomalous elution of TCEP by gel filtration.* Anal Biochem, 2000. **282**(1): p. 161-4.

100.   Ovsejevi, K., V. Grazu, K. Cuadra, and F. Batista-Viera, *Enzyme reduction on solid phase as a tool for the reversible immobilization of yeast beta-galatactosidase onto a thiol-reactive support.* Enz. Microb. Tech., 2004. **35**(2-3): p. 203-209.

101.   Lukesh, J.C., 3rd, B. Vanveller, and R.T. Raines, *Thiols and selenols as electron-relay catalysts for disulfide-bond reduction.* Angew Chem Int Ed Engl, 2013. **52**(49): p. 12901-4.

102.   Shi, X.L. and N.S. Dalal, *The role of superoxide radical in chromium (VI)-generated hydroxyl radical: the Cr(VI) Haber-Weiss cycle.* Arch Biochem Biophys, 1992. **292**(1): p. 323-7.

103.   Kuznetsov, M.L.T., F. A.; Bokach, N. A.; Pombeiro, A. J. L; Shul'pin, G. B, *Radical decomposition of hydrogen peroxide catalyzed by aqua complexes [M(H2O)n]2+ (M= Be, Zn, Cd).* Journal of Catalysis, 2014. **313**(1): p. 135-148.

104.   Wang, X., Y.O. Son, Q. Chang, L. Sun, J.A. Hitron, A. Budhraja, Z. Zhang, Z. Ke, F. Chen, J. Luo, and X. Shi, *NADPH oxidase activation is required in reactive oxygen species generation and cell transformation induced by hexavalent chromium.* Toxicol Sci, 2011. **123**(2): p. 399-410.

105.   Mohammadi-Bardbori, A. and A. Rannug, *Arsenic, cadmium, mercury and nickel stimulate cell growth via NADPH oxidase activation.* Chem Biol Interact, 2014. **224**: p. 183-8.

106.   Souza, V., C. Escobar Mdel, L. Bucio, E. Hernandez, L.E. Gomez-Quiroz, and M.C. Gutierrez Ruiz, *NADPH oxidase and ERK1/2 are involved in cadmium induced-STAT3 activation in HepG2 cells.* Toxicol Lett, 2009. **187**(3): p. 180-6.

107.   Tseng, H.Y., Z.M. Liu, and H.S. Huang, *NADPH oxidase-produced superoxide mediates EGFR transactivation by c-Src in arsenic trioxide-stimulated human keratinocytes.* Arch Toxicol, 2012. **86**(6): p. 935-45.

108. Wang, J., L. Li, H. Cang, G. Shi, and J. Yi, *NADPH oxidase-derived reactive oxygen species are responsible for the high susceptibility to arsenic cytotoxicity in acute promyelocytic leukemia cells.* Leuk Res, 2008. **32**(3): p. 429-36.

109. Li, N.C. and R.A. Manning, *Some metal complexes of sulfur-containing amino acids.* J. of the ACS, 1955. **77**(20): p. 5225-5228.

110. Jalilehvand, F., B.O. Leung, and V. Mah, *Cadmium(II) complex formation with cysteine and penicillamine.* Inorg Chem, 2009. **48**(13): p. 5758-71.

111. Mah, V. and F. Jalilehvand, *Cadmium(II) complex formation with glutathione.* J Biol Inorg Chem, 2010. **15**(3): p. 441-58.

112. Ramani, S., B. Raspor, and T. Arbneshi, *Electrochemical study of cadmium(II) complexation with cysteine.* Am. J. Anal. Chem., 2013. **4**: p. 577-583.

113. Glusic, M., P. Ropret, K. Vogel-Mikus, and J. Grdadolnik, *The binding sites of cadmium to a reduced form of glutathione.* Acta Chim. Slov., 2013. **60**: p. 61-69.

114. Scott, N., K.M. Hatlelid, N.E. MacKenzie, and D.E. Carter, *Reactions of arsenic(III) and arsenic(V) species with glutathione.* Chem Res Toxicol, 1993. **6**(1): p. 102-6.

115. Connett, P.H. and K.E. Wetterhahn, *Metabolism of the carcinogen chromate by cellular constituents.* Struct. Bond., 1983. **54**: p. 93-124.

116. Connett, P.H.W., K. E., *Reaction of Chromium(VI) with Thiols: pH Dependence of Chromium(VI) Thio Ester Formation.* Journal of the American Chemical Society, 1986. **108**(8): p. 1842-1847.

117. Zhitkovich, A., G. Quievryn, J. Messer, and Z. Motylevich, *Reductive activation with cysteine represents a chromium(III)-dependent pathway in the induction of genotoxicity by carcinogenic chromium(VI).* Environ Health Perspect, 2002. **110 Suppl 5**: p. 729-31.

118. Zhitkovich, A., V. Voitkun, and M. Costa, *Formation of the amino acid-DNA complexes by hexavalent and trivalent chromium in vitro: importance of trivalent chromium and the phosphate group.* Biochemistry, 1996. **35**(22): p. 7275-82.

119. Borges, K.M. and K.E. Wetterhahn, *Chromium cross-links glutathione and cysteine to DNA.* Carcinogenesis, 1989. **10**(11): p. 2165-8.

120. Bogumil, R. and V. Ullrich, *Phenylarsine oxide affinity chromatography to identify proteins involved in redox regulation: dithiol-disulfide equilibrium in serine/threonine phosphatase calcineurin.* Methods Enzymol, 2002. **348**: p. 271-80.

121. Foley, T.D., S.L. Melideo, A.E. Healey, E.J. Lucas, and J.A. Koval, *Phenylarsine oxide binding reveals redox-active and potential regulatory vicinal thiols on the catalytic subunit of protein phosphatase 2A.* Neurochem Res, 2011. **36**(2): p. 232-40.

122. Foley, T.D., C.M. Stredny, T.M. Coppa, and M.A. Gubbiotti, *An improved phenylarsine oxide-affinity method identifies triose phosphate isomerase as a candidate redox receptor protein.* Neurochem Res, 2010. **35**(2): p. 306-14.

123. Chang, Y.Y., T.C. Kuo, C.H. Hsu, D.R. Hou, Y.H. Kao, and R.N. Huang, *Characterization of the role of protein-cysteine residues in the binding with sodium arsenite.* Arch Toxicol, 2012. **86**(6): p. 911-22.

124. Zhang, T., H. Lu, W. Li, R. Hu, and Z. Chen, *Identification of Arsenic Direct-Binding Proteins in Acute Promyelocytic Leukaemia Cells.* Int J Mol Sci, 2015. **16**(11): p. 26871-9.

125. Zhou, X., K.L. Cooper, X. Sun, K.J. Liu, and L.G. Hudson, *Selective Sensitization of Zinc Finger Protein Oxidation by Reactive Oxygen Species through Arsenic Binding.* J Biol Chem, 2015. **290**(30): p. 18361-9.

126. Huang, B., K.H. Chiang, H.S. Yu, Y.L. Chen, H.L. You, and W.T. Liao, *Arsenic modulates posttranslational S-nitrosylation and translational proteome in keratinocytes.* ScientificWorldJournal, 2014. **2014**: p. 360153.

127. Myers, C.R., *The effects of chromium(VI) on the thioredoxin system: implications for redox regulation.* Free Radic Biol Med, 2012. **52**(10): p. 2091-107.

128. Myers, J.M., W.E. Antholine, and C.R. Myers, *Hexavalent chromium causes the oxidation of thioredoxin in human bronchial epithelial cells.* Toxicology, 2008. **246**(2-3): p. 222-33.

129. Myers, J.M. and C.R. Myers, *The effects of hexavalent chromium on thioredoxin reductase and peroxiredoxins in human bronchial epithelial cells.* Free Radic Biol Med, 2009. **47**(10): p. 1477-85.

130. Hansen, J.M., H. Zhang, and D.P. Jones, *Differential oxidation of thioredoxin-1, thioredoxin-2, and glutathione by metal ions.* Free Radic Biol Med, 2006. **40**(1): p. 138-45.

131. Go, Y.M., J.R. Roede, M. Orr, Y. Liang, and D.P. Jones, *Integrated redox proteomics and metabolomics of mitochondria to identify mechanisms of cd toxicity.* Toxicol Sci, 2014. **139**(1): p. 59-73.

132. Go, Y.M., M. Orr, and D.P. Jones, *Actin cytoskeleton redox proteome oxidation by cadmium.* Am J Physiol Lung Cell Mol Physiol, 2013. **305**(11): p. L831-43.

133. Yang, L., J. Gal, J. Chen, and H. Zhu, *Self-assembled FUS binds active chromatin and regulates gene transcription.* Proc Natl Acad Sci U S A, 2014. **111**(50): p. 17809-14.

134. Son, Y.O., J.C. Lee, J.A. Hitron, J. Pan, Z. Zhang, and X. Shi, *Cadmium induces intracellular Ca2+- and H2O2-dependent apoptosis through JNK- and p53-mediated pathways in skin epidermal cell line.* Toxicol Sci, 2010. **113**(1): p. 127-37.

135. Han, S.G., V. Castranova, and V. Vallyathan, *Comparative cytotoxicity of cadmium and mercury in a human bronchial epithelial cell line (BEAS-2B) and its role in oxidative stress and induction of heat shock protein 70.* J Toxicol Environ Health A, 2007. **70**(10): p. 852-60.

136. Mukherjee, K., T.I. Chio, D.L. Sackett, and S.L. Bane, *Detection of oxidative stress-induced carbonylation in live mammalian cells.* Free Radic Biol Med, 2015. **84**: p. 11-21.

137. Failla, M.L., R.J. Cousins, and M.J. Mascenik, *Cadmium accumulation and metabolism by rat liver parenchymal cells in primary monolayer culture.* Biochim Biophys Acta, 1979. **583**(1): p. 63-72.

138. Klug, S., F. Planas-Bohne, and D.M. Taylor, *Factors influencing the uptake of cadmium into cells in vitro.* Hum Toxicol, 1988. **7**(6): p. 545-9.

139. DelRaso, N.J., B.D. Foy, J.M. Gearhart, and J.M. Frazier, *Cadmium uptake kinetics in rat hepatocytes: correction for albumin binding.* Toxicol Sci, 2003. **72**(1): p. 19-30.

140. Peralta, D., A.K. Bronowska, B. Morgan, E. Doka, K. Van Laer, P. Nagy, F. Grater, and T.P. Dick, *A proton relay enhances H2O2 sensitivity of GAPDH to facilitate metabolic adaptation.* Nat Chem Biol, 2015. **11**(2): p. 156-63.

141. Perez-Sala, D., C.L. Oeste, A.E. Martinez, M.J. Carrasco, B. Garzon, and F.J. Canada, *Vimentin filament organization and stress sensing depend on its single cysteine residue and zinc binding.* Nat Commun, 2015. **6**: p. 7287.

142. Sun, R., L. Fu, K. Liu, C. Tian, Y. Yang, K.A. Tallman, N.A. Porter, D.C. Liebler, and J. Yang, *Chemoproteomics Reveals Chemical Diversity and Dynamics of 4-Oxo-2-nonenal Modifications in Cells.* Mol Cell Proteomics, 2017. **16**(10): p. 1789-1800.

143. Ternette, N., M. Yang, M. Laroyia, M. Kitagawa, L. O'Flaherty, K. Wolhulter, K. Igarashi, K. Saito, K. Kato, R. Fischer, A. Berquand, B.M. Kessler, T. Lappin, N. Frizzell, T. Soga, J. Adam, and P.J. Pollard, *Inhibition of mitochondrial aconitase by succination in fumarate hydratase deficiency.* Cell Rep, 2013. **3**(3): p. 689-700.

144. Wang, C., E. Weerapana, M.M. Blewett, and B.F. Cravatt, *A chemoproteomic platform to quantitatively map targets of lipid-derived electrophiles.* Nat Methods, 2014. **11**(1): p. 79-85.

145. Gupta, V., J. Yang, D.C. Liebler, and K.S. Carroll, *Diverse Redoxome Reactivity Profiles of Carbon Nucleophiles.* J Am Chem Soc, 2017. **139**(15): p. 5588-5595.

146.	Seo, M.S., S.W. Kang, K. Kim, I.C. Baines, T.H. Lee, and S.G. Rhee, *Identification of a new type of mammalian peroxiredoxin that forms an intramolecular disulfide as a reaction intermediate.* J Biol Chem, 2000. **275**(27): p. 20346-54.

147.	Smeets, A., C. Marchand, D. Linard, B. Knoops, and J.P. Declercq, *The crystal structures of oxidized forms of human peroxiredoxin 5 with an intramolecular disulfide bond confirm the proposed enzymatic mechanism for atypical 2-Cys peroxiredoxins.* Arch Biochem Biophys, 2008. **477**(1): p. 98-104.

148.	Tian, C., R. Sun, K. Liu, L. Fu, X. Liu, W. Zhou, Y. Yang, and J. Yang, *Multiplexed Thiol Reactivity Profiling for Target Discovery of Electrophilic Natural Products.* Cell Chem Biol, 2017. **24**(11): p. 1416-1427 e5.

149.	Dong, G., P.A. Wearsch, D.R. Peaper, P. Cresswell, and K.M. Reinisch, *Insights into MHC class I peptide loading from the structure of the tapasin-ERp57 thiol oxidoreductase heterodimer.* Immunity, 2009. **30**(1): p. 21-32.

150.	Schirmer, E.C., J.R. Yates, 3rd, and L. Gerace, *MudPIT: A powerful proteomics tool for discovery.* Discov Med, 2003. **3**(18): p. 38-9.

VITA

John Andrew Hitron

Education

August 2007-Present: PhD Candidate, Center for Toxicology and Cancer Biology, University of Kentucky.

August 2003-May 2007: B.S. (Biology), B.A. (Chemistry), University of Kentucky.

Research Experience

Graduate Research Assistant: University of Kentucky

Project 1: An optimized solid-phase reduction and capture strategy for the study of reversibly-oxidized cysteines and its application to metal toxicity

Professional Skills

Electron spin resonance techniques

Cysteine post-translational modification isolation and analysis techniques

Synthetic chemistry techniques

Cellular biology techniques

Molecular biology techniques

Other Experience

Lecture

Introductory lecture to TOX 509, University of Kentucky, 2012

Toxicology Student Forum

Secretary: 2009-2010

Vice President: 2010-2011

President: 2011-2013

Research Publications

Pratheeshkumar P, Son YO, Divya SP, Turcios L, Roy RV, **Hitron JA**, Wang L, Kim D, Dai J, Asha P, Zhang Z, Shi X. *Hexavalent chromium induces malignant transformation of human lung bronchial epithelial cells via ROS-dependent activation of miR-21-PDCD4 signaling.* Oncotarget. 2016 Aug 9;7(32):51193-51210.

Pratheeshkumar P, Son YO, Divya SP, Wang L, Turcios L, Roy RV, **Hitron JA**, Kim D, Dai J, Asha P, Zhang Z, Shi X. *Quercetin inhibits Cr(VI)-induced malignant cell transformation by targeting miR-21-PDCD4 signaling pathway.* Oncotarget. 2016 Jun 17;8(32):52118-52131.

Wang L, Fan J, **Hitron JA**, Son YO, Wise JT, Roy RV, Kim D, Dai J, Pratheeshkumar P, Zhang Z, Shi X. *Cancer stem-like cells accumulated in nickel-induced malignant transformation*. Toxicol Sci. 2016 Jun;151(2):376-87.

Son YO, Pratheeshkumar P, Roy RV, **Hitron JA**, Wang L, Divya SP, Xu M, Luo J, Chen G, Zhang Z, Shi X. *Antioncogenic and oncogenic properties of Nrf2 in arsenic-induced carcinogenesis*. J Biol Chem. 2015 Nov 6;290(45):27090-100.

Wang L, **Hitron JA**, Wise JT, Son YO, Roy RV, Kim D, Dai J, Pratheeshkumar P, Zhang Z, Xu M, Luo J, Shi X. *Ethanol enhances arsenic-induced cyclooxygenase-2 expression via both NFAT and NF-κB signaling in colorectal cancer cells*. Toxicol Appl Pharmacol. 2015 Oct 15;288(2):232-9.

Divya SP, Wang X, Pratheeshkumar P, Son YO, Roy RV, Kim D, Dai J, **Hitron JA**, Wang L, Asha P, Shi X, Zhang Z. *Blackberry extract inhibits UVB-induced oxidative damage and inflammation through MAP kinases and NF-κB signaling pathways in SKH-1 mice skin*. Toxicol Appl Pharmacol. 2015 Apr 1;284(1):92-99.

Pratheeshkumar P, Son YO, Divya SP, Roy RV, **Hitron JA**, Wang L, Kim D, Dai J, Asha P, Zhang Z, Wang Y, Shi X. *Luteolin inhibits Cr(VI)-induced malignant cell transformation of human lung epithelial cells by targeting ROS mediated multiple cell signaling pathways.* Toxicol Appl Pharmacol. 2014 Dec 1;281(2):230-41.

Son YO, Pratheeshkumar P, Roy RV, **Hitron JA**, Wang L, Zhang Z, Shi X. *Nrf2/p62 signaling in apoptosis resistance and its role in cadmium-induced carcinogenesis*. J Biol Chem. 2014 Oct 10;289(41):28660-75.

Pratheeshkumar P, Son YO, Wang X, Divya SP, Joseph B, **Hitron JA**, Wang L, Kim D, Yin Y, Roy RB, Lu J, Zhang Z, Wang Y, Shi X. *Cyanidin-3-glucoside inhibits UVB-induced oxidative damage and inflammation by regulating MAP kinase and NF-κB signaling pathways in SKH-1 hairless mice skin.* Toxicol Appl Pharmacol. 2014 Oct 1;280(1):127-37.

Yang YX, Li XL, Wang L, Han SY, Zhang YR, Pratheeshkumar P, Wang X, Lu J, Yin YQ, Sun LJ, Budhraja A, **Hitron AJ**, Ding SZ. *Anti-apoptotic proteins and catalase-dependent apoptosis resistance in nickel chloride-transformed human lung epithelial cells*. In J Oncol. 2013 Sep;43(3):936-46.

Wang L, Kuang L, **Hitron JA**, Son YO, Wang X, Budhraja A, Lee SC, Pratheeshkumar P, Chen G, Zhang Z, Luo J, Shi X. *Apigenin suppresses migration and invasion of*

transformed cells through down-regulation of C-X-C chemokine receptor 4 expression. Toxicol Appl Pharmacol. 2013 Oct 1;272(1):108-16.

Yin Y, Li W, Son YO, Sun L, Lu J, Kim D, Wang X, Yao H, Wang L, Pratheeshkumar P, **Hitron AJ**, Luo J, Gao N, Shi X, Zhang Z. *Quercitrin protects skin from UVB-induced oxidative damage.* Toxicol Appl Pharmacol. 2013 Jun 1;269(2):89-99.

Ding SZ, Yang YX, Li XL, Michelli-Rivera A, Han SY, Wang L, Pratheeshkumar P, Wang X, Lu J, Yin YQ, Budhraja A, **Hitron AJ**. *Epithelial-mesenchymal transition during oncogenic transformation induced by hexavalent chromium involves reactive oxygen species-dependent mechanism in lung epithelial cells.* Toxicol Appl Pharmacol. 2013 May 15;269(1):61-71.

Pratheeshkumar P, Son YO, Budhraja A, Wang X, Ding S, Wang L, **Hitron A**, Lee JC, Kim D, Divya SP, Chen G, Zhang Z, Luo J, Shi X. *Luteolin inhibits human prostate tumor growth by suppressing vascular endothelial growth factor receptor 2-mediated angiogenesis.* PLoS One 2012;7(12):e52279.

Pratheeshkumar P, Budhraja A, Son YO, Wang X, Zhang Z, Ding S, Wang L, **Hitron A**, Lee JC, Xu M, Chen G, Luo J, Shi X. *Quercetin inhibits angiogenesis mediated human prostate tumor growth by targeting VEGFR-2 regulated AKT/mTOR/P70S6K signaling pathways.* PLoS One 2012;7(10):e47516.

Son YO, Wang L, Poyil P, Budhraja A, **Hitron JA**, Zhang Z, Lee JC, Shi X. *Cadmium induces carcinogenesis in BEAS-2B cells through ROS-dependent activation of PI3K/AKT/GSK-3β/β-catenin signaling.* Toxicol Appl Pharmacol. 2012 Oct 15;264(2):153-60.

Wang L, Son YO, Ding S, Wang X, **Hitron JA**, Budhraja A, Lee JC, Lin Q, Poyil P, Zhang Z, Luo J, Shi X. *Ethanol enhances tumor angiogenesis in vitro induced by low-dose arsenic in colon cancer cells through hypoxia-inducible factor 1 alpha pathway.* Toxicol Sci. 2012 Dec;130(2):269-80.

Budhraja A, Gao N, Zhang Z, Son YO, Cheng S, Wang X, Ding S, **Hitron JA**, Chen G, Luo J, Shi X. *Apigenin induces apoptosis in human leukemia cells and exhibits anti-leukemic activity in vivo.* Mol Cancer Ther. 2012 Jan;11(1):132-142.

Son YO, Wang X, **Hitron JA**, Zhang Z, Cheng S, Budhraja A, Ding S, Lee SC, Shi X. *Cadmium induces autophagy through ROS-dependent activation of the LKB1-AMPK signaling in skin epidermal cells*. Toxicol Appl Pharmacol. 2011 Sep 15;255(3):287-296.

Wang X, Son YO, Chang Q, Sun L, **Hitron JA,** Budhraja A, Zhang Z, Ke Z, Chen F, Luo J, Shi X. *NADPH oxidase activation is required in reactive oxygen species generation and cell transformation induced by hexavalent chromium.* Toxicol Sci. 2011 Oct;123(2)399-410.

Lehner AF, **Hitron JA**, May J, Hughes C, Eisenberg R, Schwint N, Knowles DP, Timoney P, Tobin T. *Evaluation of mass spectrometric methods for detection of the anti-protozoal drug imidocarb*. J Anal Toxicol. 2011 May;35(4):199-204.

Son YO, **Hitron JA**, Cheng S, Budhraja A, Zhang Z, Lan Guo N, Lee SC, Shi X. *The dual roles of c-Jun NH2-terminal kinase signaling in Cr(VI)-induced apoptosis in JB6 cells*. Toxicol Sci. 2011 Feb;119(2):335-45.

Son YO, **Hitron JA**, Wang X, Chang Q, Pan J, Zhang Z, Liu J, Wang S, Lee JC, Shi X. *Cr(VI) induces mitochondrial-mediated and caspase-dependent apoptosis through reactive oxygen species-mediated p53 activation in JB6 CI 41 cells.* Toxicol Appl Pharmacol. 2010 Jun 1;245(2):226-35.

Brammell BF, Price DJ, Birge WJ, Harmel-Laws EM, **Hitron JA**, Elskus AA. *Differential sensitivity of CYP1A to 3,3',4,4'-tetrachlorobiphenyl and benzo(a)pyrene in two Lepomis species.* Comp Biochem Physiol C Toxicol Pharmacol 2010 Jun;152(1):42-50.

Meng D, Wang X, Chang Q, **Hitron A**, Zhang Z, Xu M, Chen G, Luo J, Jiang B, Fang J, Shi X. *Arsenic promotes angiogenesis in vitro via a heme oxygenase-1-dependent mechanism.* Toxicol Appl. Pharmacol. 2010 May 1;244(3):291-9.

Son YO, Lee JC, **Hitron JA**, Pan J, Zhang Z, Shi X. *Cadmium induces intracellular Ca^{2+} and H_2O_2-dependent apoptosis through JNK- and p53-mediated pathways in skin epidermal cell line.* Toxicol Sci. 2010 Jan;113(1)127-37.

Abdelfattah MS, Kharel MK, **Hitron JA**, Baig I, Rohr J. *Moromycins A and B, isolation and structure elucidation of C-glycosylangucycline-type antibiotics from Streptomyces sp. KY002.* J. Nat. Prod. 2008 Sep;71(9):1569-73.

Reviews

Roy RV, Son YO, Pratheeshkumar P, Wang L, **Hitron JA**, Divya SP, D R, Kim D, Yin Y, Zhang Z, Shi X. *Epigenetic targets of arsenic: emphasis on epigenetic modifications during carcinogenesis*. J Environ Pathol Toxicol Oncol. 2015;34(1):63-84. Review.

Pratheeshkumar P, Sreekala C, Zhang Z, Budhraja A, Ding S, Son YO, Wang X, **Hitron A**, Hyun-Jung K, Wang L, Lee JC, Shi X. *Cancer prevention with promising natural products: mechanisms of action and molecular targets*. Anticancer Agents Med Chem. 2012 Dec;12(10):1159-84. Review.

Chapters

Son YO, **Hitron JA**, Shi X. *Chromium(VI), Oxidative Cell Damage*, in *Encyclopedia of Metalloproteins*, RH Kretsinger, VN Uversky, EA Permyakov, editors. 2013, Springer.

Poster Presentations

Hitron JA, Son YO, Wang X, Budhraja A, Cheng S, Ding S, Zhang Z, Shi X. The oxidative stress response protein DJ-1 protects against hexavalent chromium-induced cell death. Graduate Center for Toxicology Poster Session 2010, University of Kentucky.